

EDMF parameterization during ASTEX

A. van Leeuwen

Supervisor:
Dr. S.R. de Roode

Clouds, Climate and Air Quality
Department of Multi-Scale Physics
Faculty of Applied Sciences
Delft University of Technology

June 4, 2014

Contents

1	Introduction	1
2	Theory	3
2.1	Scales and models	3
2.2	Variables	4
2.2.1	Water	5
2.2.2	Heat	5
2.2.3	Buoyancy	5
2.2.4	Overview	7
2.3	Budget equations	7
2.3.1	Horizontal mean conserved variable	7
2.3.2	Updraft conserved variables	10
2.3.3	Updraft vertical velocity	11
2.4	Eddy diffusivity parameterization	11
2.5	Massflux transport parameterization	13
2.5.1	Updraft scalar properties	13
2.5.2	Massflux development	14
3	LES diagnosis of the ASTEX transition	17
3.1	The ASTEX case study	17
3.2	LES case setup	19
3.3	Mean state	20
3.3.1	Cloud fraction	20
3.3.2	Updraft massflux heat and water transport	21
3.3.3	Turbulence dynamics	22
3.3.4	Total turbulent heat and water transport	23
3.4	Horizontal plane plots	25
3.5	Turbulence based stratification	27
4	Detailed LES analysis of the 30th hour	29
4.1	Decomposition of the sub-cloud layer	29
4.1.1	Updraft properties	31
4.1.2	Joint density plots	33
4.2	Decomposition of the cloud layer	34
4.2.1	Updraft properties - lower part cloud layer	36
4.2.2	Joint density plots - lower part cloud layer	37
4.2.3	Updraft properties - upper part cloud layer	39

4.2.4	Joint density plots - upper part cloud layer	40
4.2.5	Overview updraft properties	42
5	Parameterization	43
5.1	Eddy diffusivity parameterization during ASTEX	43
5.1.1	Sub-cloud layer	43
5.1.2	Cloud layer	45
5.2	Massflux parameterization during ASTEX	48
5.2.1	Sub-cloud layer	48
5.2.2	Cloud layer	53
6	Conclusion and discussion	61
6.1	Sub-cloud layer	61
6.2	Cloud layer	61
7	Appendix - Vertical plane plots	65
8	Appendix - Joint PDF plots large domain LES	73

Chapter 1

Introduction



Figure 1.1: Stratocumulus clouds (foreground) cover the entire sky and are the top of a turbulent mixed layer. Cumulus clouds in the back are saturated rising thermals in a conditionally stable environment. The parameterization of these cloud-types is the topic of this research. (personal picture: Mahdi (2012))

Clouds have a significant role in the heat and moisture balance of the earth. Cumulus (figure 1 - background) and stratocumulus (figure 1 - foreground) clouds are the most important cloud types in the lowest part of the earth's atmosphere. The role of these cloud-types is uncertain in the global warming problems. First, the stratocumulus clouds have a contradictory type of feedback. They are known to reflect solar radiation, but they also reduce longwave radiative heat losses. Second, it is uncertain whether a warmer atmosphere leads to less or more clouds. The Intergovernmental Panel on Climate Change (IPCC) recognizes the uncertainty for these clouds as one of the key parameters in the global warming problem (IPCC (2007)).

The horizontal grid size of Global climate models (GCMs) and numerical weather prediction (NWP) models is much coarser than the dimensions a large part of the cloud dynamics and even the entire cumulus clouds. Transport by turbulent eddies and cumuli are therefore represented in a parameterized model.

Parameterization of the separate cumulus and stratocumulus boundary layer is widely studied. The GCMs and NWPs use models for both boundary layer types based on these studies. Heat and water transport in cumulus cloud layers is most often parameterized with *massflux parameterization*. Transport in stratocumulus topped boundary layers is

most often parameterized by the *eddy diffusivity parameterization* or a combined scheme called EDMF.

Stratocumulus topped boundary layers sometimes develop into cumulus boundary layers. This transition is observed in the ASTEX case study in 1992 (Albrecht et al. (1995)). Most GCMs and NWP models have this transition incorporated in their model by an abrupt change of parameterization scheme. This results in quite irregular prediction of e.g. the cloud fraction (figure 1.2). The colored lines indicate the cloud fraction as results from GCMs and NWP-models.

The grey band indicates the cloud fraction as results from different large eddy simulations (LES). These models use a smaller grid-size, but also have a small domain. As a consequence much of the cloud dynamics are large enough to resolve. However these models are only usable for diagnosis of small characteristic domains, since the calculation costs of these models are large. The main focus of this research is the diagnosis of the heat and water transport parameterization during the ASTEX transition. LES output is used to diagnose the applicability of the combined EDMF model, with two updrafts in the sub-cloud layer (Neggers et al. (2009a)).

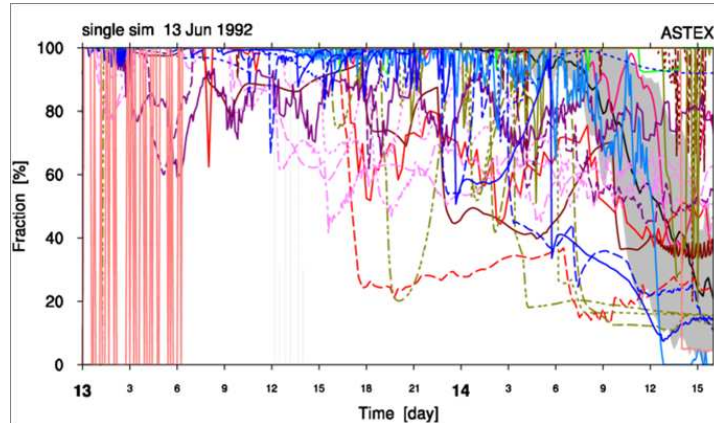


Figure 1.2: Cloud fraction as a function of time, indicating the breakup of the stratocumulus clouds. Parameterization by single column versions of climate models (in color) give varied moments for the break up whereas LES simulations produce more accurate predictions (grey band).

Chapter 2 contains a short explanation of different basic atmospheric subjects and an overview of the eddy diffusivity (2.4) and massflux parameterization (2.5).

An LES model is used to diagnose the heat and water transport during ASTEX (chapter 3). First the horizontal mean properties are diagnosed during the entire transition(3.3). The decomposed heat and water transport terms are more elaborate diagnosed in chapter 4 for the 30th hour of the ASTEX transition, using i.a. probability-density-functions (PDF). Chapter 5 diagnoses the parameters of the dual massflux heat and water transport model. The final chapter contains the conclusion and discussion (chapter 6).

Chapter 2

Theory

Heat and water transport in the boundary layer is already modelled since the 1950's. Even though the processor speed of computers has increased greatly, much of the vertical transport still has to be parameterized. The planetary boundary layer is large and even the smallest eddies are relevant. Only a small part of the eddies is resolved in numerical weather forecast (NWF) models and general circulation models (GCMs). In this chapter the equations that such models typically use are described.

2.1 Scales and models

Heat and water transport is calculated by budget equations for conserved variants of temperature and water content. These equations use three dimensions and need simplifications, because the atmosphere contains an enormous spectrum of length scales. It is not possible to resolve these budget equations, for both the smallest and the largest movements in the atmosphere. Table 2.1 gives an indication of some length scales in the atmosphere. In the 3th and 4th column is indicated whether these scales are too large to fit in the simulation domain (not), are large enough to be resolved (res), or are parameterized (par) in global numerical weather forecast models and large eddy simulations.

Table 2.1: Scales of atmospheric phenomena and explanation whether the phenomena are too large (not), resolved (res) or parameterized (par) in global numerical weather forecast (NWF) and large eddy simulations (LES)

Atmospheric phenomenon	Magnitude	In Global NWF	In LES
Atmospheric pressure system	1000 <i>km</i>	res.	not
mesoscale convective system	100 <i>km</i>	res.	not
boundary layer depth	1-3 <i>km</i>	res.	res.
diameter cumulus cloud	0.1-1 <i>km</i>	par.	res.
smallest eddies (Kolmogorov dissipation scale)	0.1 <i>mm</i>	par.	par.
droplet size at initiation	80 μ <i>m</i>	par.	par.

NWF and GCMs have to deal with scales, which differ in order of 10^6 in horizontal and 10^4 in vertical direction. Climate models cover the entire world and calculate over years. Every day numerical global weather models produce a weather forecast for the next 14 days. Limited by calculation costs, the global weather forecast model of the

ECMWF (European Centre for Medium-Range Weather Forecasts) uses grid boxes of $15 \times 15 \text{ km}^2$ in horizontal and 90 levels in vertical direction (ECMWF (2010)). The KNMI (Royal Netherlands Meteorological Institute) model *Harmonie* uses grid boxes with dimensions up to $2.5 \times 2.5 \text{ km}^2$ in horizontal in a limited domain of about $750 \times 750 \text{ km}^2$ (HIRLAM (2009)). Cumulus clouds are by far too small to be resolved explicitly in all mentioned models. These clouds (and many other phenomena) are incorporated by parameterization; subgrid-scale phenomena are related to variables which are available on grid size.

Horizontal advection of heat and water is in most GCMs and NWF models satisfactorily represented, but especially the representation of vertical turbulent transport causes problems, since subgrid-scale turbulence has a significant role in the heat and water transport. Parameterization of turbulent vertical heat and water fluxes is based on and validated by measurement series and LES runs on characteristic weather situations (figure 2.1).

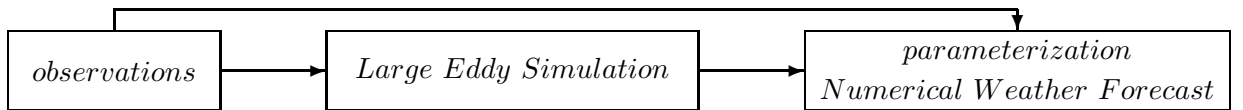


Figure 2.1: LES and observations during measurement series are used to develop parameterization in global circulation models and numerical weather forecast models.

LES domains have a much smaller domain than GCMs, but resolve a large part of the three-dimensional turbulence. Two different ways of diagnosis of the vertical component are first the diagnosis of horizontal homogeneous parts of the boundary layer and second Lagrangian diagnosis. The ASTEX case is a Lagrangian case study, therefore this approach is also used in this research. In the Lagrangian approach, a parcel of air is tracked, while travelling over the earth's surface. The entire history of the parcel is hereby well-known, but the boundaries of the chosen domain are changing in time. The horizontal domain is often chosen small with respect to horizontal boundary layer development length scales, making it possible to assume horizontal statistical homogeneity within the domain. The LES results in this research therefore use periodic vertical boundary layers and horizontal homogeneous forcings, which change in time as if the domain travels along with a parcel. Three-dimensional LES results are horizontally averaged. The horizontal mean profiles are used to find simplified budget equations in the GCMs.

2.2 Variables

In atmospheric sciences, variables are typically used that are conserved for pressure changes and condensation/evaporation of water. The use of such variables greatly simplifies the conservation equations. The budget equation of a general conserved variable ϕ reads :

$$\frac{\partial \phi}{\partial t} + u_j \frac{\partial \phi}{\partial x_j} = F_\phi \quad (2.1)$$

Here $\partial/(\partial t)$ indicates the tendency, u_j is velocity vector in a Cartesian coordinate system (x_j) and sources and sinks are represented by F_ϕ (equations in this section are based on de Roode et al. (2004))

2.2.1 Water

The amount of water is often related to the mass of dry air, expressed in kilogram water per kilogram dry air. The sum of the water vapor content (q_v) and liquid water content (q_l , cloud water), is called total water content (q_t). The total water content is in contrast to the water vapor content conserved for condensation and is used in many models.

A distinction is made between liquid cloud water and liquid rain water. The latter is often excluded from the total water content. Rain therefore acts as sink term for parcels in which rain droplets are formed and as source term at lower levels where the rain is evaporated again.

2.2.2 Heat

It is more difficult to formulate a conserved variable for heat. The temperature of an air parcel is conserved for adiabatic horizontal displacements. But when a parcel rises, the pressure decreases due to hydrostatic pressure decrease. As a consequence the parcel expands and gets colder.

The potential temperature (θ) is introduced with the aim to conserve the temperature for vertical displacement in hydrostatic atmosphere. The definition is:

$$\theta = T \left(\frac{p_0}{p} \right)^{\frac{R_d}{c_p}} \quad (2.2)$$

in which T is the temperature, p_0 is the pressure at the reference height, R_d is the specific gas constant of dry air and c_p is the heat capacity. Although conserved for adiabatic displacements, this only holds until the water vapor pressure approaches the saturation pressure. Exceeding this pressure, water vapor condenses and clouds are formed. The saturation pressure decreases with height due to the (real) temperature decrease of the rising parcel. Exceeding the saturation pressure condensation heat is released. The potential temperature then is no longer conserved. The linearized form of the liquid water potential temperature (θ_l) is used in order to have a conserved temperature-scale, even when water phase changes take place:

$$\theta_l \cong \theta - \frac{L_v}{c_p} q_l \quad (2.3)$$

Here, L_v is the latent heat of evaporation of water and q_l is the liquid water content. The liquid water potential temperature is used as basic variable in many large eddy simulations. Typical values for c_p and L_v are 1000 J/kgK and $2.5 \cdot 10^6 \text{ J/kg}$.

2.2.3 Buoyancy

The liquid water potential temperature simplifies calculations on heat transport. Although θ_l is conserved for condensation and vertical adiabatic displacements, it is not directly related to the density. The virtual temperature is introduced as a temperature

scale which is especially related to the density. The ideal gas law gives a first relation between the density and the temperature:

$$\rho = \frac{\overline{M}p}{R_u T} \quad (2.4)$$

The density is, besides for temperature, a function of pressure (p), the universal gas constant (R_u) and the mean molar mass (\overline{M}). Since air contains many chemical components, the mean molar mass can be written as:

$$\sum x_i M_i = \overline{M}, \quad (2.5)$$

in which x_i are the molar fractions of the chemical components in a parcel air. Water vapor f.e. is less dense (0.804 g/L) than dry air (1.29 g/L) and therefore has a lowering effect on the mean density. When all effects due to the molar fractions are incorporated in the virtual temperature scale, the ideal gas law is transformed into:

$$\rho = \frac{p}{T_v R_d} \quad (2.6)$$

The molecular weight of dry air is substituted out by the use of the specific gas constant R_d for dry air. Hereby the virtual temperature (T_v) is a function of the water vapor and liquid water content:

$$T_v = \left[1 + \frac{1 - \epsilon}{\epsilon} q_t - \frac{q_l}{\epsilon} \right] T, \quad (2.7)$$

The molar mass of water vapor is included in the specific gas constant of water vapor (R_v) in $\epsilon = R_d/R_v \cong 0,622$. The second term between the brackets of equation 2.7 can be interpreted as the buoyancy contribution of water vapor. The third term is a load term in which the volume of liquid water is neglected. The decrease in temperature due to a pressure drop due to adiabatic vertical displacement is often, in similarity with equation 2.2, compensated by the introduction of a potential temperature scale. When furthermore the potential temperature is expressed in terms of θ_l and q_l , the expression for the virtual potential temperature (θ_v) reads:

$$\theta_v = \left[1 + \frac{1 - \epsilon}{\epsilon} q_t - \frac{q_l}{\epsilon} \right] \left(\theta_l + \frac{L_v}{c_p} q_l \right) \quad (2.8)$$

Whereas liquid water content was only a sink term in equation 2.7, it is also a source for θ_v in equation 2.8, due to latent heat release. θ_v as a consequence is in contrast with T_v , conserved for hydrostatic pressure differences due to vertical displacements.

The lapse rate of the horizontal mean θ_v is an important indicator for stability of the atmosphere. When $\overline{\theta_v}$ is increasing with height, the upper parcels are less dense and turbulence is suppressed. When the lapse rate is large enough, this effect could be even sufficient for saturated parcels ($\frac{\partial \overline{\theta_v}}{\partial z} > \frac{\partial \theta_{v,saturated}}{\partial z}$, absolutely stable). Though when the

lapse rate is negative, the density increases with height. Parcels are denser than lower ones, so the atmosphere is absolutely unstable. Temperature profiles with lapse-rates between the moist-adiabatic and dry-adiabatic lapse rate are called conditionally stable.

2.2.4 Overview

Most results in this research are based on LES results. The main used variables and their most significant limitations and relations are given in table 2.2.

Table 2.2: Symbol and brief description of the main variables in this research.

	variable	description	units
w	vertical velocity	vertical component of velocity vector	$[m/s]$
u, v	horizontal velocity	horizontal components of velocity vector	$[m/s]$
θ_l	liquid water potential temperature	vertical displacement and condensation conserved temperature. Not conserved for radiation, surface fluxes and rain evaporation.	$[K]$
q_t	total water content	kg liquid water and vapor per kg air. Not conserved for rain, surface fluxes.	$[kg/kg]$
p_{mod}	modified pressure	pressure fluctuation with respect to horizontal mean hydrostatic pressure (de Roode et al. (2012), eq.12)	$[m^2/s^2]$
q_l	liquid water content	kg liquid water per kg air. The saturation pressure is strongly related to the normal temperature. The liquid water content is therefore a function of temperature, pressure and total water content.	$[kg/kg]$
θ_v	virtual potential temperature	temperature scale, for small deviations inversely proportional to the density. It is therefore not conserved for phase transitions, radiation and rain, only for vertical displacement under hydrostatic, adiabatic circumstances.	$[K]$

2.3 Budget equations

The heat budget is often parameterized for the variable θ_l , whereas the water budget uses q_t . These variables are conserved for many processes within the boundary layer. The budget equation for the horizontal mean conserved variable is elaborated in the first part of this chapter, whereas the budget of the main updraft properties is elaborated in the second part.

2.3.1 Horizontal mean conserved variable

This research uses a simplified budget equation for the variable's θ_l and q_t , which are represented by the conserved variable ϕ :

$$\frac{\partial \bar{\phi}}{\partial t} = -\frac{\partial \overline{w'\phi'}}{\partial z} + F_\phi \quad (2.9)$$

The overbar is used for a horizontal mean, the $'$ indicates a fluctuation with respect to the horizontal mean and F_ϕ is a source and sink term for processes as mentioned in table 2.2. The research presented in this report, focusses on the parameterization of the vertical transport. Other terms, such as horizontal advection, subsidence, radiation and precipitation are therefore not treated here, although their effect is not negligible.

The tendency of a conserved variable ϕ is, as a consequence of equation 2.9, defined by the vertical lapse rate of the $\overline{w'\phi'}$ term. This is called turbulent transport term since transport is not performed by vertical advection, but due to transport by turbulent eddies. Under the condition of horizontal statistical homogeneity this is the only term, since mass balance requires a zero mean vertical velocity (which is forced in the used LES model). Turbulent eddies with large q_t' and low θ_l' eddies move upwards performing upward water and downward heat transport, whereas small q_t' and high θ_l' eddies move downwards. So after averaging, all transport is performed by the covariance (figure 2.2) of the vertical velocity fluctuations with the variable fluctuations, whereas the horizontal mean vertical velocity is negligible small.

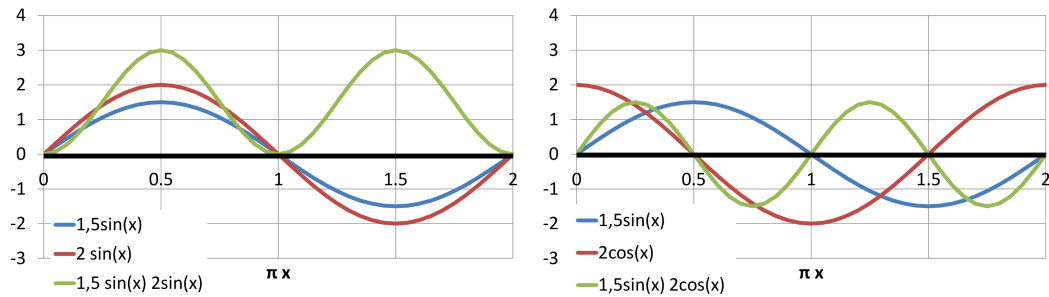


Figure 2.2: Two sine functions have a non-zero covariance (right), since their mean value is non-zero after multiplication. A sine and cosine functions though are uncorrelated and have zero covariance(left).

Decomposition of the turbulent transport term

For parameterization it appears convenient to use a decomposition of the turbulent transport term into an updraft and non-updraft contribution (called environment). This causes non-zero horizontal mean vertical velocity within the decomposed parts of the boundary layer (more about this subject by Heus and Jonker (2008)). Rising updrafts have a strong vertical velocity (up to 5 m/s), so the mean non-updraft part of the boundary layer as a consequence is subsiding. Figure 2.3 shows the notation of different vertical velocities, needed for an expression of the decomposed turbulent transport term.

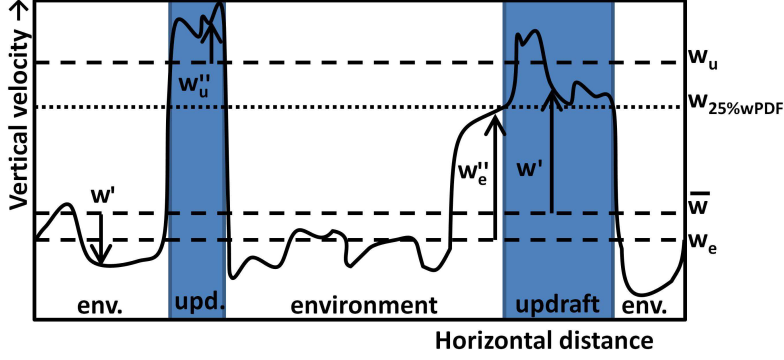


Figure 2.3: Notation of fluctuations and means of the vertical velocity in a decomposed boundary layer. As an example the 25 % wPDF sample criterion is used; parts satisfying the sample criterion ($w > w_{25\%wPDF}$) are blue-shaded.

A common horizontal mean variable $\bar{\psi}$ is expressed in sample and environmental mean values, when weighted by their updraft fractions.

$$\bar{\psi} = a_u \psi_u + (1 - a_u) \psi_e \quad \psi \in \{\theta_l, \theta_v, q_t, w\} \quad (2.10)$$

The subscripts indicate horizontal mean value within updraft (u) or environment (e) for the concerning variable. The environmental fraction is equal to $(1 - a_u)$ when a decomposition in two parts is used

The decomposition of the boundary layer is often diagnosed by sampling of LES output. Different sample criteria are used in this diagnosis of the ASTEX case, which are explained in table 2.3. The set of criteria with a the-liquid-water-condition, will be mentioned as conditional sampling criteria. Probability density function based criteria define at every height a limit value of the fastest or moistest percentile of the probability density function, which is used as sampling criterion at that height.

Table 2.3: Sample criteria, used to diagnose updrafts in the ASTEX case

Name	Sample criterion	Abbreviation
cloud	$q_l > 0$ g/kg (liquid water content)	cld
cloudup	$q_l > 0$ g/kg, $w > 0$ m/s (rising)	cldup
cloudcore	$q_l > 0$ g/kg, $\theta'_v > 0$ K (positive buoyant)	cldcr
PDF-based	The fastest or moistest $x\%$ of the probability density function of the variable ϕ	$x\%$ ϕ PDF

The decomposition of the horizontal mean turbulent flux ($\overline{w'\phi'}$, eq 2.9) leads to a subplume transport term within the sample $a_u \overline{w''\phi''^u}$ and environment $(1 - a_u) \overline{w''\phi''^e}$ and in one or two vertical advection terms. The overbars with u or e indicate averaging within sample or environment. The decomposed transport term then reads (Siebesma and Cuijpers (1995)):

$$\overline{w'\phi'} = a_u \overline{w''\phi''^u} + (1 - a_u) \overline{w''\phi''^e} + a_u (w_u - \bar{w}) (\phi_u - \phi_e) \quad (2.11)$$

The third term on the right-hand-side is the advection term caused by the non-zero w_s and w_e . The first part of the term is called the massflux of the updraft:

$$M_u \equiv a_u (w_u - \bar{w}) \quad (2.12)$$

A decomposed massflux transport term is diagnosed in this study, since multiple updrafts are used. Therefore the massflux transport terms are expressed in terms of sample value with respect to horizontal mean value (Siebesma and Cuijpers (1995) and Neggers et al. (2009a)). For a single updraft the result is:

$$\overline{w'\phi'} = a_u \overline{w''\phi''^u} + (1 - a_u) \overline{w''\phi''^e} + \underbrace{a_u (w_u - \bar{w})}_{M_u} (\phi_u - \bar{\phi}) + \underbrace{(1 - a_u) (w_e - \bar{w})}_{M_e} (\phi_e - \bar{\phi}) \quad (2.13)$$

Both massflux transport terms could be expressed in sample and horizontal-mean values, using equation 2.10. The resulting adapted expression of equation 2.13 reads:

$$\overline{w'\phi'} = a_u \overline{w''\phi''^u} + (1 - a_u) \overline{w''\phi''^e} + M_u (\phi_u - \bar{\phi}) + \frac{a_u}{1 - a_u} M_u (\phi_u - \bar{\phi}) \quad (2.14)$$

The ratio of the environmental and updraft massflux transport contributions is $a_u / (1 - a_u)$. Consequently the environmental massflux ϕ transport contribution is negligible to the updraft contribution for small updraft fractions. A general notation of a multiple decomposed turbulent flux is:

$$\overline{w'\phi'} = \sum_i a_i \overline{w''\phi''^i} + M_i (\phi_i - \bar{\phi}) \quad (2.15)$$

2.3.2 Updraft conserved variables

The properties of the LES sampled updraft change in time and therefore also need parameterization. Though the budget is often diagnosed for a steady state situation. The updraft content for the conserved variable budget reads (Siebesma et al. (2007)):

$$\frac{\partial \phi_u}{\partial z} = -\epsilon_\phi (\phi_u - \bar{\phi}) + r_u^\phi \quad (2.16)$$

r_u^ϕ represents sources or sinks due to processes as defined in table 2.2. ϵ_ϕ is the fractional entrainment rate. No detrainment rate is added, since the updraft mean ϕ does not change due to detrainment when the detrained parcel is assumed to have mean sample value. Though the massflux does change due to detrainment (Siebesma et al. (2007)):

$$\frac{\partial M_u}{\partial z} = M_u (\epsilon - \delta) \quad (2.17)$$

δ is the fractional detrainment rate. Equations 2.17 and 2.16 can use the same ϵ ; although often different entrainment rates are used for different variables. This research will use the variable q_t for the entrainment-rate diagnosis, since this variable has less sources and sinks than θ_l .

2.3.3 Updraft vertical velocity

Instead of the massflux budget, also the vertical velocity budget is used to define the updraft massflux. This is especially convenient for PDF sampled updrafts and for cumulus cloud-top height calculations. The vertical velocity budget by de Roode et al. (2012) contains 7 terms: tendency (tend), buoyancy (buo), advection (adv), entrainment (ent), subplume (sub), pressure (pres) and Coriolis effects (cor):

$$\underbrace{\frac{\partial w_u}{\partial t}}_{\text{tend}} = \underbrace{B_u}_{\text{buo}} - \underbrace{\frac{1}{2} \frac{\partial w_u^2}{\partial z}}_{\text{adv}} - \underbrace{\frac{\epsilon_w w_u^2}{1 - a_u}}_{\text{entr}} - \underbrace{\frac{1}{a_u} \frac{\partial a_u \overline{w'' w''^u}}{\partial z}}_{\text{subpl}} - \underbrace{\left[\frac{\partial p_{mod,u}}{\partial z} \right]}_{\text{pres}} + \underbrace{2\Omega \cos \phi_l a_u u_u}_{\text{cor}} \quad (2.18)$$

The Coriolis term is a function of the angular velocity of the earth (Ω) and the latitude (ϕ_l) The buoyancy term B_u is often expressed as a function of θ_v :

$$B_u = [g/\theta_0 (\theta_{v,u} - \overline{\theta_v})] \quad (2.19)$$

using g as the acceleration due to gravity and θ_0 as a reference temperature.

2.4 Eddy diffusivity parameterization

Eddy diffusivity (ED) parameterization relates vertical turbulent transport of a conserved variable (equation 2.9) to the vertical gradient of its horizontal mean value as follows:

$$\overline{w' \phi'} = -K_\phi(z) \left(\frac{\partial \overline{\phi}}{\partial z} \right) \quad (2.20)$$

In order to have down-gradient diffuse transport from high values to low values, a minus sign is added in front of the eddy diffusivity profile (K_ϕ). The term eddy is used since transport by turbulent eddies is modelled. Atmospheric turbulence in mixed layers, such as stratocumulus topped layers and sub-cloud layers, are characterized by strong turbulent mixing. The largest eddies typically extend from the top to the bottom of these layers. These largest eddies break up into smaller eddies, which again break up, up to dissipation scale, until the entire layer is involved in this transport. Though the horizontal mean vertical velocity is negligible small with respect to the variance. The term diffusivity is used since the flux is related to the lapse rate of the horizontal mean value of ϕ . Hereby the flux is related to the local ϕ profile. Eddy diffusivity profiles are often parameterized with the next equation,

$$K_\phi = \sqrt{E} L_m \quad (2.21)$$

in which L_m is a mixing length and E is the turbulent kinetic energy. Many NWP use a prognostic equation to determine E (Soares et al. (2008)).

Counter-gradient heat fluxes and potential temperature profiles heat fluxes appeared are quite common (Deardorff (1966)). This urged to find an more advanced scheme than

the bare ED model (2.20), taking care for non-local transport. Figure 2.4 shows a deep layer in which the heat flux is opposite directed to what would be expected from the local gradient.

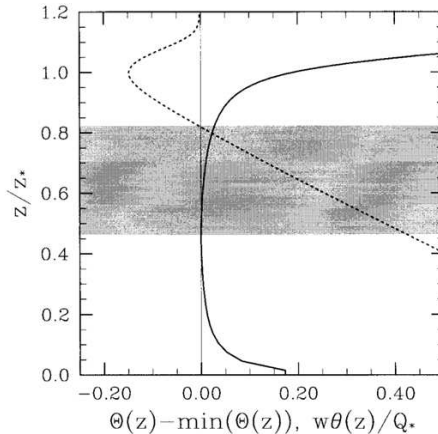


Figure 2.4: normalized flux(dotted) and potential temperature(solid line) in a convective boundary layer. A counter-gradient-transport region is present (shaded) when $\overline{w'\phi'}$ is non-zero at an height with a zero- ϕ gradient. (used from Stevens (2000))

Most convective boundary layers, stratocumulus sub-cloud layers and stratocumulus topped boundary layers have two heat sources; an upward-directed surface heat flux and an downward directed entrainment heat flux. As a consequence first the θ_l profile has a minimum (a zero-gradient) and at least one height has zero heat flux. Often these heights do not coincide, causing a region with counter gradient heat transport (figure 2.4). First approach was to add a counter gradient term(γ_h):

$$\overline{w'\phi'} = -K_\phi(z) \left(\frac{\partial \bar{\phi}}{\partial z} + \gamma_h \right) \quad (2.22)$$

Different variables are used to define the counter gradient term (Holtslag and Moeng (1991), Deardorff (1972) e.a.). Though the use of this counter-gradient term appears to have some undesirable side effects. Stevens (2000) diagnosed analytical solutions for θ profiles and poses some restrictions on the use of counter-gradient terms and investigates the role of the different parts of the ED parameterization on the θ profiles. The K_θ single column models with non-local fluxes tend to relax the profiles of scalars toward a similarity form, whose non-dimensional shape is implicitly determined by the shape of the K-profile and the choice of scaling. The non-local term is only valid in a limited range of counter-gradient-term values, creating unrealistic θ -profiles outside this range. Using LES simulations, Siebesma et al. (2007) shows the need for combined eddy diffusivity massflux parameterization (EDMF), to deal with the stabilizing influence of the eddy diffusivity on the top of the mixed layer. The counter-gradient term should provide instability in the cloud-top and a sharp temperature drop as found in measurements. But actually it causes the θ_l profile to develop in such a manner that the counter gradient flux neutralizes the eddy diffusivity transport. The eddy diffusivity term is always positive, as it tends to create a stable cloud top, which forces the top entrainment flux to decrease.

This gives unrealistic slow cloud layer development. On the contrary, EDMF parameterization represents well the evolution of the main properties of convective boundary layer (equation 2.23)

$$\overline{w'\phi'} = -K_\phi(z) \left(\frac{\partial \bar{\phi}}{\partial z} \right) + M_u (\phi_u - \bar{\phi}) \quad (2.23)$$

The use of a combined eddy diffusivity and massflux transport model excludes the need of a non-local term. Another application of the EDMF scheme is found in the sub-cloud layer. Besides for redistribution of heat and water within the sub-cloud layer, the massflux model is used for initialization of the cloud-layer updraft. Neggers et al. (2009a) shows how cumulus updrafts are deeply rooted in the sub-cloud layer. In the dual massflux parameterization, a 'dry' and 'wet' updraft is used. The dry updraft detrains in the top of the sub-cloud layer in order to deal with non-local fluxes, whereas the saturated updraft is used as initial updraft in the cumulus-cloud layer. As a result both the updraft has an initial velocity, θ_l and q_t and the cumulus heat and water transport out of the sub-cloud layer is coupled to the transport within the sub-cloud layer. Even though the decomposition of turbulent fluxes leads to multiple subplume transport terms, these terms are parameterized in one term in the dual massflux model:

$$\overline{w'\phi'} = -K_\phi(z) \left(\frac{\partial \bar{\phi}}{\partial z} \right) + \sum_{i=1}^2 M_{u,i} (\phi_{u,i} - \bar{\phi}) \quad (2.24)$$

In the sub-cloud layer two updrafts are present ($i \subset 1, 2$). One fully detrains in the top of the sub-cloud layer and only one enters the cloud layer ($i \subset 1$).

2.5 Massflux transport parameterization

The massflux transport contribution in the heat and water transport budget represents 60 to 90 % of the total vertical q_t and θ_l transport in the cumulus cloud layer of the BOMEX case. The parameters have been diagnosed with LES models in different cumulus case studies (Siebesma and Cuijpers (1995), Stevens et al. (2001), Siebesma et al. (2007), de Roode et al. (2012)). The next variables are needed for a complete massflux model.

1. Mean updraft $q_{t,u}$ or $\theta_{l,u}$ value (scalar properties).
2. Updraft massflux M_u or vertical velocity w_u .
3. Mean \bar{q}_t or $\bar{\theta}_l$.

The mean q_t or θ_l value is a result of the mean conserved variable budget equation 2.9. So only the updraft scalar properties and the massflux or vertical velocity need parameterization.

2.5.1 Updraft scalar properties

The entrainment rates for cumulus updrafts are diagnosed from LES by sampling with the next equation:

$$\epsilon_\phi \cong -\frac{\frac{\partial\phi_u}{\partial z}}{\phi_u - \bar{\phi}} \quad (2.25)$$

The entrainment rates for q_t and θ_l are found to be almost equal and more or less constant in the BOMEX cloud layer with values of about 0.003 m^{-1} for the updraft criterion ($w > 0$) and 0.002 m^{-1} for the cloudcore updraft (Siebesma and Cuijpers (1995)). The updraft in the ATEX case is quite similar, though the entrainment rate increases in the highest 400 m to a value of about $0.006\text{-}0.008 \text{ m}^{-1}$, since the ATEX cloud layer is capped by a warm layer (Stevens (2000)). The increasing temperature is called the temperature inversion. The upper part of the cloud layer of ASTEX is similar to the ATEX case capped by warm layer.

The entrainment rates for updrafts in convective boundary layers and sub-cloud layers are diagnosed with wPDF sampling criteria (Siebesma et al. (2007)). The rates appear not constant in height, but the entrainment rate profiles collapse reasonably well on a single parabolic curve, using the inversion height (z_{inv}):

$$\epsilon \cong c_\epsilon \left(\frac{1}{z} + \frac{1}{z_{inv} - z} \right) \quad (2.26)$$

c_ϵ is a constant with a value of about 0.4 for 1 to 5 % wPDF sampled updrafts (Siebesma et al. (2007)) and 0.5 for the 30 % wPDF sampled (Soares et al. (2008)). The entrainment rate strongly depends on the updraft environment and the applied sample criterion. Dawe and Austin (2011) recommends to diagnose the rates separately for the different variables, since many processes occur in the cloud shell, which are related to the vertical velocity, q_t and θ_l and the sample-criteria itself.

2.5.2 Massflux development

The massflux is calculated by the massflux budget equation (2.17). Even though the updrafts have positive entrainment rates, most cumulus case studies have a net decreasing massflux after cloud initiation. The detrainment rates in the BOMEX and ATEX cases are slightly larger than the entrainment rates ($\delta_{BOMEX} = 0.004 \text{ m}^{-1}$, $\delta_{ATEX} = 0.003 \text{ m}^{-1}$), with as a result a slowly decreasing massflux with height.

Probability-density-function-based sample criteria have a constant updraft fraction. As a consequence the massflux budget is totally defined by the vertical velocity budget. The vertical velocity budget equation (2.18) as mentioned in section 2.3 is often used in models in the next simplified form:

$$\frac{1}{2} \frac{\partial w_{up}^2}{\partial z} = a B_u - b \epsilon_w w_{up}^2 \quad (2.27)$$

Similar to equation 2.18 the buoyancy (B) of the updraft is expressed in the sample mean θ_v with respect to the horizontal mean. The parameterization in equation 2.27 has less terms than equation 2.18, so these terms have to be related to the buoyancy and advection term by the a and b constants. The effects of non-hydrostatic pressure perturbations and subplume fluctuations are supposed to be taken into account by a reduction of the buoyancy

term ($a < 1$) and by multiplication of the lateral entrainment by a proportionality factor b . de Roode et al. (2012) gives an overview of the used parameters of 15 different models. The relationship between the pressure, advection and buoyancy term and the subplume and entrainment term are also diagnosed from sampled LES results for three different case studies. Using least-error analysis the a factor appeared to be in the order of 0.35 to 0.55 and b between 0.0 and 0.45. The parameterization coefficients are case dependant. The pressure term appears to be the dominant damping term, in odds with former models that use the lateral entrainment term as main damping term of the vertical velocity. The entrainment term and vertical velocity entrainment rate in the extended budget equation (2.18) are calculated as residual term. The term appeared small and even positive, indicating a negative entrainment rate.

Chapter 3

LES diagnosis of the ASTEX transition

The background and the main characteristics of the ASTEX measurement series are given in section 3.1. This research uses an LES model (more in section 3.2) validated on these measurements. Output is used to diagnose the mean state (chapter 3.3) and turbulence dynamics during the first 40 hours of the ASTEX transition. The heat and water transport terms and dynamics in the ASTEX cloud layer are different to f.e. the BOMEX case and change during the transition. The mean state diagnosis is therefore used to choose a suitable moment in the transition, which is more elaborate diagnosed in chapter 4. Chapter 5 presents parameters of the EDMF model.

3.1 The ASTEX case study

The ASTEX case study concerns the transition from a stratocumulus topped boundary layer into a cumulus perturbed boundary layer. Data was collected between 12 to 14 June 1992, during the first Lagrangian measurement series of the Atlantic Stratocumulus Transition Experiment (ASTEX). The transition took place in about 40 hours over a distance of 1000 km (Albrecht et al. (1995), C. S. Bretherton (15 aug 1995)).

The measurements in the ASTEX case study consist of aircraft, satellite, ship and balloon observations on a parcel travelling over the sea surface. The observed, advected parcel is part of the tradewinds. The tradewinds themselves are part of a planetary atmospheric circulation cell, which is called the Hadley cycle.

Hadley cycle

The Hadley cycle is an atmospheric circulation system, redistributing heat and water over a large part of the earth. Heated dry air rises at the equator and moves in the direction of the poles (figure 3.1). At 30°N and S and dry air flow descends and travels back over the sea surface to the equator. Each side of the earth contains three of these cells in which the second, the middle-latitude cell has opposite direction. Due to the opposed streams, the atmospheric pressure builds-up at 30°N and S latitude. This forces the lower streams at the earth's surface to turn back.

The lower Hadley stream is heated and moistened at the sea surface. Water is transported from the surface to the top of the cloud layer. An uprising parcel encounters

a sudden increase in environmental temperature as it reaches the upper stream (the temperature inversion). The environmental temperature increment is accompanied by a smaller density, so the rising parcel will fall back into the lower layer. The dynamics in the upper and lower stream therefore are separated. The upper heated, dry stream is not directly influenced by the surface of the earth and is called "free atmosphere". The lower stream is called "planetary boundary layer".

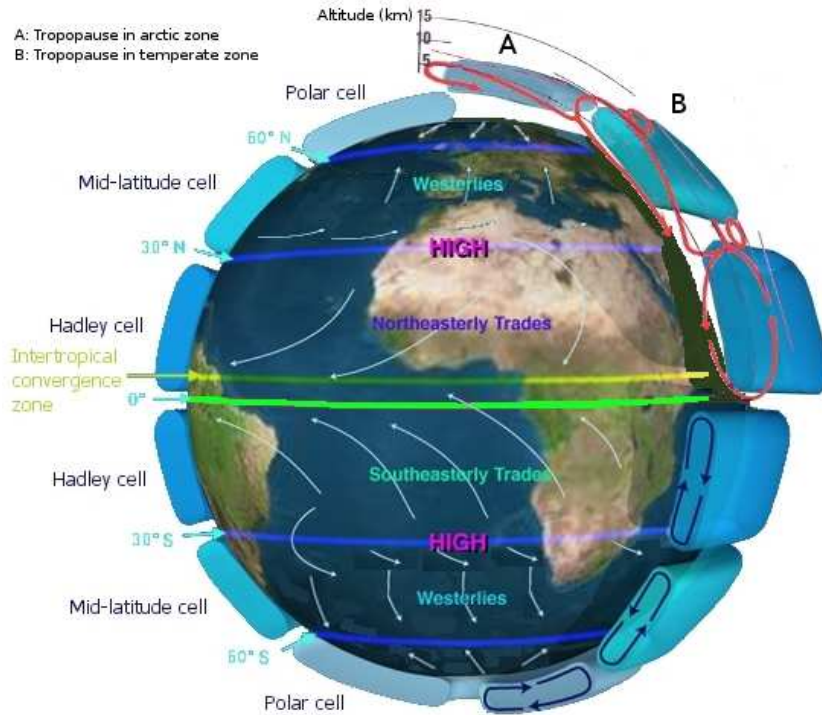


Figure 3.1: Global circulation. Heated dry air rises at the equator and moves to 30°N and S. Reaching the next cell, the air cools down and travels back over the sea surface. (NASA (2005))

Boundary layer clouds

The ASTEX boundary layer is initially relative shallow, unstable and turbulent. Stratocumulus clouds are formed, since the boundary layer is relative moist due to water evaporation at the sea surface. The entire boundary layer is turbulent mixed and as a result all surface is covered by stratocumulus clouds. Moving to the equator, the temperature inversion is getting weaker and air with small q_t and high θ_l is entrained downwards from the upper layer into the lower layer. The boundary layer depth increases, the cloud top is getting dryer, less dense and finally the stratocumulus clouds break up.

The sea surface temperature of the Atlantic ocean increases from 290.4 K to 294.2 K during the transition (de Roode and Duijkerke (1997)). As a consequence, the surface moisture flux remains and moist parcels become saturated far below the stratocumulus clouds. These saturated parcels evolve in rising cumuli. When saturated, parcels become positive buoyant due to latent heat release and gain relative large upward velocities. The stability of the cloud-layer increases due to cloud top entrainment, whereas the cumulus clouds detrain air with low θ_l and large q_t values in upper part of the cloud layer. During

the track the next cloud regimes are present:

1. extensive sheets of stratocumulus
2. cumulus under stratocumulus
3. trade wind cumulus

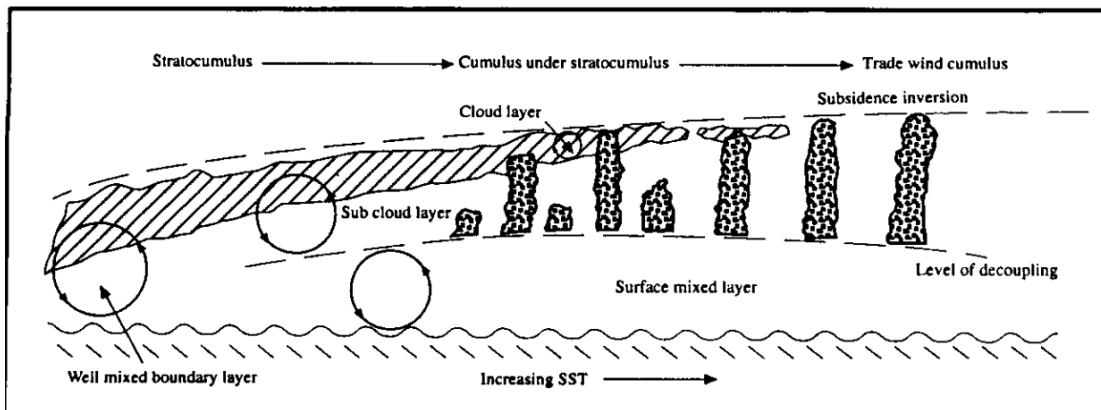


Figure 3.2: Schematic representation of the ASTEX boundary layer development during two days. The figure start in the early morning of June the 13th in the left. (adapted from Albrecht et al. (1995))

3.2 LES case setup

This thesis uses output of the DALES LES model (Heus et al. (2010)). The model results agree remarkably well with aircraft observations. In particular, the models are able to closely reproduce the ASTEX transition of a vertically well-mixed stratocumulus-topped boundary layer into a much deeper decoupled boundary layer, with shallow cumulus clouds penetrating the stratocumulus clouds above (Van der Dussen et al. (2013)).

Two different LES runs are used in this research. They are mentioned as 'small' or 'large', according to their relative domain size. The small domain results are used for the diagnosis of the entire transition (chapter 3.3). Diagnosis of updrafts with small probability density function based sample criteria is only applied on the large domain simulation. Saturated cumuli are not continuously present in the small domain LES, since the minimum hourly mean fraction is in the order of 0.001. This is no problem for conditional sampling criteria (f.e. cloud or cloudup criterion), since these have fraction weighted contribution to hourly averaged vertical profiles. On the contrary, the 0.1% wPDF sampled updraft, uses fixed updraft fractions and is therefore only able to select liquid water when a saturated updraft is present. However, the saturated updraft is always present in the large LES domain. Detailed analysis, using wPDF updraft diagnosis, therefore uses results from the large domain LES. Details of the models are given in table 3.1:

Table 3.1: Dimensions of the used LES models.

SMALL	Vertical dimensions: 15 m/gridbox up to 600 m, 5 m/gridbox to 2100, total 2465 m in 361 levels Horizontal dimensions: 128×128 boxes of 35×35 m^2 in total 4480×4480 m^2 Output 1: instantaneous 3D fields in hour 30 to 34 for every minute. Output 2: horizontal mean values per 6 minutes during the entire transition.
LARGE:	Vertical dimensions: 184 levels with 15 m/gridbox up to 2760 m Horizontal dimensions: 512×512 gridboxes of 50×50 m^2 in total 25.6×25.6 km^2 Output: instantaneous 3D fields for hour 30 and 31 per minute.

The LES model uses the Lagrangian approach as explained in section 3.1. The side borders of the simulations have periodic boundary conditions. The air entering on the left hand side is given the properties (velocities, pressure, water content and temperature etc.) of the air leaving at the right hand side border and vice versa.

3.3 Mean state

3.3.1 Cloud fraction

In the transition from stratocumulus topped boundary layer into cumulus perturbed boundary layer we see two developments in the cloud fraction profiles. First the layer with stratocumulus cloud fractions below the temperature inversion becomes shallower and disappears. Second a deep layer with cumulus cloud fractions (+- 0 to 10%) develops:

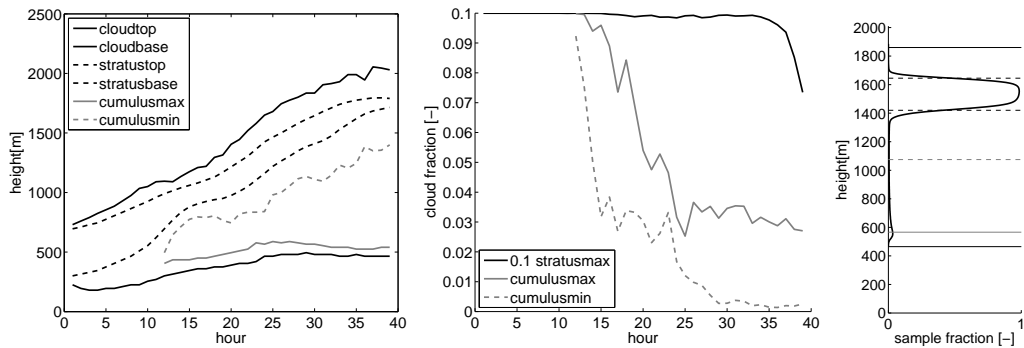


Figure 3.3: Time development of cloud heights (left) and cloud fractions (middle) using line styles as indicated in the cloud fraction profile (right). Black solid lines indicate the highest and lowest level with any saturated parcel ($q_i > 0$). The black dashed lines indicate stratocumulus cloud, which is chosen to be defined by ($\sigma_{cl} > 0.4$). The grey line indicates the height with maximum (solid) and smallest (dashed) cloud fraction below the stratocumulus cloud. (LES_{small})

The development is described in four periods. First period concerns the hours with significant shortwave solar radiation during the first day (hour 10-15). The second period

concerns the hours with reduced solar radiation and a relative shallow boundary layer (hour 15-25). The third period is the part of the night in which the boundary layer has grown deeper (hour 25-30) and latter period concerns sunrise (hour 30-36).

Hour 10 to 15: A minimum cloud fraction develops between the cloud base and the stratocumulus cloud, indicating cumulus clouds which often have a decreasing cloud fraction with height.

Hour 15-25: The depth of the layer with decreasing cloud fraction is getting shallower. A larger depth with increasing cloud fraction develops between the minimum cloud fraction and the stratocumulus cloud. The minimum cloud fraction is almost constant with a value of about 3 %.

Hour 25-30: In the last part of the night the minimum cloud fraction is strongly reduced. A fraction in the order of only 0.1% is only left. Hereby both layers (with $\frac{\partial \sigma}{\partial z} < 1$ and $\frac{\partial \sigma}{\partial z} > 1$) grow deeper. The minimum cloud fraction is found over 300 m below the stratocumulus cloud base and 500 m below the stratocumulus cloud top. These saturated updrafts should not be confused with the initiation of the stratocumulus cloud, since the sudden strong cloud-fraction increment is found at much higher level. A similar increasing cloud fraction is also found for the ATEX case study (+350 m below the inversion Stevens et al. (2001)).

Hour 30 to 35: After sunrise the stratocumulus cloud is being dissolved.

3.3.2 Updraft massflux heat and water transport

The cloudup sampled updraft is performing a major part of the heat and water transport within the parts with decreasing cloud fraction. The cloudup sampled massflux heat and water terms are slightly larger than the ones sampled by cloud sampling and significant larger than the terms for cloudcore sampling (see also figure 4.7):

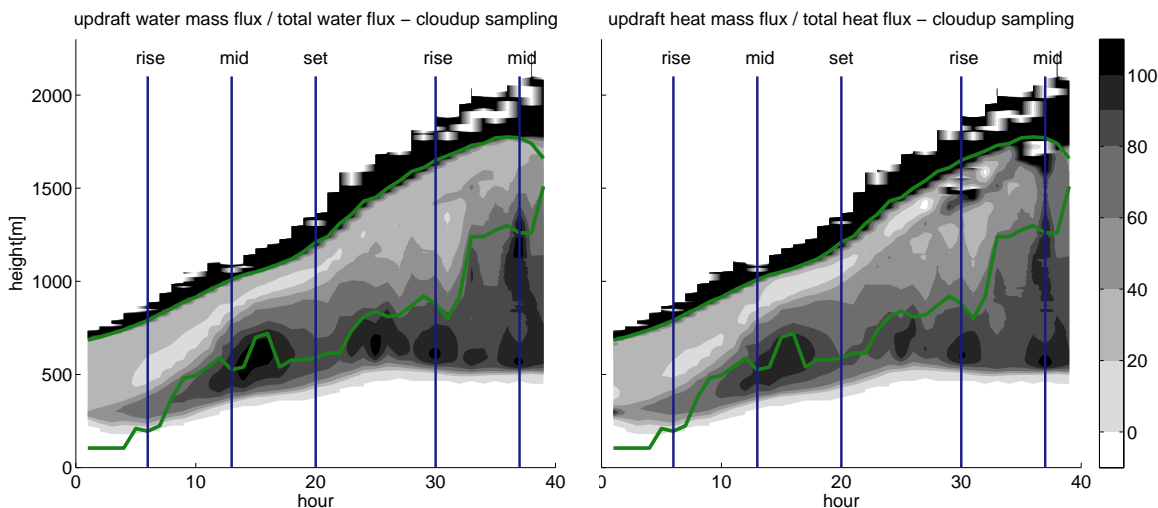


Figure 3.4: Cloudup sampled massflux water (left) and heat (right) transport contributions as percentile of the total fluxes during ASTEX. Vertical lines indicate moments of sunrise (rise), strongest solar radiation (mid) and sunset (set). Green lines indicate the part of the boundary layer with concave w^3 profile (figure 3.6), indicating downdraft-related dynamics. (LES_{small})

Hour 10 to 15: The cloudup sampled updraft is performing almost all heat and water

transport in a significant large part of the cloud layer. Similar massflux transport contributions are modelled with only mass-flux parameterization (Neggers et al. (2009a), Soares et al. (2008))

Hour 15-25: During the night other terms than the updraft massflux transport term become significant in the decomposed heat and water transport budget. Only 150 m with 80% massflux water transport contribution is left at the cloud base. Other terms are larger than the updraft massflux contribution, since significant parts of the cloud layer have massflux transport contributions smaller than 50%.

Hour 25-30: The layer with small massflux transport contributions remains quite deep, although an increasing layer with large massflux heat and water transport contributions is developed close to the cloud base. The development of this layer is similar in figure 3.3, in which a deeper layer with decreasing cloud fraction was found.

Hour 30 to 35: After sunrise, the non-updraft-massflux contributions of the decomposed turbulent heat and water transport disappear, since almost all transport is performed by the cloud up sampled updraft.

3.3.3 Turbulence dynamics

Moments with significant non-updraft-massflux contributions coincide with moments with large vertical velocity variance in the cloud layer:

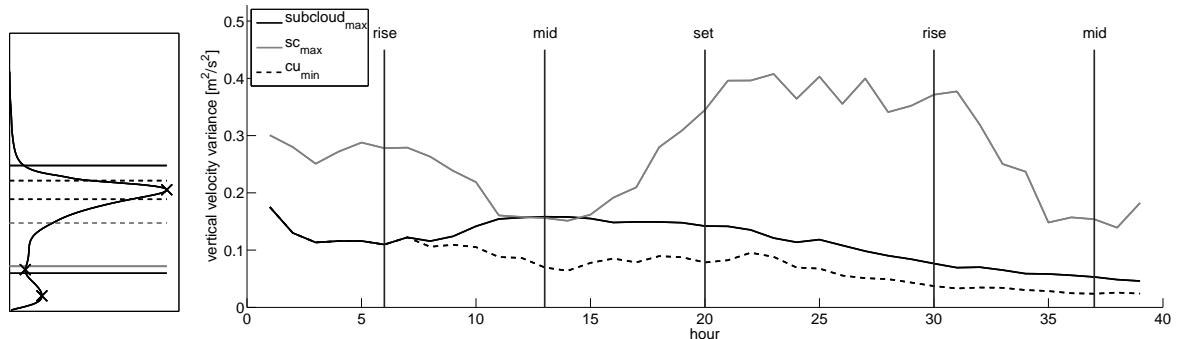


Figure 3.5: Vertical velocity variance maximum values in the sub-cloud layer and cloud layer. The minimum (dotted) between the maxima indicates the decoupling of cloud and sub-cloud layer dynamics. Until the 7th hour only one maximum is found, which is in the cloud layer. Layout similar to figure 3.3. (LES_{small})

Hour 10 to 15: The cloud top dynamics are decoupled from the sub-cloud layer dynamics as indicated by a strong minimum $\overline{w'^2}$ between the cloud top and the sub-cloud layer. $\overline{w'^2}$ is very small in the entire cloud layer, the maximum value in the cloud top is even smaller than the sub-cloud-layer maximum value.

Hour 15-25: During the night the cloud layer maximum $\overline{w'^2}$ reaches large values which are known for nocturnal stratocumulus topped boundary layers (Stevens et al. (2005)). The ASTEX maximum is found in the stratocumulus cloud, in contrast with maximum in the DYCOMS case, which has no decoupled sub-cloud and cloud layer dynamics. The decoupling in the ASTEX case is getting weaker, since the cloud-layer minimum $\overline{w'^2}$ approaches the sub-cloud layer maximum.

Hour 25-30: The cloud-top remains to have a $\overline{w'^2}$ in the order of $0.4 \text{ m}^2/\text{s}^2$. Both the sub-cloud layer maximum and the cloud layer minimum $\overline{w'^2}$ become smaller during these hours.

Hour 30 to 35: After sunrise, the cloud-top $\overline{w'^2}$ decreases strongly.

A disadvantage of $\overline{w'^2}$ is the disability to distinguish updrafts and downdrafts, since it is positive for both positive and negative vertical velocity fluctuations. Therefore the green line in figure 3.4 indicates the part of the cloud layer with significant downdraft turbulence with a concave vertical velocity skewness (w'^3) profile. Cumuli cause strong positive w'^3 profiles whereas cloud-top-downdraft related turbulence is characterized by negative (de Roode and Duynkerke (1997)) or concave profiles. Often $\overline{w'^3}$ is made dimensionless by dividing by $(\overline{w'^2})^{3/2}$. The turning points in the vertical velocity skewness profiles are indicated by crosses in figure 3.6.

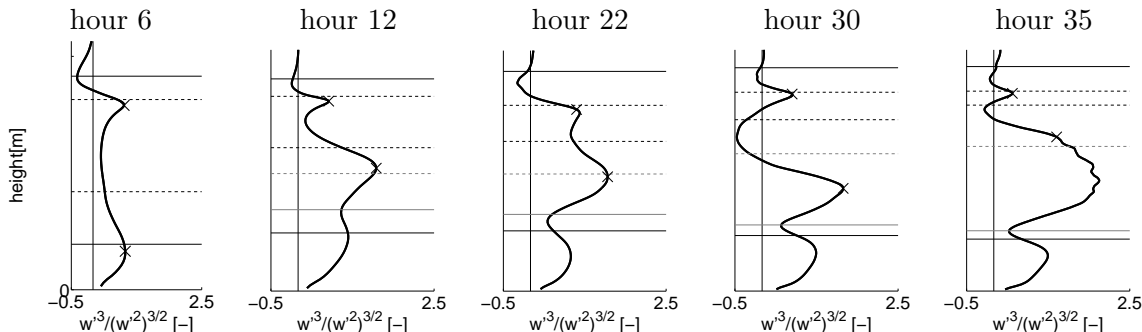


Figure 3.6: Vertical velocity skewness during ASTEX. The crosses indicate the turning points indicating the stratocumulus dominated layer as used in figure 3.4. They are defined as the extremes of the second derivative of the skewness profiles. The 30th hour shows a deep layer dominated by downdrafts, with even negative skewness values. Horizontal lines in the left side figures indicate heights according to figure 3.3. (LES_{small})

Similar range of skewness values is found in diagnosis of aircraft measurements on this case (de Roode and Duynkerke (1997)). A strong relation between the non-updraft-massflux heat and water flux and downdrafts is found as indicated by the vertical velocity skewness (figure 3.4). The non-updraft massflux contribution strongly coincides with heights with downdrafts, as indicated by the decreasing (hour 17,30) and increasing (hour 22,33) depth of the downdraft-turbulence dominated layer (figure 3.4).

3.3.4 Total turbulent heat and water transport

The magnitude of the total turbulent heat and water flux is according to figure 3.7 dependent on the boundary layer depth, the cloud-layer dynamics, decoupling and the diurnal cycle:

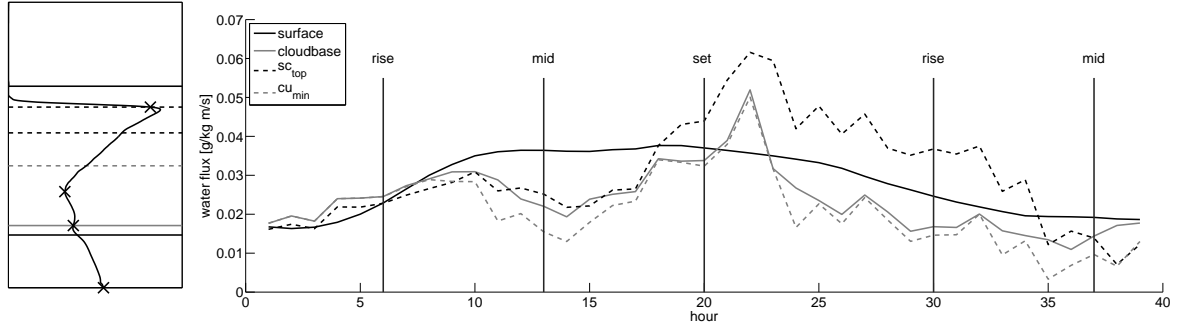


Figure 3.7: Development of surface, cumulus cloud-base, cloud layer minimum and stratocumulus cloud-top water flux using hourly averaged vertical profiles. After the 15th hour the water transport term at the cumulus cloud-base starts to deviate from the term at the inversion. Layout similar to figure 3.3. (LES_{small})

Hour 10 to 15: During the first day, almost all water and heat is directly from the cloud base into the stratocumulus cloud top, since the cloud-top, cloud-base and cloud-layer minimum water flux almost coincide.

Hour 15-25: The turbulent water flux into the cloud layer increases. As the decoupling is getting weaker the water flux out of the sub-cloud layer even exceeds the surface water flux (hour 21).

Hour 25-30: The water flux from sub-cloud layer into the cloud layer is only half of the water flux in the cloud top. A significant amount of dry air entrained and redistributed within the cloud layer.

Hour 30 to 35: All water fluxes in the cloud layer decrease strongly.

The cloud top processes are even more significant for the cloud layer heat fluxes. The heat flux in almost the entire cloud-layer is downwards due to a negative updraft massflux heat term and downward cloud-top entrained high θ_l parcels;

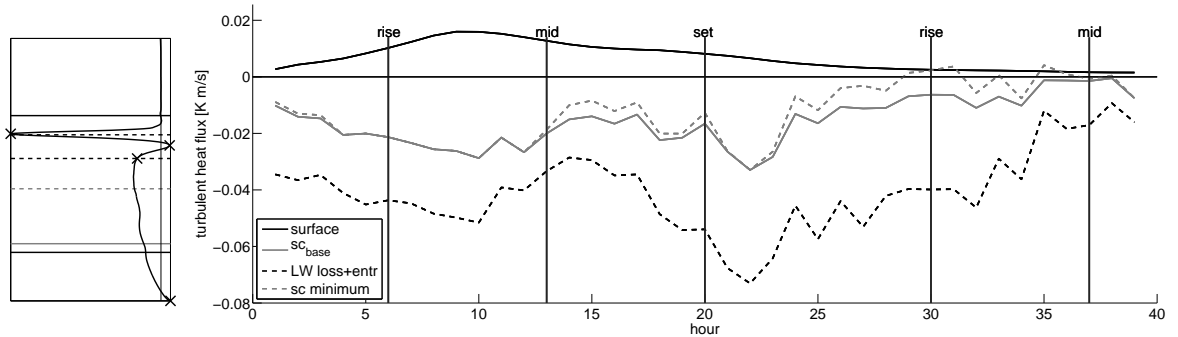


Figure 3.8: Development of surface, stratocumulus cloud-base, stratocumulus minimum and stratocumulus cloud-top heat flux using hourly averaged vertical profiles. The downward heat flux in the cloud top is relative small during the day, but increases heavily when cloud-top w'^2 increases after the 20th hour (sunset). Layout similar to figure 3.3. (LES_{small})

Hour 10 to 15: The heat fluxes in the cloud-top are relative small with respect to the nightly hours before.

Hour 15-25: The cloud top entrainment flux increases heavily. The same holds for the flux at stratocumulus cloud base, although the increment is much weaker. A significant part of the entrained air is used to raise θ_l within the stratocumulus cloud. A large

maximum is found in the 22nd hour, which coincides with the large water flux into the cloud-layer.

Hour 25-30: The surface heat flux and the heat flux at the stratocumulus cloud base have become very small with respect to the stratocumulus cloud-top heat flux. Heat from different sources, sinks, entrainment and downdraft processes is therefore redistributed within the stratocumulus cloud. Though this study focusses mainly on heat transport below the stratocumulus clouds.

Hour 30 to 35: When turbulence in the cloud top is suppressed ($\overline{w'^2}$ decrement, fig3.5), the cloud top heat flux shows similar decrease.

3.4 Horizontal plane plots

Apart from the cloudup massflux transport term, a significant downward heat and upward water flux is present. Figure 3.9 gives insight in the structure and the dynamics of the updraft and the other transport terms slightly below the stratocumulus cloud in the 30th hour of the transition. The updrafts are represented by small dots with strong upward vertical velocity, a large q_t , high θ_v and low θ_l . The environment of the updrafts is fully covered by turbulent structures, as indicated by the vertical velocity (lower right). In contrast with the vertical velocity, the variance for q_t , θ_l and θ_v is relative low within the environment.

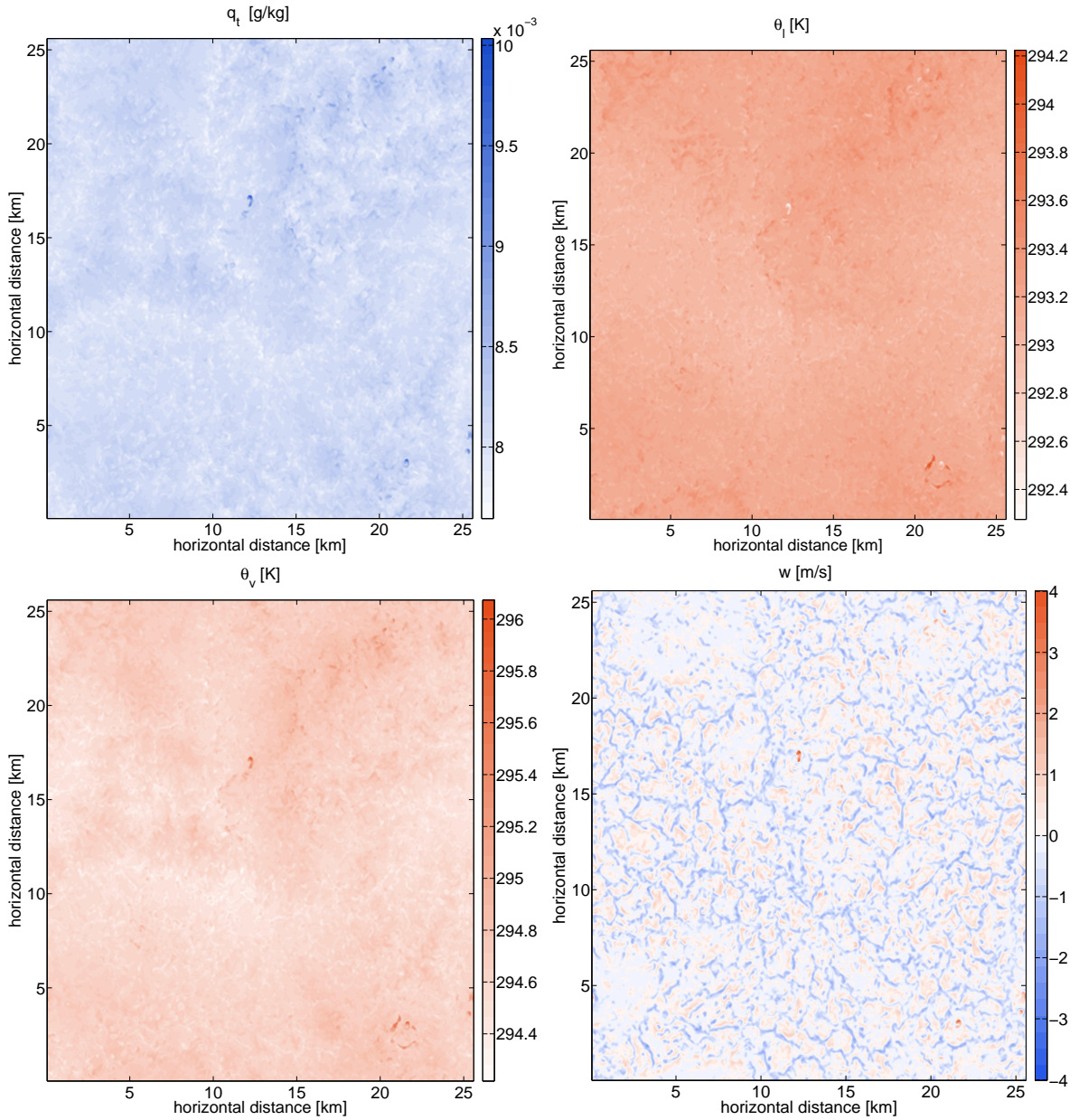


Figure 3.9: Instantaneous horizontal plane properties at the beginning of hour 30, showing q_t (upper left), θ_l (upper right), θ_v (lower left) and w (lower right) at an height of 1402.5 m, 200 m below the stratocumulus cloud base. Moist, buoyant updrafts rise in a turbulent mixed environment, as indicated by the low q_t -variance and the turbulent structures. (*LESlarge*)

Figure 3.10 gives the horizontal plane plots at the same timestep of the LES run, but at a height of 825 m (at a distance of 325 m from the cumulus cloud-base, 775 m from the stratocumulus cloud top and 575 m from the stratocumulus cloud base). The variance of q_t , θ_l and θ_v in the updraft environment is much larger than in figure 3.9. These variables even point at coexistence of two different environmental types. A part of the horizontal plane contain parcels with relative large q_t , low θ_l and high θ_v . These parcels are spatially separated from an area with opposite properties. The latter part is characterized by a small q_t -, θ_l - and θ_v -variance, whereas the variance for w is slightly larger than in the part with small q_t . Furthermore the mean q_t and θ_l in these regions

is remarkable close to the environmental mean value in figure 3.9 ($7.8 \text{ g/kg} < q_t < 8.3 \text{ g/kg}$ and $292.8 \text{ K} < \theta_l < 293.3 \text{ K}$).

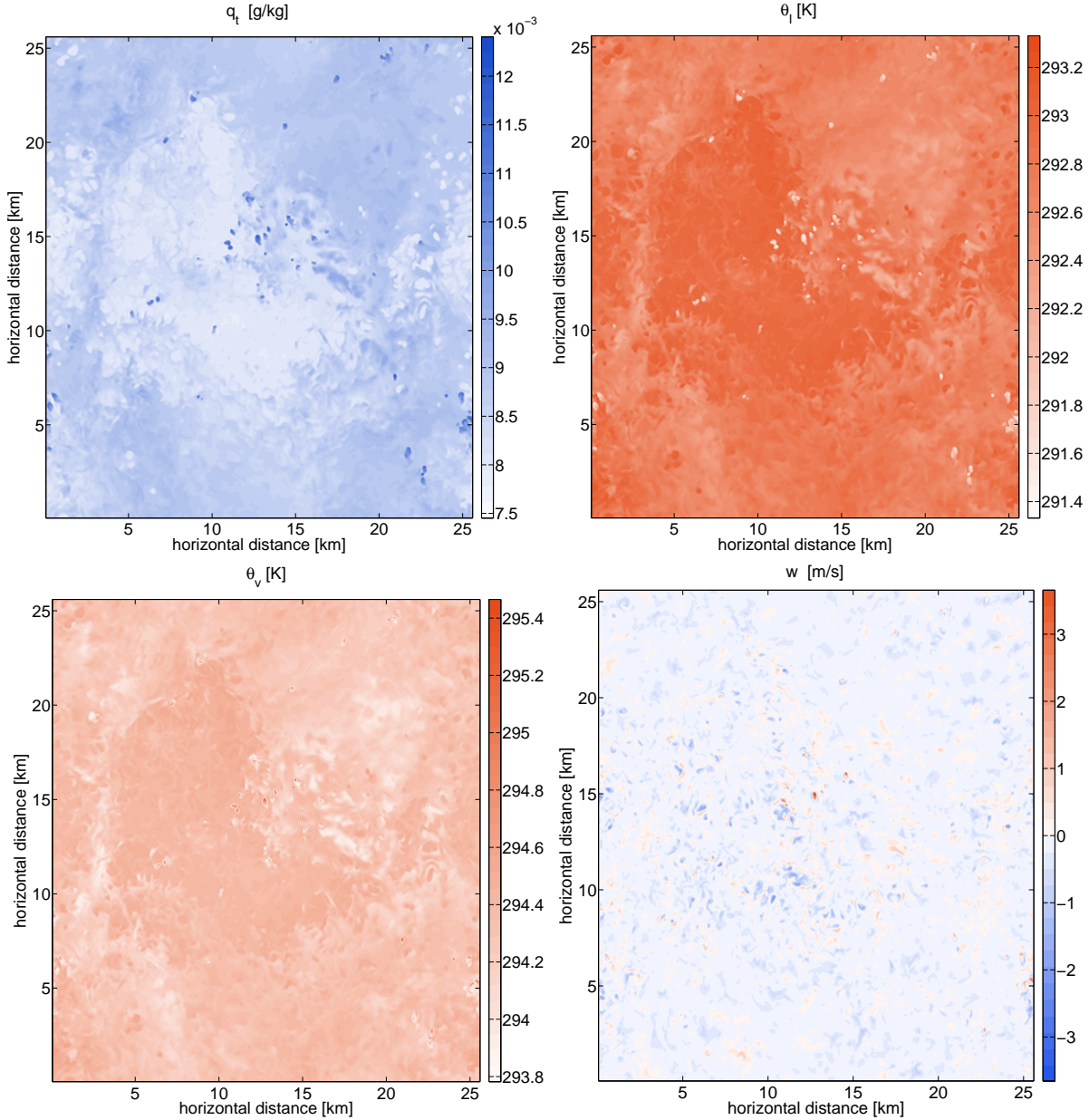


Figure 3.10: Instantaneous horizontal plane properties at the beginning of hour 30, showing q_t (upper left), θ_l (upper right), θ_v (lower left) and w (lower right) at an height at 825 m in the lower part of the cloud layer. The bimodal environment is also spatially visible. The area with cloud-top mean q_t is characterized by high θ_v value and large w fluctuations. (*LESlarge*)

3.5 Turbulence based stratification

The magnitude of the transport contributions of the turbulent updraft environment are not directly observable in the plots of q_t , θ_l and w (figure 3.9). Although these turbulent structures at the stratocumulus cloud base cover all environment and are known to bring

parcels with relative low q_t and high θ_l over 500 m downwards. In the contrary at heights without these parcels, the cloudup sampled updraft is the only source in the heat and water transport budget. The upper part of the cloud layer is therefore called 'downdraft dominated environment' and the lower part is called 'undisturbed cumulus environment'. A schematic representation gives an overview of an adapted stratification:

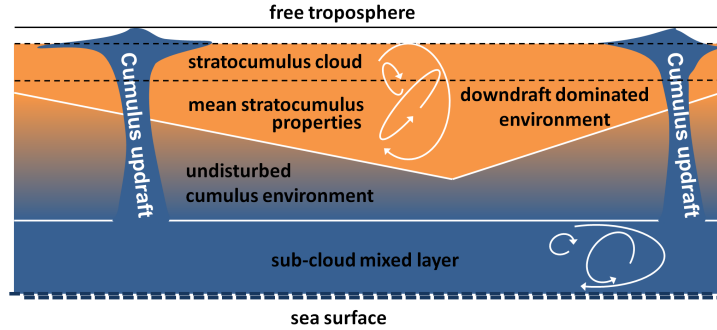


Figure 3.11: Stratification according to the cloud-dynamics in the 30th hour. Blue indicates a large q_t and low θ_l value, orange indicates a small q_t and high θ_l value. The sub-cloud layer and turbulent cloud-stop have almost constant content with height, compared to the undisturbed cumulus environment, which has a gradually decreasing q_t and increasing θ_l with height.

The exact depth of these layers in the 30th hour for the large domain LES simulation is given in table 3.2:

Table 3.2: stratification according to the joint PDF plots in the 30h hour of the transition

Stratification	large LES hour 30
Sub-cloud layer	0-500 m
Solely undisturbed cumulus environment	500 to 675 m
Bimodal environment	675 to 1275 m
Solely downdraft-dominated environment	1275 to 1600 m
Parcels with free atmospheric properties	1450 to 1600 m

Neggers et al. (2009a) also uses the term 'transition layer' for the lower part of the cloud layer with both moist and dry updrafts. wPDF and q_t PDF sampling and joint density plots are used to diagnose the transport contributions of the updraft and the two types of environments in the next chapter. The 30th hour is chosen to diagnose most elaborate, since both a deep layer with undisturbed cumulus environment and a layer with deep downdraft turbulence dominated environment are present.

Chapter 4

Detailed LES analysis of the 30th hour

The dual massflux parameterization scheme (Neggers et al. (2009a)) uses two updrafts in the sub-cloud layer and one in the cloud layer. Another difference between these layers is the applied sample criterion. The cloudcore criterion is used in the cloud layer, whereas the sub-cloud layer is diagnosed by wPDF criteria. The heat and water transport therefore are separately diagnosed for these layers.

Furthermore the environment of the updraft in the lower part of the ASTEX cloud layer is different to the environment in the upper part (chapter 3). The updraft properties and joint density plots are therefore also separately diagnosed for the lower and upper part of the cloud layer.

4.1 Decomposition of the sub-cloud layer

The 'dry updraft' in the dual massflux model is initiated at the sea-surface and is supposed to detrain in the top of the sub-cloud. The main purpose is 'non-local' heat redistribution within the sub-cloud layer. A moist updraft is modelled in order to initiate the cloud layer updraft, since the initial cloud-layer updraft is firmly rooted in the sub-cloud layer (Neggers et al. (2009a), or chapter 7).

Only limited wPDF sampling percentiles have appropriate massflux transport terms. The 40% wPDF sampled updraft produces larger water massflux transport contributions than the horizontal mean turbulent water flux, causing heights with counter gradient fluxes (figure 4.1). The same updraft has negative massflux heat transport at the sea surface and positive massflux heat transport in the top of the sub-cloud layer. This causes extra counter-gradient turbulent transport parameterization. By enhancing non-local transport these criteria fail to achieve their purpose.

wPDF sampled updrafts with smaller fraction than 4% do not detrain at the cloud top. The dry updraft wPDF criterion should therefore larger than 4% and by far smaller than 40%. The height with zero heat flux is found relative close to the sea surface, although the same applies to the height with maximum $\bar{\theta}_l$ (figure 4.4). wPDF sampled massflux with updraft fraction between 1 and 30% are not able to bring these heights closer.

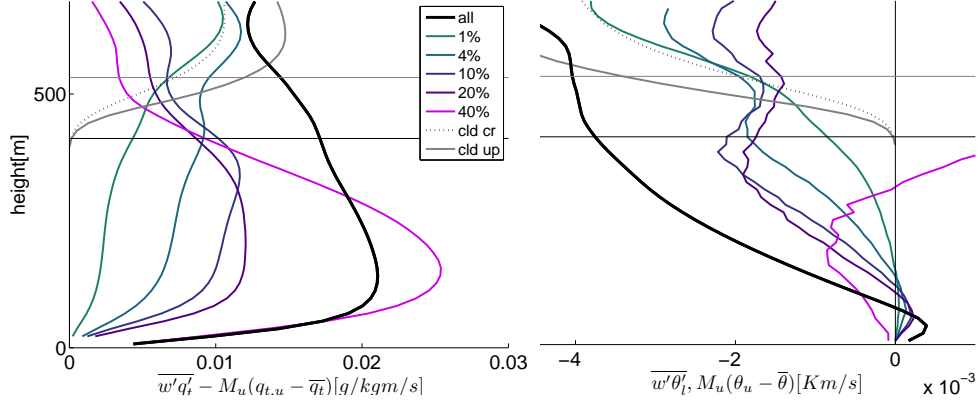


Figure 4.1: Conditional (dashed/grey), wPDF (colored) sampled massflux transport terms and total (black) water and heat transport in the 30th hour of the ASTEX case. The 10% wPDF sampled (dry) updraft detrains strongly at the cloud base. wPDF sampled updrafts, with smaller fraction than 2%, increase at that height and approach the cloudcore massflux transport contributions (moist updraft model). Horizontal lines in the figures indicate heights according to figure 3.3. (*LESlarge*)

The 4 to 20% wPDF sampled updrafts have significant massflux heat and water transport contributions. The 10% wPDF massflux water transport term (used for BOMEX by Neggers et al. (2009a)) contributes 40 to 65% and strongly decreases in the top of the sub-cloud layer. The relative heat massflux transport contributions show similarity with the relative water massflux contributions, although they deviate at the height with small horizontal mean heat fluxes (figure 4.2), because $\overline{w'\theta'_t}$ is in the numerator of the relative heat massflux contribution.

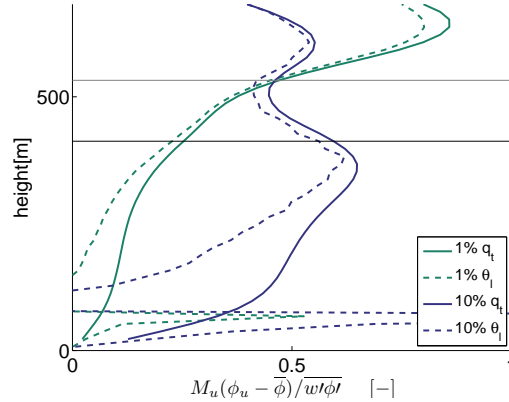


Figure 4.2: Relative massflux transport contribution by wPDF sampled updrafts for water (solid) and heat (dashed). The relative heat and water massflux contributions show similarity, although they are significant different at the height with small $\overline{w'\theta'_t}$. Horizontal lines in the figures indicate heights according to figure 3.3. (*LESlarge*)

The 1% wPDF massflux heat and water transport terms do not detrain in the transition layer, but slowly increase to a contribution of about 85% of the horizontal mean transport in the transition layer. Similar moist relative water massflux transport contributions are diagnosed for BOMEX (Neggers et al. (2009a)).

The environmental massflux contributions are about 0.11 and 0.01 times smaller than the contributions of the 10% wPDF and 1% wPDF sampled massflux transport terms

(equation 2.14). The remaining part of the transport budget is in the environmental and updraft subplume term (figure 4.3). 4% and smaller wPDF sampled subplume contributions are negligible small in the largest part of the sub-cloud layer. Larger wPDF sampled updrafts have more significant contributions.

The dual massflux model does not have separate updraft and environment subplume transport models and uses the lapse rate of the horizontal mean q_t and θ_l profiles. As a result the parameterized turbulent fluxes of the 20% wPDF sampled updraft are for 20% based on updraft values. Therefore it is for these updrafts quite reasonable to use the joint ED scheme, because the subplume transport contributions are in the same order to the sample fraction.

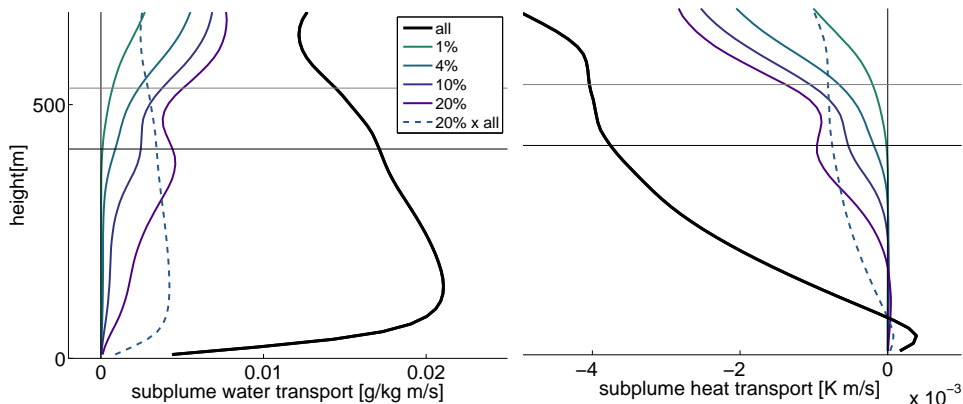


Figure 4.3: Conditional (dashed/grey) and wPDF (colored) sampled water and heat subplume transport terms in the 30th hour of the ASTEX case. The subplume contributions are negligible small for the smallest updrafts. The subplume term for the 20% wPDF is not negligible but in the order of 20% of the total fluxes. Horizontal lines in the figures indicate heights according to figure 3.3. (*LESlarge*)

4.1.1 Updraft properties

The wPDF sampled heat massflux contribution in the heat transport budget is upwards directed close to the sea surface, but changes sign within 200 meter. $\bar{\theta}_l$ is only close to the sea surface decreasing, by which the updrafts attain low θ_l with respect to horizontal mean in the upper part of the sub-cloud layer (figure 4.4). The wPDF sampled updrafts with smallest fraction have largest q_t and lowest θ_l , although the 0.1% wPDF sampled updraft has much lower q_t and higher θ_l than the 0.1% q_t PDF sampled updraft. In the transition region the 0.1% wPDF sampled updrafts reach larger q_t and lower θ_l . Though all wPDF criteria have far too high θ_l and small q_t in the relevant part of the transition layer. At the initiation the cloudup sampled updraft has about the same q_t and θ_l as the 0.1% q_t PDF sampled updraft.

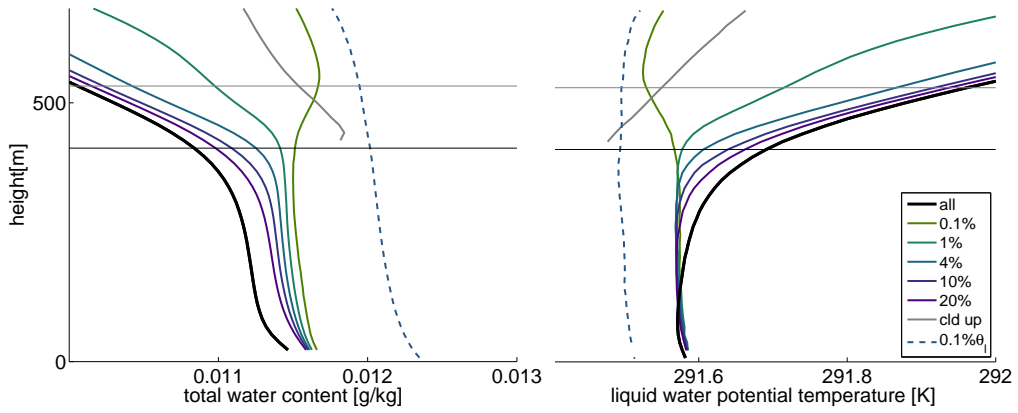


Figure 4.4: Conditional (dashed/grey) and wPDF(colored) sampled q_t and θ_l profiles in the 30th hour of the ASTEX case. Small wPDF criteria are moister than larger wPDF criteria, although the 0.1% wPDF sampled updraft is much dryer than the 0.1 q_t PDF and cloudup and cloudcore samples. The 0.1% wPDF sampled updraft has increasing q_t and decreasing θ_l with height in the transition region. Horizontal lines in the figures indicate heights according to figure 3.3. (*LESlarge*)

The cloud and cloudcore sampled w and θ_v values at cloud-base height are similar to the q_t and θ_l values remarkable close to the 0.1% q_t PDF sampled values at that height (figure 4.5):

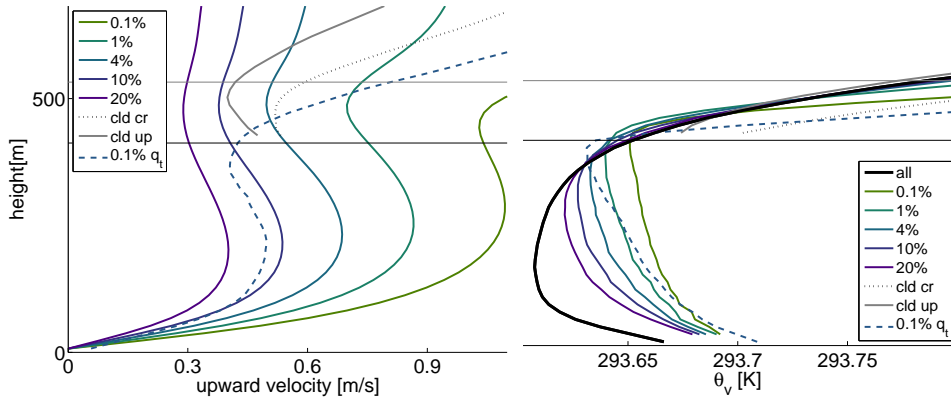


Figure 4.5: conditional (dashed/grey) and wPDF(colored) sampled w and θ_v profiles in the 30th hour of the ASTEX case. All PDF sampled updrafts accelerate in the lower part of the cloud-layer and decelerate in the upper part. The cloudup and cloudcore sampled updrafts are relative slow with respect to wPDF updrafts in the transition layer. The θ_v of updrafts with larger fraction than 0.1% have hardly an higher θ_v than horizontal mean. Horizontal lines in the figures indicate heights according to figure 3.3. (*LESlarge*)

The 4% wPDF sampled vertical velocity is much larger than the cloudup sampled updraft in the entire transition region. Though the cloudup sample fraction is only 2% and smaller. As a consequence, a significant part of the cloudup updraft found outside the fastest part of the vertical velocity PDF. Similar discontinuity is present for θ_v , for which the cloudup values in the transition layer are higher than the wPDF values at that height. The cloudup updraft apparently has at cloud-base height more in common with the moistest part of the q_t PDF, than with the fastest part of the wPDF.

Slightly below the lowest condensation level, the PDF sampled updrafts become negative

buoyant. The 0.1% q_t PDF sampled updrafts becomes significant positive buoyant within a few tens of meters rising. The cloudup and cloudcore updraft are positive buoyant at the lowest level either, although the cloudup sample quickly approaches the horizontal mean θ_v . The updraft even becomes slightly negative buoyant. Joint density plots are used to diagnose the different sampling criteria in the lower part of the cloud-layer in chapter in chapter 4.2.2. Before that, the joint density plots are used to diagnose the updrafts before saturation.

4.1.2 Joint density plots

The sub-cloud layer wPDF is quite symmetric, except for a small rising tail in the large q_t , slightly low θ_l part of the joint PDFs. wPDF criteria sample a fastest percentile of the wPDF. In the joint PDF's plots in this chapter, the sample criterion limit value is represented by a horizontal line (dashed), separating the updraft and its environment. According to figure 4.6 the asymmetric part of the joint w - q_t and w - θ_l PDF's is selected in the sub-cloud layer.

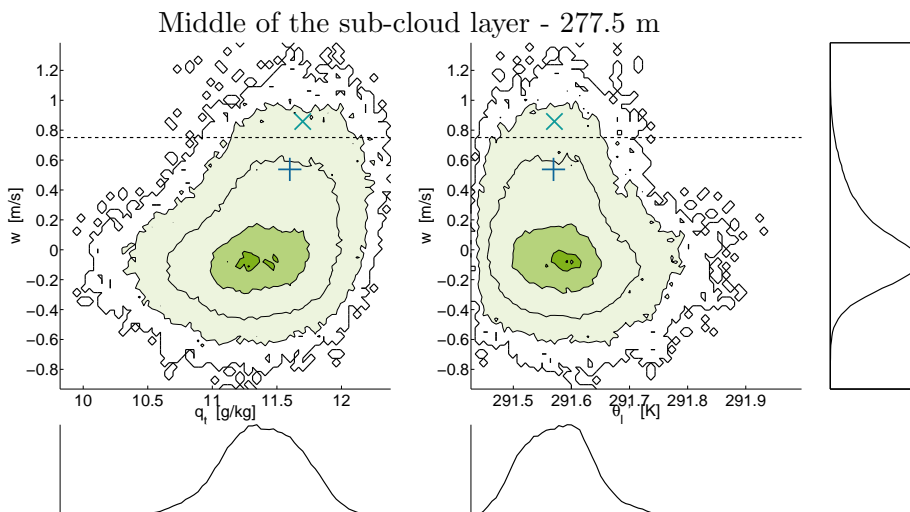


Figure 4.6: Joint probability density functions (PDF) of θ_l and w (left) and q_t and q_l (right). \times indicates the 1% wPDF mean updraft properties, the horizontal dashed line the 1% wPDF criterion limit value and the $+$ the 10% wPDF mean updraft properties. The joint PDFs have quite symmetric wPDFs, except for the upward moving, large q_t and low θ_l part of the functions. Contours indicate a larger PDF than {0%, 1%, 10%, 50%, 90%, 99% and 99.5%} of the PDF maximum value. The probability to have w and q_t or θ_l fluctuations on the third contour is 10 times more likely than having them on the second contour. (based on 12 even distributed instantaneous fields in the 30th hour - *LESlarge*)

Besides symmetry with respect to the horizontal mean vertical velocity (0 m/s), symmetry with respect to horizontal mean q_t or θ_l is needed for a massflux transport contribution. Since the centre of mass of the sampled parts in the joint w - q_t PDFs are moist with respect to the horizontal mean q_t , the updraft has significant contribution in the water transport budget. On the other hand, the 1 and 10% wPDF sampled $\theta_{l,u}$ have almost the same value as the centre of the θ_l PDF. The updrafts therefore only have a small contribution in the heat transport budget.

The maximum value in the wPDF is found to at a small negative vertical velocity. Using the model of a fast rising updraft and a slowly descending environment, the wPDF peak

vertical velocity could be used to determine a appropriate updraft fraction at this height. The environment of the 14% wPDF sampled updraft has similar vertical velocity to the descending peak velocity in the wPDF. This percentile is in the same order of 10% wPDF sampled updraft in the dual massflux model. However, this approach is not directly applicable in the dual massflux, because multiple updrafts have an another mass flux balance with the environment.

4.2 Decomposition of the cloud layer

In chapter 3.3, the differences between the lower and upper part of the ASTEX cloud layer are described. Cloud fraction and atmospheric environmental dynamics of the lower part of the ASTEX cloud layer are similar to i.a. the BOMEX and ATEX case. The same applies for the cloudup sampled relative mass-flux transport contributions in the heat and water transport budget, which is close to unity (figure 3.4). The wPDF sampled updrafts also have significant massflux transport contributions in this part of the cloud layer. Though all wPDF sampled updrafts have smaller heat and water transport contributions than the conditional sampled updrafts. The criteria are not able to improve the low relative massflux transport contributions in the heat and water transport budget of the upper part of the cloud layer. The massflux heat and water transport term is slightly larger for the cloudup criterion, than for the cloud or cloudcore criterion. The differences between these criteria are larger in the lower part of the cloud layer and smaller in the upper part of the cloud layer.

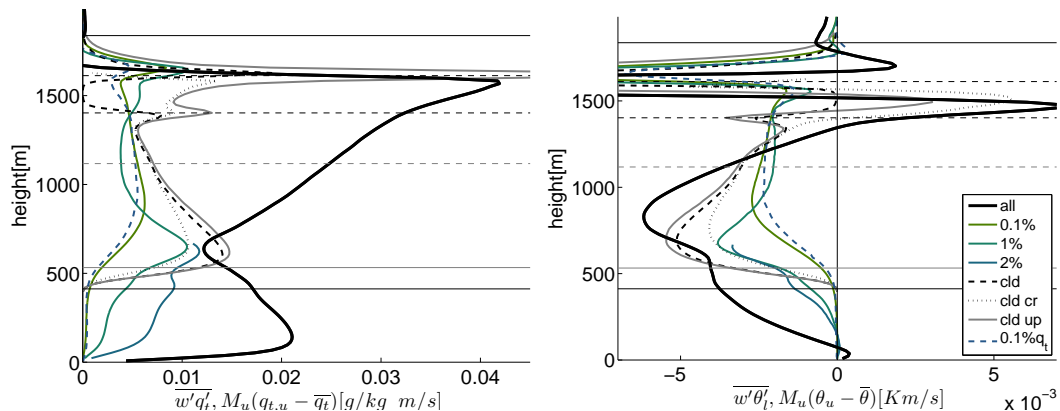


Figure 4.7: conditional (dashed), ϕPDF (solid) and wPDF (colored) sampled heat and water massflux transport terms in the 30th hour of the ASTEX case. The the cloudup massflux term is able to take care for all transport in the lower part of the boundary layer; wPDF sampled updrafts are smaller. Horizontal lines in the left side figures indicate heights according to figure 3.3. (*LESlarge*)

The wPDF sampled updraft with similar fraction to the cloud-fraction at a certain height, has the largest heat and water transport contribution of all wPDF sampled updrafts. The cloud layer updraft apparently benefits from the use of a height-dependant updraft fraction which is in the order of the cloud fraction. In the largest part of the boundary layer, the 0.1% q_t PDF sampled massflux heat and water transport contributions are smaller than the contributions of the 0.1% wPDF sampled updraft. Although not at the most significant height with small cloud-fractions. At this height, the q_t PDF sampled massflux water and heat transport contribution is slightly larger. Still the 0.1%

q_t PDF sampled transport contribution is significantly smaller than the cloudup sampled updraft, since updraft fraction is smaller than the smallest mean cloud up sampled fraction (0.3%).

The environmental massflux transport contributions in the heat and water transport budget are about 2% or smaller than the updraft massflux contributions (equation 2.14). The residual fluxes are performed by subplume transport in the environment and updraft (figure 4.8)

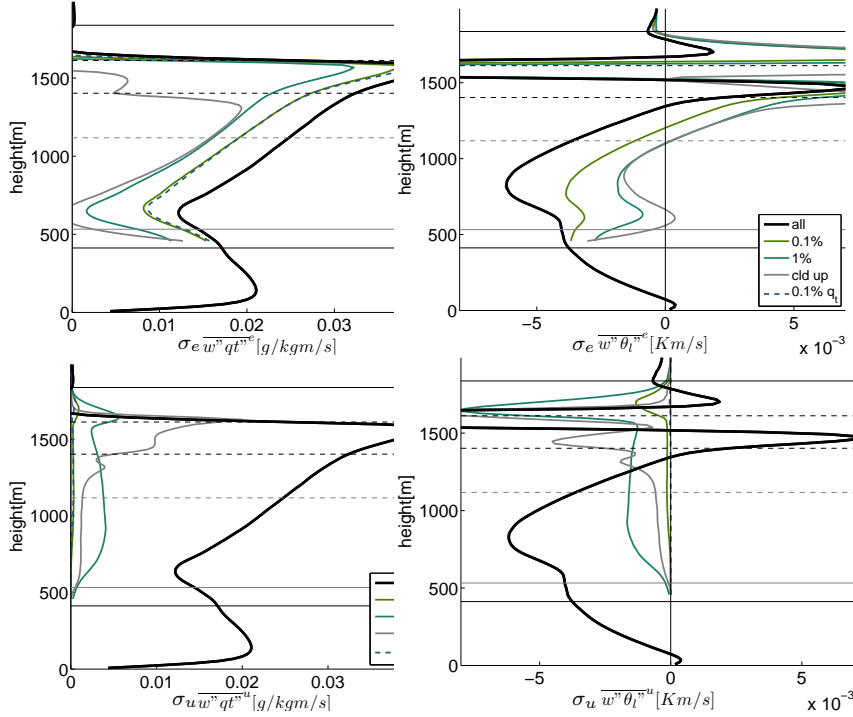


Figure 4.8: Conditional (dashed), ϕ PDF (solid) and wPDF (colored) subplume water(upper) and heat (lower) transport term in the updraft (left) and the environment (right) in the 30th hour of the ASTEX case. Environmental subplume transport is the largest of all transport terms slightly below the stratocumulus cloud. Updraft subplume terms also have significant contributions. Horizontal lines in the left side figures indicate subplume heights according to figure 3.3. (*LESlarge*)

The environmental subplume term is dominant in a large part of the cloud layer for almost all used sample criteria. Although the updraft subplume terms are relative large with respect to the their fraction. The cloudup subplume water flux is performing over 10% of the total water transport contribution, even though the cloudup fraction is smaller than 1%. The subplume heat flux increases up to -0.002 K m/s within the same 1% of the horizontal plane. Another remarkable difference with the sub-cloud layer subplume terms, is the sign of $\overline{w''\theta_l''^u}$. In the water transport budget, both the updraft and environmental term have an upward contribution. The updraft subplume contribution in the heat transport budget is downward directed, similar to the direction of the updraft massflux term, but in opposite direction to the environmental subplume term.

4.2.1 Updraft properties - lower part cloud layer

The cloud fraction based sample criteria satisfactorily select the heat and water transporting updraft in the lower part of the cloud layer (figure 3.4). The cloudup and cloud sampled updrafts have almost same $q_{t,u}$, $\theta_{l,u}$ and $\theta_{v,u}$. The cloudcore updraft has slightly larger $q_{t,u}$, lower $\theta_{l,u}$ and higher $\theta_{v,u}$ than the other criteria.

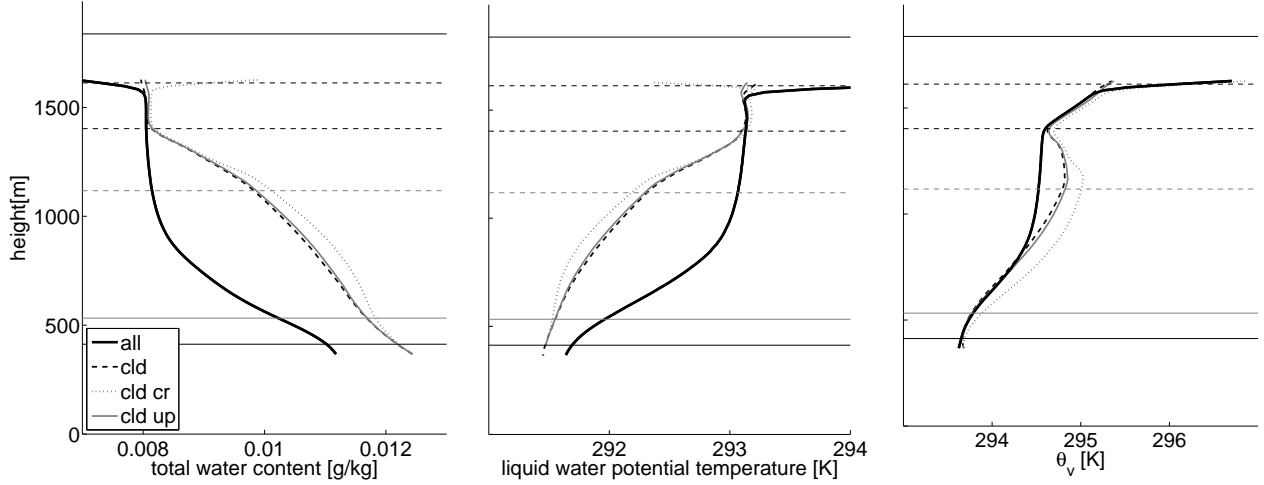


Figure 4.9: Conditional sampled scalar updraft properties in the 30th hour of the ASTEX case. Cloud and cloudup sampled content hardly deviate. The cloud and cloudup updraft are slightly negative buoyant with respect to the mean values. Horizontal lines in the left side figures indicate heights according to figure 3.3. (*LESlarge*)

The difference between updraft and environment mean θ_l and q_t increases strongly with height (figure 4.10) in the lower part of the cloud layer. On contrary, the updraft θ_v is hardly larger than the horizontal mean. The cloudup and cloud sample appear even slightly negative buoyant. The decreasing difference between updraft and horizontal mean q_t and θ_l is clearly related with updraft-fraction decrement; the 0.1, 0.5 and 1% wPDF sampled $q_{t,u}$ and $\theta_{l,u}$ profiles have a more constant offset. The smallest updrafts have more distinct mean θ_l and q_t values. The 0.1% q_t PDF sampled θ_l and q_t are significant lower and higher than the profiles of the 0.1% wPDF criterion. This difference is relevant, since the mean cloudup $q_{t,u}$ and $\theta_{l,u}$ are at the lowest level closer to the 0.1% q_t PDF than to the 0.1% wPDF updraft. The wPDF and q_t PDF criteria apparently select a different part of the transition layer and the cloudup sample has more in common with the 0.1% q_t PDF than with the 0.1% wPDF.

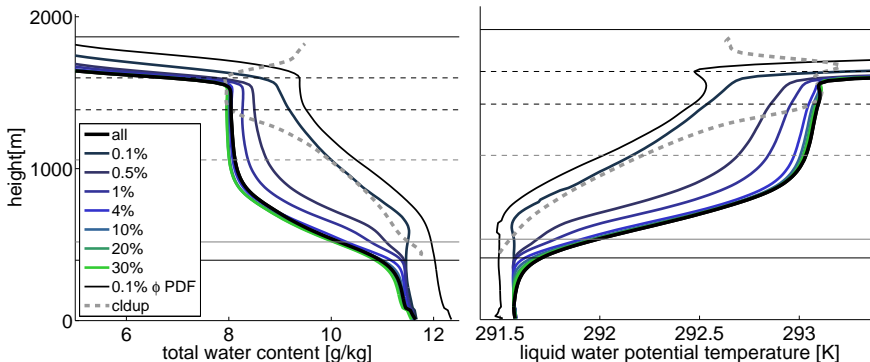


Figure 4.10: conditional (dashed), ϕPDF (solid) and wPDF (colored) sampled q_t and θ_l values at hour 30 in the ASTEX case. The 0.1 to 1% wPDF sampled updrafts have distinct content in the cloud layer. Horizontal lines in the left side figures indicate heights according to figure 3.3. (*LESlarge*)

Another remarkable result in figure 4.10 are the 4 to 30% wPDF sample $\theta_{l,u}$ and $q_{t,u}$ profiles. $\theta_{l,u}$ is between a height of 650 and 850 m almost equal to the horizontal mean θ_l and $q_{t,u}$ is even slightly dryer than the horizontal mean q_t . These criteria apparently are dominated by fast rising small q_t parcels. The next section uses joint w - q_t and w - θ_l PDFs, to diagnose the ability of smaller wPDF criteria to select the saturated updraft.

4.2.2 Joint density plots - lower part cloud layer

Figure 4.11 shows the probability density function (PDF) of the w , q_t and θ_l fluctuations in the transition layer. Both updraft, stable cumulus environment and downdraft turbulence dominated environment (chapter 3.5, $7.8 \text{ g/kg} < q_t < 8.3 \text{ g/kg}$ and $292.8 \text{ K} < \theta_l < 293.3 \text{ K}$) are represented in this figure. The wPDF seems more symmetric than the sub-cloud layer wPDF (figure 4.6), although a much smaller updraft is present in the large q_t and low θ_l part of the q_t and θ_l PDFs. $q_{t,u}$ and $\theta_{l,u}$ are indicated for the cloudup sampled updraft with a '+' and for the 1% wPDF sampled updraft with a 'x'. These updrafts have almost the same updraft fraction, although they have significant different mean $q_{t,u}$ and $\theta_{l,u}$ values.

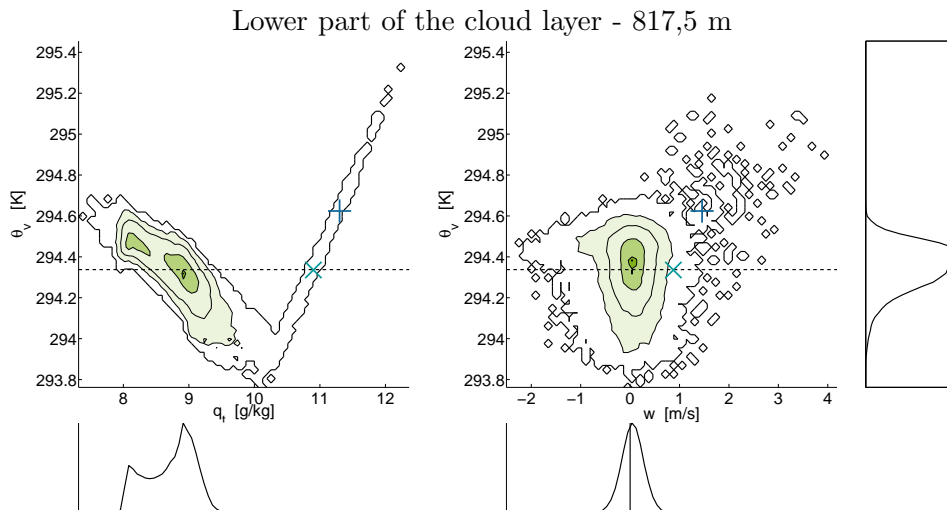


Figure 4.12: Joint PDFs of q_t and θ_v (left) and w and θ_v (right). \times indicates the cloud mean updraft properties, the horizontal dashed line the horizontal mean θ_v value and the + the cloud-core updraft mean properties $\sigma_{cld} = 0.54\%$, $\sigma_{cldcr} = 0.24\%$. The moistest part of the environment is dense with respect to the dryer part of the environment and the updraft. (based on 12 even distributed instantaneous fields in the 30th hour, line-style similar to figure 4.6 - *LESlarge*)

A wide range of θ_v values are found within the non-environmental part of the joint θ_v - q_t PDF. Both the joint PDF and the q_t PDF have bimodal behaviour (more in chapter 3.5 and 4.2.4). The driest q_t PDF peak-value coincides with the peak with downdraft-mean properties in figure 4.11. The part of the joint density function below the horizontal mean θ_v and smaller q_t than 10.3 g/kg belongs to the unsaturated undisturbed cumulus environment, which is spatially separated from the downdraft turbulence dominated part of the environment. Since θ_v in this part is lower than mean (horizontal dashed line figure 4.12), it explains the acceleration of the cloudup sample in despite of its low buoyancy with respect to $\overline{\theta_v}$.

The fraction undisturbed cumulus environment decreases with height and is disappeared at a height of about 1250 m (figure 8.5). The absence of the negative buoyant environment and shell will strongly affect the updraft-environment interaction. The updraft properties in the upper and lower part of the cloud layer as a consequence are evidently different.

4.2.3 Updraft properties - upper part cloud layer

At the height of about 1150 m, the mean vertical velocity profiles of the cloudup and cloudcore updrafts suddenly deflect and heavily decrease height. Figure 4.13 shows the same for the modified pressure:

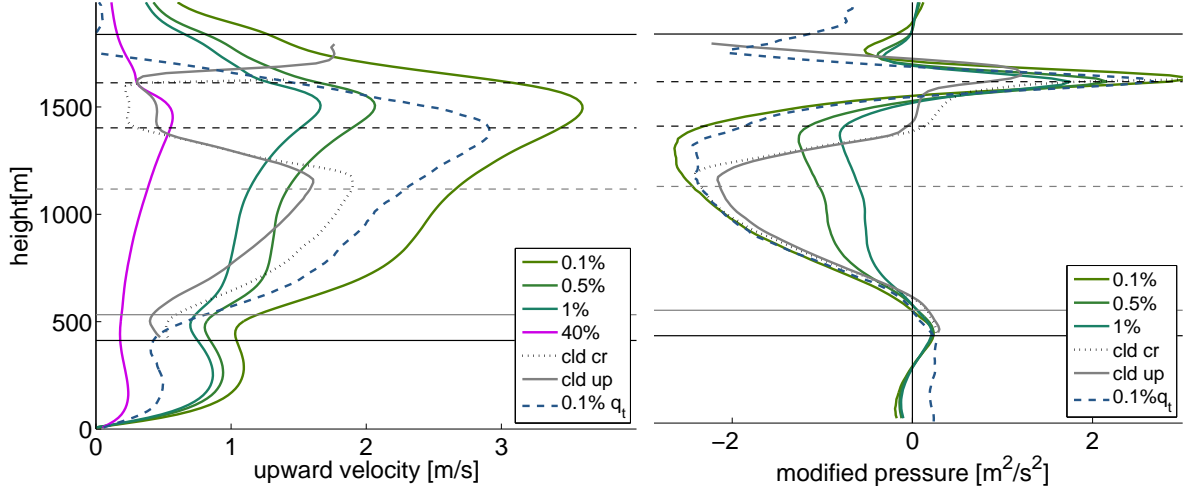


Figure 4.13: Vertical velocity (left) and modified pressure at hour 30. The cloud up sampled updraft velocity and modified pressure decrease strongly at a height of 1100 m, whereas all PDF criteria have distinct properties up to the stratocumulus cloud. Horizontal lines in the left side figures indicate heights according to figure 3.3. (*LESlarge*)

The increasing modified pressure is not the main reason for the deceleration. The sudden deflection of the cloudup and cloudcore updraft profiles namely also occurs in the θ_l , q_t and θ_v profiles (figure 4.9 and 4.10). Furthermore the wPDF sampled profiles of these variables do not approach the horizontal mean values and these updrafts have even increasing w and p_{mod} with height. The maximum vertical velocity of all wPDF sampled updrafts with percentiles up to at least 40% is found within the stratocumulus cloud (figure 4.13). The increasing updraft fraction of the saturated updrafts therefore has a significant role in the decreasing w_u .

The cloudup fraction increment has similar effect on $p_{mod,u}$, $\theta_{l,u}$, $q_{t,u}$ and $\theta_{v,u}$, since all of these updrafts approach horizontal mean value. The subplume heat and water transport contributions and subplume vertical velocity variance heavily increase (figure 4.8 and 5.12) at these heights. These effects raise the question whether liquid-water-content-condition based sample criterion is able to select the updraft in this part of the boundary layer, or possibly an another criterion should fit better. The updraft and environment are visualized in joint w - q_t and w - θ_l PDFs in the next chapter in order to diagnose the cloudup and wPDF criteria and the subplume transport terms.

4.2.4 Joint density plots - upper part cloud layer

In similarity with the lower part of the cloud layer, three distinct parts are observable in the joint w - q_t PDF (figure 4.14). Again the downdraft turbulence dominated environment is present between a q_t of 7.8 and 8.3 g/kg. The weight of this environmental type has increased in the PDF. This part of the boundary layer is clearly driven by downdrafts, since downward velocities are significant larger than upward. The turbulent transport in this part of the boundary layer is indicated by the covariance of the w and q_t or θ_l fluctuations. The joint PDF's are not symmetric for q_t , θ_l and w but are slightly slanted towards the diagonal with positive w' and q_t' and the diagonal with positive w' and negative q_t' . This indicates a positive subplume water transport term and a negative subplume heat transport term in the environment.

The weight of undisturbed cumulus environment decreases and is almost disappeared.

The region between updraft and downdraft-dominated environment is fully disappeared at the height of 1270 m (8.4). Although at a height of 1117 m the rising updraft is still found in the large q_t and low θ_l part of the joint w - q_t and w - θ_l PDFs (4.15).

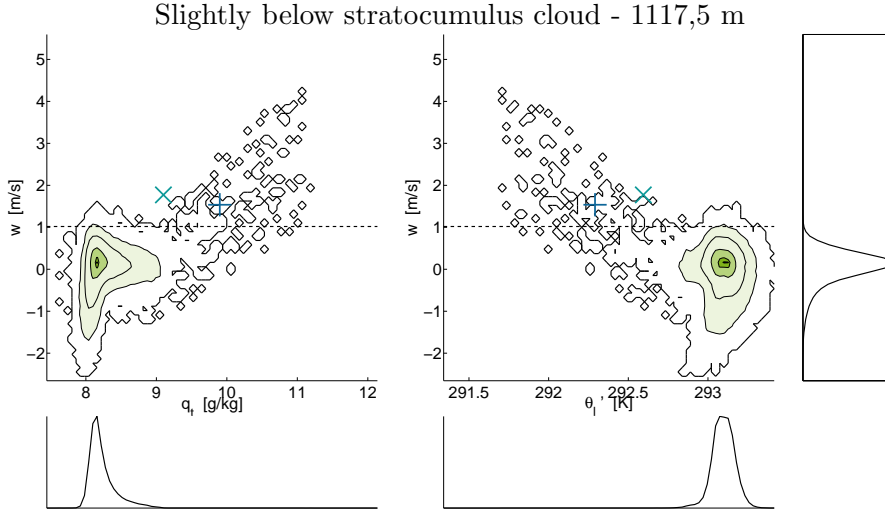


Figure 4.14: Joint PDFs of θ_l and w (left) and q_t and q_l (right). indicates the 0.2% wPDF sampled mean updraft properties, the horizontal dashed line the 0.2% wPDF criterium limit value and the + the cloudup mean properties ($\sigma_{cloudup} = 0.25\%$). The bimodal PDF within the environment has almost disappeared. (based on 12 even distributed instantaneous fields in the 30th hour, line-style similar to figure 4.6 - *LESlarge*)

The cloudup sampled w_u , $q_{t,u}$ and $\theta_{l,u}$ are found in the middle of this updraft. $w_{u,cloudup}$ is only slightly slower than the velocity sampled by the 0.2% wPDF criterion, whereas the cloudup fraction is even slightly larger (0.25%). Though the cloudup sampled mean $q_{t,u}$ is much larger and $\theta_{l,u}$ is much lower. In similarity with the lower part of the cloud layer, significant parts of the downdraft turbulence dominated environment are selected by the 0.2% wPDF criterion.

In contrast with the cloud and cloudup fraction, the updraft in the joint w - q_t and w - θ_l PDFs has a quite a constant fraction in height. A similar part of the joint w - q_t and w - θ_l PDF is selected in figure 4.6. A fast rising 'core' with distinct properties and a more or less constant fraction is present after the height with minimum cloud fraction. No bimodal environment is present at this height, so this updraft is directly located on the top of the part of the joint PDFs that represent the downdraft turbulence dominated environment 4.15.

Middle of the stratocumulus cloud - 1507,5 m

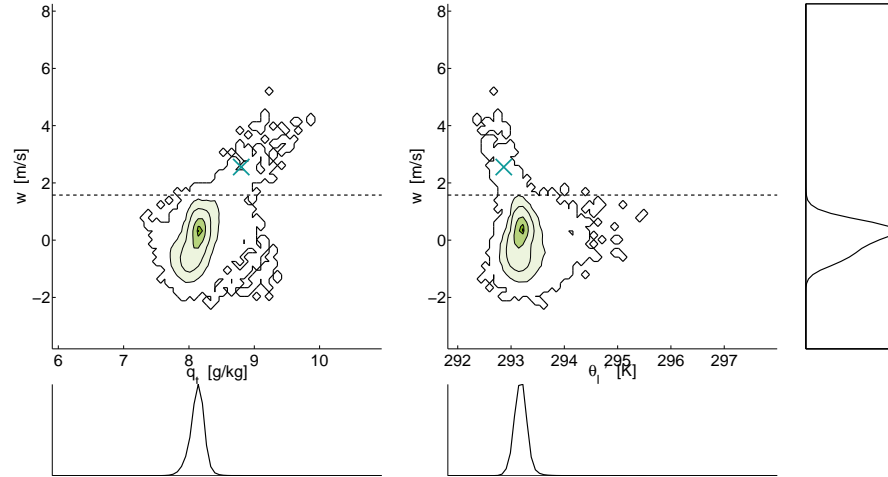


Figure 4.15: Joint PDFs of θ_l and w (left) and q_t and q_l (right). The low θ_l and moist updraft continuously accelerates up into the stratocumulus cloud. The slanted PDFs show turbulent transport within the environment. (based on 12 even distributed instantaneous fields in the 30th hour, line-style similar to figure 4.6 - *LESlarge*)

4.2.5 Overview updraft properties

The cloudup updraft has quite different properties in the part of the boundary layer with downdraft dominated turbulence and undisturbed cumulus environment.

Variable	Undisturbed environment	Downdraft dominated environment.
(σ_{cldup})	decreasing	increasing
$(\theta_{v,cldup} - \overline{\theta_v})$	very small due to bimodal environment	large
$(q_{t,cldup} - \overline{q_t})$	increasing	decreasing
(w_{cldup})	increasing	decreasing
$\sigma_u \overline{w'' q_t''}$	< 10% of $\overline{w' q_t'}$	> 10% of $\overline{w' q_t'}$
$\sigma_u \overline{w'' \theta_l''}$	< 10% of $\overline{w' \theta_l'}$	opposed sign to $\overline{w'' \theta_l''}$

Chapter 5

Parameterization

This chapter uses LES output (chapter 3.2) to diagnose parameters of the dual mass-flux heat and water transport parameterization scheme. The first section (5.1) concerns the eddy diffusivity parameterization of the residual turbulent heat and water transport term according to equation 2.24. The second section (5.2) concerns the massflux transport parameterization. The dry updraft in the sub-cloud layer will be diagnosed by the 10% wPDF criterion (similar to Neggers et al. (2009a) and f.e. Siebesma et al. (2007)), the moist updraft by the 1% wPDF criterion and the cloud layer updraft by the cloudup and cloudcore criterion. The cloud-layer is diagnosed for two criteria, because the cloudup criterion has largest massflux heat and water transport contribution (chapter 3.3), whereas the cloudcore parameters are used by Neggers et al. (2009a). The vertical velocity budget is also diagnosed for both criteria using LES results of the BOMEX and RICO case (de Roode et al. (2012)).

5.1 Eddy diffusivity parameterization during ASTEX

The eddy diffusivity vertical profiles are diagnosed from sampled heat and water massflux and total transport terms and the horizontal mean q_t and θ_l profiles (adapted from equation 2.24):

$$K_\phi(z) = - \frac{\overline{w'\phi'} - \sum_i M_{u,i} (\phi_{u,i} - \bar{\phi})}{\frac{\partial \bar{\phi}}{\partial z}} \quad (5.1)$$

The residual environmental fluxes as mentioned in equation 5.1 are diagnosed for one updraft in the cloud layer and for a combined moist and wet updraft scheme in the sub-cloud layer.

5.1.1 Sub-cloud layer

The sub-cloud layer is heated from below by sea-surface with increasing temperature and from the top by downward turbulent transport of high θ_l free-atmospheric parcels. The sea surface is the only source of water and the water is partially transported into the cloud layer. Therefore both q_t and $\overline{w'q'_t}$ both decrease with height. The $\overline{w'\phi'}$ and $\bar{\phi}$ profiles for heat and water have quite different characteristics. Therefore the diagnosis

of the parameterization is performed separately for heat and water, even though heat and water transport models often shows strong similarity.

Water transport

The $\overline{q_t}$ lapse rate is small in the middle of the boundary layer and larger at the cloud base and at the sea surface (figure 4.4). The difference between massflux and the total water transport term is also smaller at the sea surface and at the cloud base compared to the residual term halfway the sub-cloud layer (figure 4.1). As a consequence we have a maximum $K_{q,t}$ in the sub-cloud layer:

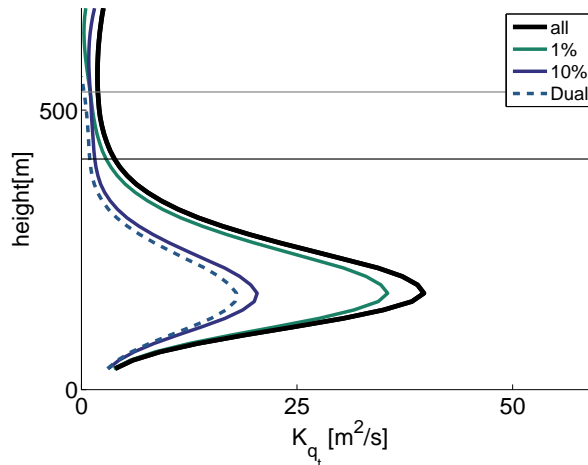


Figure 5.1: Eddy diffusivity profiles based on the total turbulent water transport (black) and the residual fluxes after subtraction of the massflux transport by dry (10%wPDF), moist (1%wPDF) and both massfluxes (dual, dotted). Sub-cloud layer eddy diffusivity profiles have similar shape to the profiles as known from the BOMEX and ATEX cases. Horizontal lines in the left side figures indicate heights according to figure 3.3. (*LESlarge*)

The eddy diffusivity profiles of the different ED, EDMF and dual MF schemes are almost evenly shaped below the cloud base. The maximum value is found slightly below the middle of the sub-cloud layer; which is similar to f.e. the BOMEX $K_{q,t}$ profile (Siebesma et al. (2003)).

In the sub-cloud layer the profile of the 10% wPDF-EDMF scheme is about half as large as the profile in the ED scheme. The 1% wPDF sampled updraft causes a smaller reduction of the required EDMF profile, but causes a large reduction in the transition layer. Using the dual massflux scheme, with moist (1% wPDF) and dry (10% wPDF) updraft massflux terms, the $K_{q,t}$ profile approaches $0 \text{ m}^2/\text{s}^2$ at the height with largest cumulus-fraction. Compared to the BOMEX sub-cloud layers, the ASTEX sub-cloud layer surface flux is small, but the cloud base entrainment is fluxes large. Though the resulting eddy diffusivity profile for q_t transport is still similar-shaped but about half as large.

Heat transport

Eddy diffusivity profiles for heat transport are more complicated than profiles for water transport. A minimum θ_l value is found, since the sub-cloud layer has two heat sources (increasing sea-surface temperature and top-entrainment of high θ_l air). This causes an

asymptote in the eddy diffusivity profile since the θ_l lapse rate is in the denominator of equation 5.1, unless when the numerator is zero too. The height with zero θ_l lapse rate is found quite near the sea surface. The total heat flux appears to be zero at the same height. The massflux heat transport terms are positive in this part of the sub-cloud layer. The height with zero heat flux as a consequence, is found at a slightly higher level when the EDMF scheme is used. The resulting θ_l eddy diffusivity profiles are given in figure 5.2

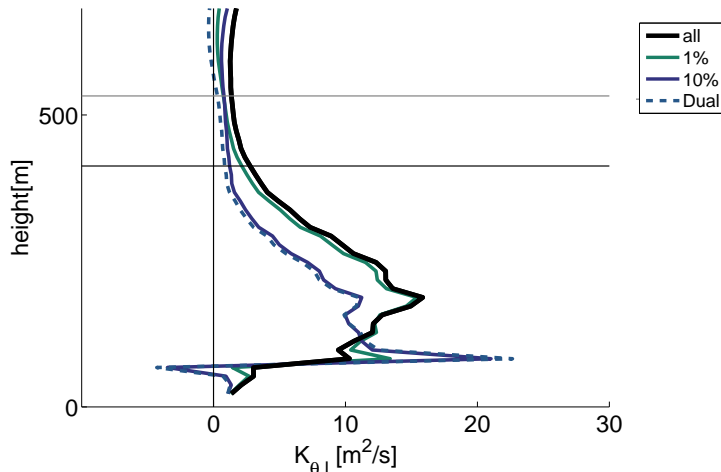


Figure 5.2: Eddy diffusivity profiles based on the total turbulent heat transport (black) and the residual fluxes after subtraction of the massflux transport by dry (10%wPDF), moist (1%wPDF) and both massfluxes (dual, dotted). The profiles based on the residual fluxes, have stronger asymptotic behaviour, since the height of zero heat flux no longer coincides with the height of zero gradient. Horizontal lines in the left side figures indicate heights according to figure 3.3.(*LESlarge*)

The use of the combined EDMF scheme instead of the ED scheme causes stronger asymptotic behaviour. The asymptote in the dry massflux EDMF $K_{\theta,l}$ profile avoids a maximum value, which is found in the total heat flux $K_{\theta,l}$ profile. Therefore only the total heat-flux parameterization could be used to diagnose the relation of the θ_l K -profile with the q_t K -profile. The peak value in the sub-cloud layer θ_l -profile is 40% of the q_t -peak value.

The 1% wPDF sampled heat transport contribution is very small. This updraft therefore causes only a small reduction of the 1% wPDF - EDMF eddy diffusivity profile with respect to the ED scheme. The 10% wPDF heat massflux term in contrast contributes for 60% in the top the sub-cloud layer, which is quite similar to the water massflux contribution (see figure 4.2). The use of the EDMF scheme with the 10% wPDF sampled massflux heat transport contribution therefore leads to a significant reduction of the $K_{\theta,l}$ profile, whereas the main difference between the diagnosed EDMF $K_{\theta,l}$ and $K_{q,t}$ profiles is found in the asymptotic behaviour due to the zero θ_l lapse rate.

5.1.2 Cloud layer

Significant large downward heat and upward water fluxes need turbulent transport parameterization, even though large massflux heat and water transport contributions are found in the cloud layer. This turbulent transport is related to downdraft turbulence in the top of the cloud layer (chapter 3.3 and 4.2.3). In these turbulent parts the horizon-

tal mean q_t and θ_l profiles have very small lapse-rates. The diagnosed eddy diffusivity profiles therefore explode within the stratocumulus cloud (see figure 5.3). The change of sign of K_ϕ within the cloud in the 6th to 30th hour of the transition for q_t and at the 30th hour for θ_l , indicates even a increasing $\overline{q_t}$ and decreasing $\overline{\theta_l}$ with height. The eddy diffusivity profiles for heat and water could be assumed to be simply very large within the stratocumulus cloud.

At heights without downdraft related turbulence, the profiles using the cloudup massflux residual fluxes approach $0 \text{ m}^2/\text{s}^2$. This concerns large parts of the boundary layer, f.e. in the 13th, 30th and 35th hour of the ASTEX transition.

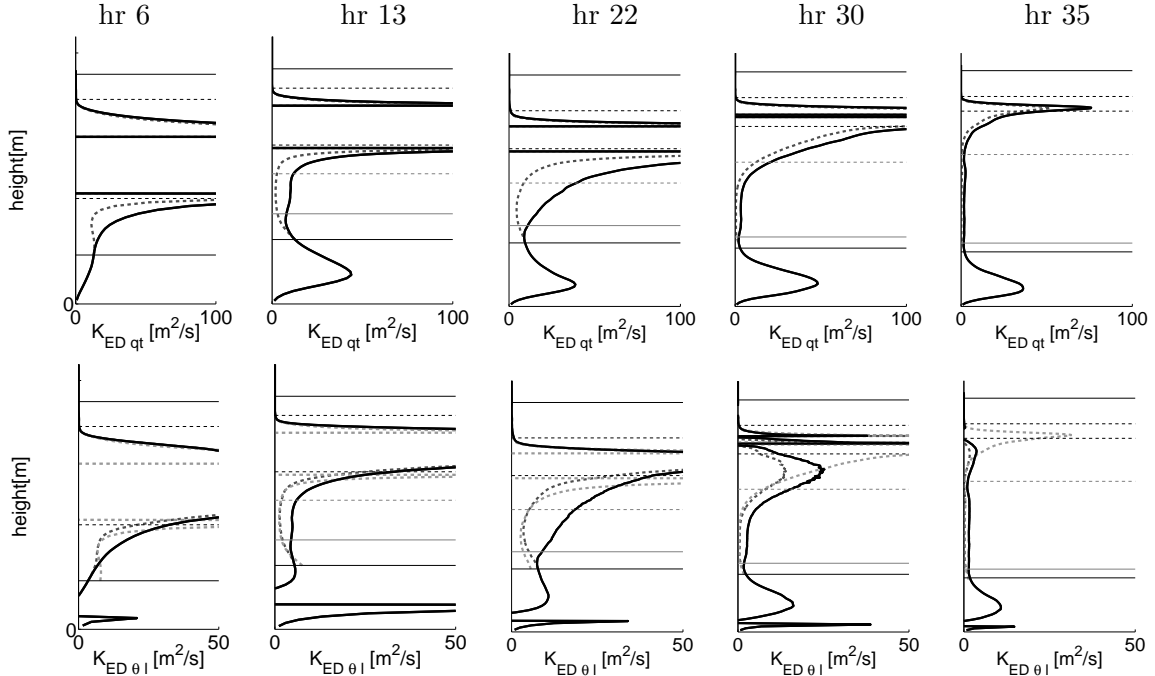


Figure 5.3: Eddy diffusivity profiles calculated in reverse by relating the total transport (solid) or the deficit with the cloudup massflux to the lapse rate of q_t (upper figures) and θ_l (lower figures). The q_t eddy diffusivity profiles is also plotted, multiplied with 0.6, in the lower plots in grey. Horizontal lines in the left side figures indicate heights according to figure 3.3. (*LES_{small}*)

The eddy diffusivity profiles in the lower part of the cloud-layer are similar shaped for the θ_l and q_t variables. $K_{\theta,l}$ can be well approximated by $K_{q,t}$ multiplied by a factor of 0.6. Though in presence of any downdraft related turbulence, significant differences between the profiles show up. During the 13th and 35th hour the profiles differ only slightly below the stratocumulus clouds, whereas the profiles diverge much more in the 22nd and 30th hour. An explanation is the opposed sign of the updraft and environmental subplume heat terms, causing lower θ_l eddy diffusivity profiles than found for q_t (as explained in chapter 4.2). As a consequence the difference between the EDMF $K_{q,t}$ and $K_{\theta,l}$ are especially found during the night when the downward environmental subplume heat transport term is present. This term is hardly present below the stratocumulus cloud, when downdraft turbulence is suppressed by short-wave radiative heating of the cloud top.

A way to define the magnitude of the eddy diffusivity profiles below the stratocumulus cloud is the relation with the turbulent kinetic energy (equation 2.21). The resulting mixing length profiles are displayed in figure 5.4.

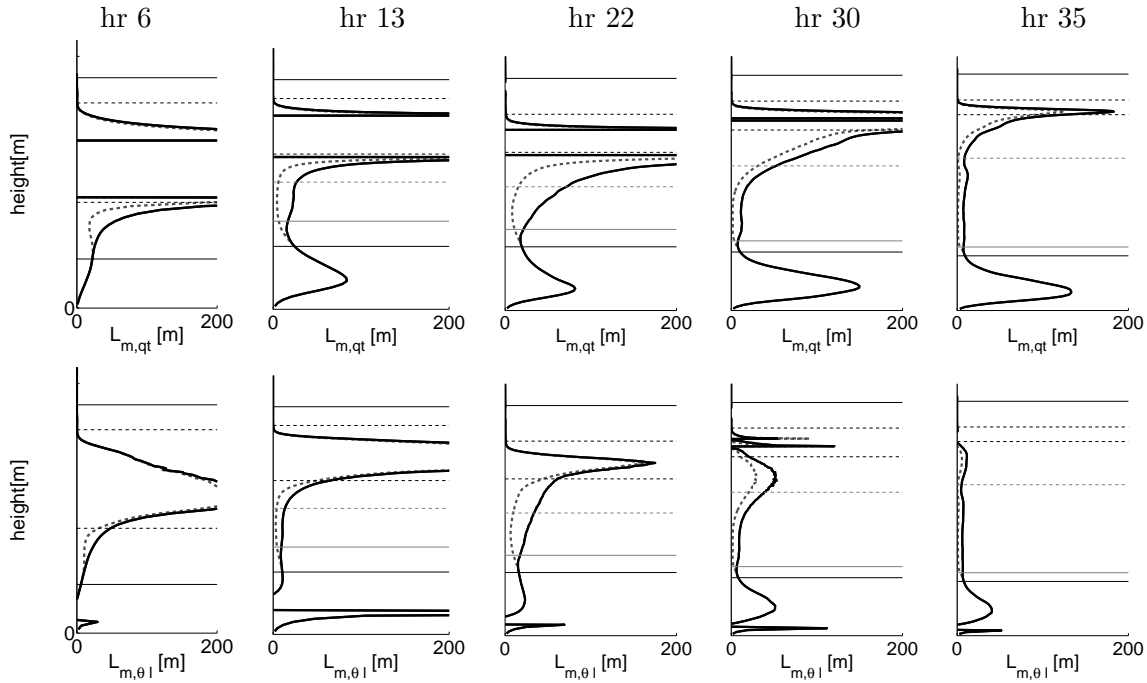


Figure 5.4: Required mixing lengths, needed to relate the eddy diffusivity profiles of figure 5.3 to the turbulent kinetic energy (Soares et al. (2004)). The use of a cloudup EDMF scheme (dashed lines) leads to a reduction of the required mixing lengths. Horizontal lines in the left side figures indicate heights according to figure 3.3. (*LESsmall*)

The turbulent kinetic energy and the eddy diffusivity profiles are related, since the differences of magnitude between different hours and heights of the mixing length profiles are smaller than for the $K_{q,t}$ and $K_{\theta,l}$ profiles. Although the profiles have hardly different characteristics and the asymptotic values are still present in the cloud top.

5.2 Massflux parameterization during ASTEX

A complete massflux transport model consists of the next properties (2.5, equation 2.9):

- $q_{t,u}$ and $\theta_{l,u}$ values at the bottom of the parameterized layer.
- An entrainment rate as a function of height, defining the $q_{t,u}$ and $\theta_{l,u}$ vertical lapse-rate (equation 2.16).
- Massflux entrainment and detrainment rate (equation 2.17) or a and b factors for a simplified solution of the vertical velocity budget for updrafts with fixed updraft fraction (equation 2.27).

The horizontal mean q_t and θ_l values result from the parameterization of the budget equation, in which the turbulent transport term itself results from the massflux transport parameterization. Different models are used for the source and sink terms in the budget equations, but these are no part of this research.

5.2.1 Sub-cloud layer

Updraft initialization

The dry and moist $q_{t,u}$ and $\theta_{l,u}$ at the lowest level of the sub-cloud layer are almost similar to the sea surface temperature and the associated saturation water vapor content (figure 4.10). Even though the updrafts have quite low q_t and high θ_l values with respect to the 0.1% q_t PDF sampled updraft, the wPDF sample criteria select the heat and water transporting updraft in the sub-cloud layer. The transporting rising updraft is especially found in the fastest part of the wPDF criterion and not in the high q_t and low θ_l parts of the q_t and θ_l PDFs (figure 4.6 upper plots, chapter 4.2.2).

The mean sea surface properties could be used for the moist updraft initialization. The same holds for the 1% wPDF updraft. Although the transition from moist sub-cloud layer updraft into cumulus updraft is poorly represented by any wPDF sampled updraft. The cloudup sampled updraft at the cloud-base has larger q_t and lower θ_l value than the sea surface properties (more elaborate in chapter 4.2.1). The wPDF updrafts therefore are appropriate to perform heat and water transport, but show no continuity from sub-cloud into the cloud layer updraft. Therefore these criteria are not suitable to use for moist updraft criterion.

Entrainment rate

The entrainment rate is diagnosed by the $q_{t,u}$ and the horizontal mean \bar{q}_t profiles (equation 2.25). Diagnosis for q_t is preferred above θ_l , because it is conserved for more processes like radiation and because the zero $\bar{\theta}_l$ lapse rate causes an asymptote. Figure 5.5 gives entrainment rates for different wPDF sampled updrafts.

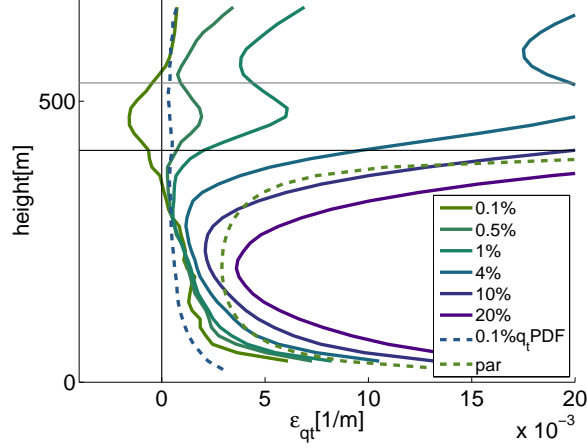


Figure 5.5: $\epsilon_{q,t}$ of different wPDF (solid) and 0.1% q_t PDF (blue dotted) sampled updrafts. A parameterization of the entrainment rate is given (green dotted) using $c_\epsilon = 0.3$ (equation 2.26), similar to the parameterization of a 'dry' updraft in a convective boundary layer (Siebesma et al. (2007)). Horizontal lines in the left side figures indicate heights according to figure 3.3. (*LESlarge*)

The 10 and 20% wPDF sampled entrainment rates are consistent with what is expected from a dry updraft. The profiles have an asymptote at the sea surface and the cumulus cloud base. Because the updraft massflux is relative constant due to the constant updraft fraction, entrainment implies detrainment and the dry updraft is supposed to detrain in the top of the sub-cloud layer.

The 0.5 to 4% wPDF sampled updrafts also detrain at the bottom of the cloud layer, though they lack the asymptotic behaviour within the transition layer. On the contrary the 0.1% wPDF sampled updraft, is negative in the transition layer. This implies that relative dry parcels are replaced by moister parcels in this part of the sub-cloud layer. This is not consistent with the meaning of the moist updraft. The dry updraft is supposed to become only slightly moister due to entrainment and to show continuity between sea surface into the cloud-layer updraft. Both positive and negative detrainment rates in the transition layer point at discontinuity. In the meantime, the entrainment rate of the 0.1% q_t PDF sampled updraft is small and almost constant in the entire transition layer.

The parameterization of the entrainment rate (equation 2.26) therefore is especially useful for the 10% wPDF sampled updraft, since the dry updraft is supposed to detrain. The entrainment rate constant was found to be $c_\epsilon = 0.5$ for an updraft fraction of 0.3 (Soares et al. (2008) and $c_\epsilon = 0.4$ for updraft fractions of 1 to 3% (Siebesma et al. (2007)) in a convective boundary layer. The LES results in the ASTEX case, also have smaller entrainment rates for smaller updraft fractions, though the constant is also smaller for similar updraft fractions. The parameterization in figure 5.5 produces a good model for the 10% wPDF sampled updraft, with $c_\epsilon = 0.3$. The appropriate entrainment rate constant of different wPDF sampled updrafts can be red, halfway the layer, using the next relation for the entrainment rate halfway the sub-cloud layer ($\epsilon_{1/2}$):

$$c_\epsilon = \frac{\epsilon_{1/2}}{4} z_{subcloud} \simeq 100 \cdot \epsilon_{1/2} \quad (5.2)$$

Massflux budget

The wPDF sampled updrafts have a constant fraction. Thereby the massflux and vertical velocity are related (equation 2.12). Vertical velocity parameterization is diagnosed because it doesn't assume similarity with an q_t or other entrainment rate. The vertical velocity budget contains a buoyancy, advection, entrainment, subplume, pressure and Coriolis term (de Roode et al. (2012), equation 2.18). The subplume and pressure term are often related to the buoyancy and entrainment term using an a and b factor, resulting in equation 2.27. The vertical velocity of both the 1 and 10 % wPDF sampled updraft increases in the lower part of the boundary layer, but slowly decreases in the upper part (figure 4.5, left). The θ_v value of both updrafts is higher than the mean value in the largest part of the sub-cloud layer (figure 4.5, right). So these updrafts are positive buoyant in this part of the boundary layer. Reaching the lowest condensation level, first the dry updraft becomes negative buoyant and second the moist updraft, which again become positive buoyant below the height with largest cloud fraction (grey line).

With a positive buoyancy and a decreasing vertical velocity, a significant sink term is needed in the top of the sub-cloud layer. The moist updraft (1% wPDF) is partially slowing down due to a slowly increasing subplume vertical velocity variance (figure 5.6, right). Though the dry updraft (10% wPDF) even has a decreasing w'' variance in the top of the sub-cloud layer, indicating a positive w -budget contribution. The modified pressure term instead increases strongly in the upper part of the boundary layer, so the pressure term acts as a sink in this part of the boundary layer.

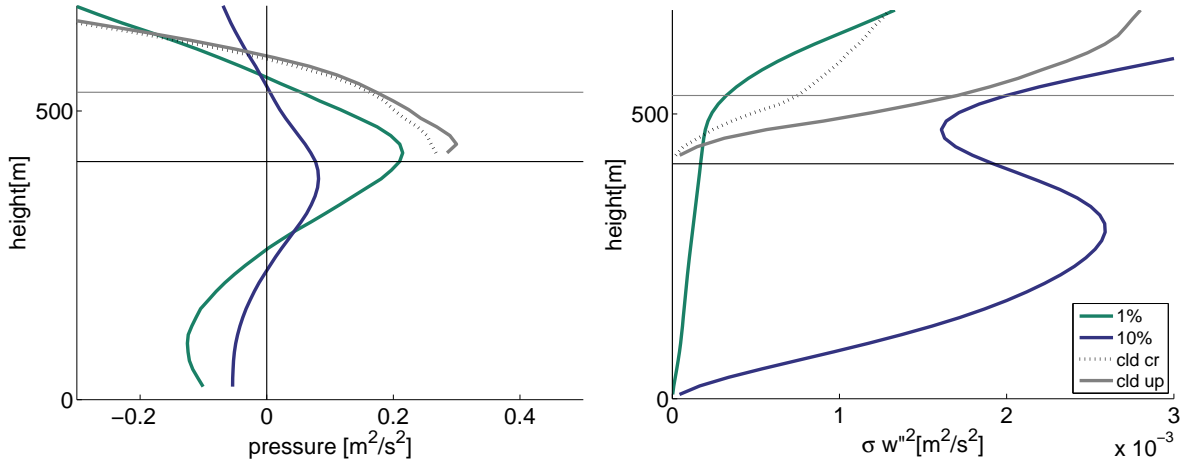


Figure 5.6: The modified pressure within the 1 and 10% wPDF sampled updrafts increases. The same holds for the 1% wPDF sampled subplume vertical velocity variance. These terms therefore act as sink term in the vertical velocity budget (equation 2.18) Horizontal lines in the left side figures indicate heights according to figure 3.3. Horizontal lines in the left side figures indicate heights according to figure 3.3. (*LESlarge*)

The different sources and sinks result in the next moist (1% wPDF) and dry (10% wPDF) updraft vertical velocity budget terms:

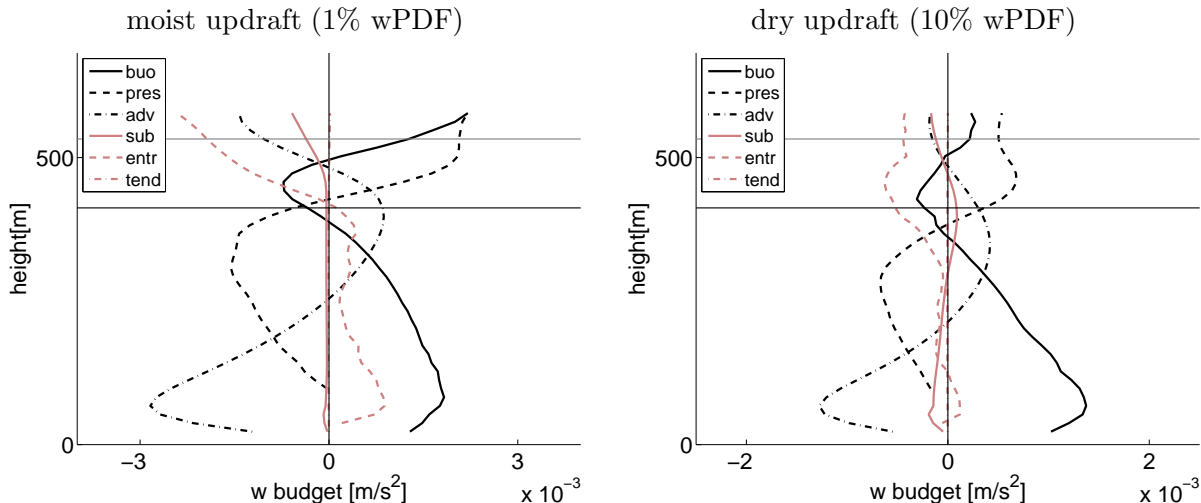


Figure 5.7: Terms of the vertical velocity equation (eq 2.18) of the 1% and 10% wPDF sampled updraft in the 30th hour of ASTEX. The entrainment term of the 1% wPDF sampled updraft (calculated as residual term in equation 5.7) acts as a source term in almost the entire layer, whereas the term is a sink for the 10% wPDF sampled w . Horizontal lines in the left side figures indicate heights according to figure 3.3. (*LESlarge*)

The 1 and 10% wPDF sampled vertical velocity budget terms show similar characteristics, but deviate especially in the top of the sub-cloud layer. The 10% wPDF sampled updraft shows strongest similarity with the terms in the convective boundary layer (Siebesma et al. (2007)).

The *tendency* of both updrafts is very small with respect of the other terms.

The *pressure* term in the ASTEX case is the main sink in the largest part of the sub-cloud layer. Reaching the cloud layer the 10% wPDF pressure term decreases again and in the transition layer it turns into a source. This is different to the pressure term in f.e. the convective boundary layer (CBL, Siebesma et al. (2007)). The pressure appears significant for the updraft to rise and to become saturated.

The term is however not directly related to any of the other terms of the w budget, since it is the only term which is constantly increasing without a change of sign in the middle of the sub-cloud layer.

Close to the sea surface the *advection* term is the main sink term in the vertical velocity budget. On the contrary in the upper part of the boundary layer, it is a significant source. This implies that no vertical velocity source term is present at this height and that the updraft mean vertical velocity as a consequence decreases. The dry updraft starts to slow down at a slightly lower level than the moist updraft. Compared to the convective boundary layer updraft (Siebesma et al. (2007)) a larger part of the budget is used to accelerate. This is in agreement with the purpose of the 'moist' updraft, because this updraft is supposed to have a remaining upward velocity at the cumulus cloud base.

The *subplume* contribution is a negligible small sink term for the moist updraft. The 10% wPDF sampled vertical velocity variance (dry updraft) acts as a source in the upper

part of the sub-cloud layer, although the term is still quite small.

The *entrainment* term was calculated as residual term, since the entrainment rate is not yet known. In the convective boundary layer this term is found to be the a sink in the largest part of the mixed layer. Though entrainment appears to have a quite unusual effect on the 1% wPDF sampled updraft mean velocity. The moist updraft requires a positive entrainment term in order to have a balanced budget equation. The updraft is not slowing down due to entrainment, but even accelerates when relative fast air is sampled. We have to keep in mind that we have a fixed updraft fraction, so entrainment and detrainment actually means exchange of slow parcels by faster parcels. However in the transition region the entrainment term becomes the largest sink term.

The 10% wPDF sampled w_u takes only advance of entrainment in the lower part of the sub-cloud. The entrainment term turns into a small sink as the updraft rises, and becomes even the largest sink term in the transition layer. This is quite reasonable, since the dry updraft is supposed to detrain at this height. Figure 5.8 gives the resulting entrainment rates for these updrafts:

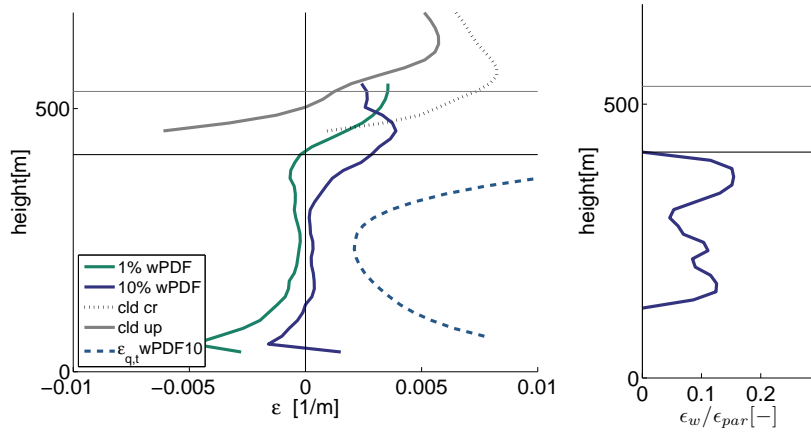


Figure 5.8: Vertical velocity entrainment rate, calculated from the entrainment term in the vertical velocity budget(left). The 1% wPDF sampled updraft is accelerating in the largest part of the sub-cloud layer due to entrainment. On the contrary the 10% wPDF sampled updraft, is continuously entraining relative slow parcels. The 10% wPDF sampled ϵ_w scales with a factor 0.1 with the parameterized $\epsilon_{q,t}$ in figure 5.5. Horizontal lines in the left side figures indicate heights according to figure 3.3. (*LESlarge*)

The entrainment term is a source term for the 1% wPDF sampled w_u between sea surface and the transition layer. The 10% fastest updraft in contrast is entraining slower parcels in the largest part of the sub-cloud layer. The vertical velocity entrainment rate of the 1% wPDF sampled updraft has opposite sign to the q_t entrainment rate. The 10% wPDF sampled ϵ_w is negative near the sea surface, but scales with a factor 0.1 with respect to the parameterized $\epsilon_{q,t}$ in figure 5.5 (Siebesma et al. (2007)). In agreement with de Roode et al. (2012) it appears a good choice to calculate the entrainment rate as residual, in order to have adjusted entrainment rates for different updrafts and variables.

a and *b* factors

The subplume and pressure term are according to equation 2.27 related to the buoyancy and entrainment term. No parameterization is needed to represent the 1% wPDF subplume term in the w budget, since this term is negligible small. The dry updraft

subplume term has a more significant value and could be related to the buoyancy term, although it is only a reduction of the buoyancy term in the order of 10%. The pressure term is an important sink term, which appears uncorrelated with any other term of the w budget. Another solution than the a and b parameterization is needed for the vertical velocity budget of the dry updraft.

5.2.2 Cloud layer

Updraft initialization

The cloud-base cloudup and cloudcore sampled updrafts are found at the moist and low θ_l part of the q_t and θ_l PDFs. The cloudcore sampled updraft has initially even larger q_t and lower θ_l value than the 0.1% q_t PDF sampled updraft, whereas the cloudup sampled updraft has only slightly smaller deviation with respect to the mean value. According to the 0.1% q_t PDF sampled q_t and θ_l profiles and the joint probability density function (PDF) plots (figure 4.11) the q_t PDF criteria are preferred above the wPDF criteria, since the moistest part of the q_t PDF appears to have more in common with the saturated updraft. This supports the approach by Neggers et al. (2009b), using a q_t variance-budget equation in order to parameterize the q_t PDF at every height.

Entrainment rate

Close to the cloudbase the q_t and θ_l rates of the cloudup and cloudcore updraft are relative small, with a value of about 0.007 m^{-1} . The rates slowly increase in the lower half of the cloud layer (figure 5.9).

In line with chapter 4.2.3, the entrainment rates suddenly increase up to values over 0.02 m^{-1} when the updrafts enter the height with downdraft related turbulence. This is accompanied by a strong relative massflux increment (figure 5.10). The q_t and wPDF sampled updrafts do not have this sudden increment. These updrafts remain to have distinct mean q_t and θ_l values with respect to the environment. The entrainment rates of these fixed-updraft-fraction-criteria as a consequence, have a constant entrainment rate of about 0.0015 m^{-1} , up to the stratocumulus cloud.

The q_t and θ_l entrainment rate profiles show strong similarity in a large part of the cloud layer. Only slightly below stratocumulus cloud (conditional criteria) and below the stratocumulus cloud top (PDF criteria) the profiles start to deviate. The q_t PDF sampled entrainment rate is getting smaller in the stratocumulus cloud and becomes even slightly negative for θ_l , due to heat and water accumulation below the temperature inversion. The 0.1% q_t PDF sampled $q_{t,u}$ is increasing and $\theta_{l,u}$ is decreasing with height (see figure 4.10) due to detrainment of the updraft and cloudtop radiative losses (similar to the ATEX case (Stevens et al. (2001))).

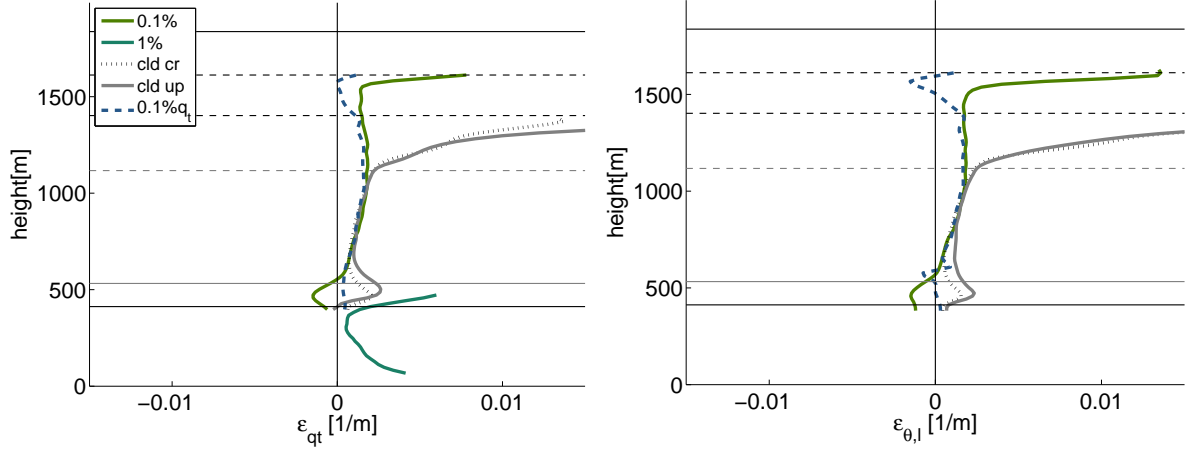


Figure 5.9: q_t and θ_l entrainment rates in the cloud layer. The cloudup and cloudcore entrainment rates heavily increase with the cloud fraction increment at 1100 m. Horizontal lines in the left side figures indicate heights according to figure 3.3. (*LESlarge*)

Massflux budget

The cloudup and cloudcore sampled massfluxes strongly decrease in the lower part of the cloud layer. Though slightly before the height at which the cloud fraction starts to increase, the massflux starts to increase already. The fractional massflux increment is growing up to values of over 0.01 m^{-1} , even more than 100 m below the stratocumulus cloud base. This sudden increment is not present for the PDF based sample criteria. These updrafts continuously grow with a fraction of 0.001 m^{-1} up to the stratocumulus cloud.

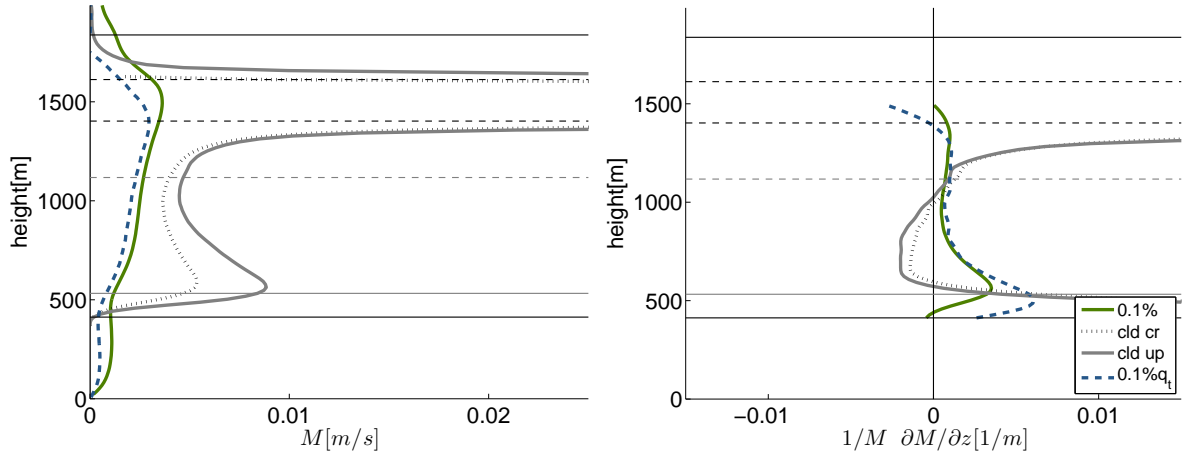


Figure 5.10: Cloudup, cloudcore, 1%wPDF and 1% q_t PDF sampled massflux and relative massflux increment. The cloudup massflux decreases in the lower part of the cloud layer, but starts to increase even below the minimum cloud fraction. Horizontal lines in the left side figures indicate heights according to figure 3.3. (*LESlarge*) .

The relative massflux increment is equal to the difference of the entrainment and detrainment rate. The detrainment rate is larger than the entrainment rate in the lower part of the cloud layer, since the conditional sampled massflux is decreasing with height.

The entrainment rate slowly increases, whereas the massflux decrement is getting smaller with height and even starts to grow. Slightly below the stratocumulus cloud the relative massflux increment becomes larger than the q_t entrainment rate. When the updraft massflux is increasing faster than the updraft q_t is changed by this massflux increment, the entrained parcels should be moister than the horizontal mean value. The bimodal environment as mentioned in chapter 4.2.2 explains the presence of relative moist parcels at these heights. Although the concept of a larger relative massflux increment than entrainment rate is quite unusual (figure 5.11). This situation even causes a negative detrainment-rate, which meaning is quite hard to understand.

The 0.1% wPDF and q_t PDF sampled updraft have in contrast to the former updrafts, almost constant fractional massflux lapse rates and q_t entrainment rates in this part of the boundary layer. They remain detraining with about 0.001 m^{-1} up to the stratocumulus cloud.

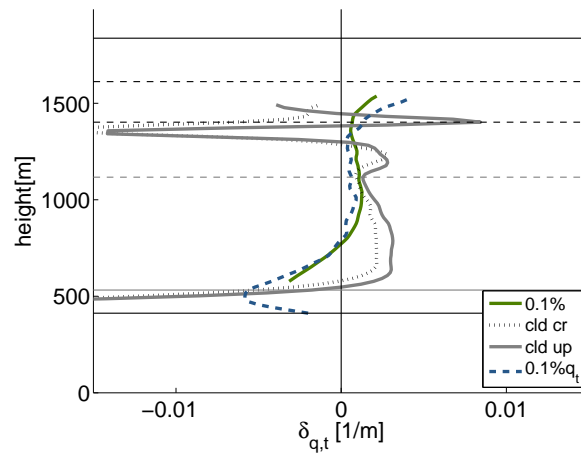


Figure 5.11: The cloudup and conditional sampled updrafts have slowly decreasing detrainment rate. Below the stratocumulus cloud the fractional massflux increment is larger than the q_t entrainment rate, causing a negative detrainment rate. For the 0.1% q_t and wPDF sampled updraft the detrainment rate of 0.001 m^{-1} is almost constant in the upper part of the cloud layer. Horizontal lines in the left side figures indicate heights according to figure 3.3. (*LESlarge*)

Vertical velocity budget

Another approach of the massflux model is the use of the vertical velocity budget equation in combination with a solution for the updraft fraction. Figure 5.12 shows the cloudup, cloudcore and 0.1% q_t and wPDF sampled vertical velocity and updraft $\overline{\sigma w'^2}$ profiles.

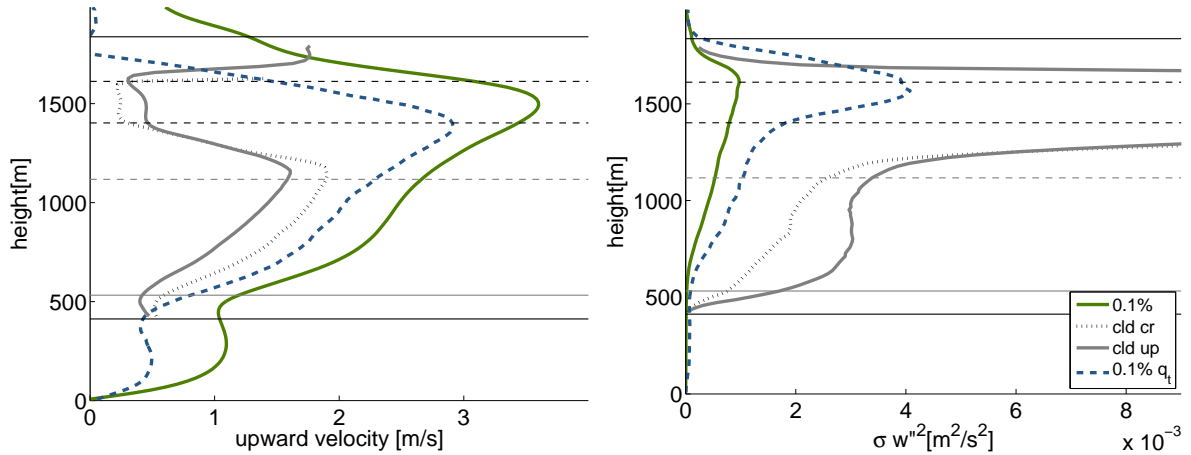


Figure 5.12: The mean vertical velocity of the cloudup and cloudcore sampled updraft decreases strongly at a height 1100 m. On the contrary, the 0.1% wPDF and q_t PDF sampled updrafts have increasing vertical velocity, up to the stratocumulus cloud (left). The subplume vertical velocity variance is increasing for all sample criteria; the cloudup variance even explodes at 1100 m. Horizontal lines in the left side figures indicate heights according to figure 3.3. (*LESlarge*)

The cloudup and cloudcore sampled updrafts accelerate in the lower part of the cloud layer, but heavily decelerate at a height of 1100 m. The deflection is not explained by the buoyancy of these updrafts, which is very small in the lowest part of the cloud layer and even increases at a height of 1100 m (more elaborate in chapter 4.2.3). The increasing subplume vertical velocity variance gives a first explanation for the sudden decreasing w_u (figure 5.12, right). Second the pressure term is quite different than in f.e. the BOMEX case, due to downdraft turbulence (figure 4.13). The mean modified pressure within all updrafts decreases quite strongly with height (figure 4.13) and acts thereby as a source in the w_u budget for the updrafts entering the cloud layer. At the height of about 1100 m the modified pressure of the cloudup and cloudcore sampled updrafts collapses and approaches horizontal mean value. Thereby the pressure term turns into a sink for the w_u budget. The 0,1% q_t and wPDF sampled updrafts though still have a decreasing modified pressure, whereas the mean cloud and cloudup sample approach horizontal mean pressure. Similar to q_t , θ_l and w_u a distinct core is found, whereas mean cloudup properties approach horizontal mean values due to sample fraction growth.

Figure 5.13 show the resulting cloudup (left) and cloudcore (right) vertical velocity budget terms:

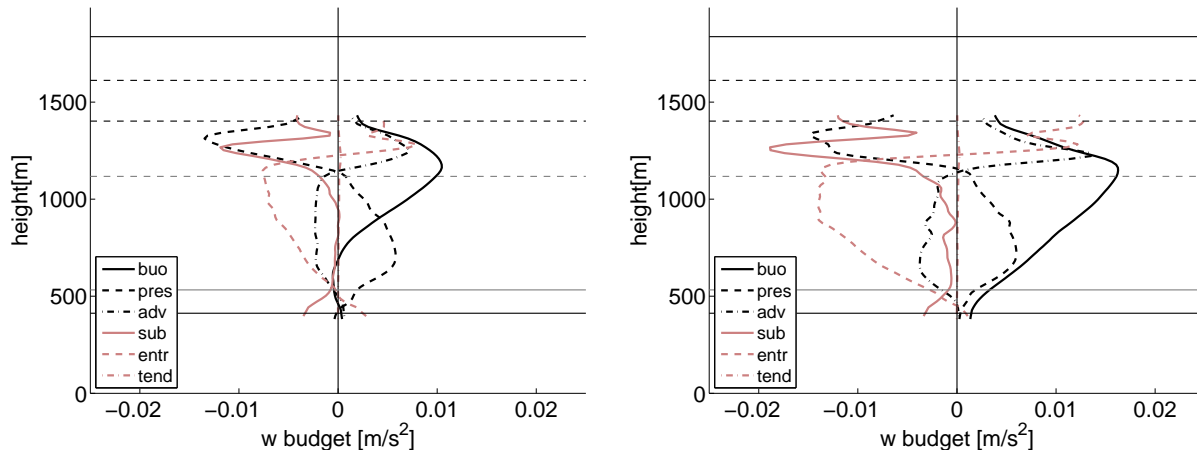


Figure 5.13: Terms of the vertical velocity equation (eq 2.18) based on the cloudup sampled updraft (left) and the cloudcore sampled updraft (right) in the 30th hour of the ASTEX transition. Horizontal lines in the left side figures indicate heights according to figure 3.3. (*LESlarge*)

The *tendency* of the cloudcore and the cloudup sampled updraft again is very small with respect of the other terms.

The cloudcore updraft is fed by a steady increasing *buoyancy*, which decreases when the updraft reaches heights with mainly downdraft dominated environment. The cloudup sampled buoyancy term is in the lower part of the cloud layer very small and the *pressure* term is only source term in the vertical velocity budget. The term is an important source for both criteria, whereas the pressure term was found to be the main sink term in the BOMEX case (de Roode et al. (2012)). Although it becomes a sink for ASTEX a higher level, when the cloudup and cloudcore fraction starts to increase. Another reason is the capping temperature inversion, since also the 0.1% fastest and moistest PDF sampled updrafts have in similarity with the CBL a decreasing pressure in the cloud top (figure 4.13).

The *advection* term is a quite significant sink term in the lower part of the cloud layer. This term is even almost constant for the cloudup sampled updraft. When the updraft fractions start to increase, the advection term becomes positive. The sources are no longer able to accelerate the updraft, so w_u^2 is decreasing with height.

The cloudup *subplume* term is a negligible small sink term in the lower part of the boundary layer. When the sample fraction starts to increase the subplume terms initially increase but then decrease again. The increment is explained by the decreasing mean sampled vertical velocity combined with an continuously accelerating core as found in the 0.1% q_t and wPDF sampled updrafts (figure 4.13). The accelerating core turns into a subplume fluctuation. Since the cloudup fraction still increases, the mean vertical velocity variance becomes dominated by the part outside the accelerating core and the mean subplume term decreases again. The cloudcore subplume term is slightly larger than the similar term in the cloudup w -budget.

The *entrainment* term was calculated as residual term. The cloudup and cloudcore sampled vertical velocity budget need a sink term in the lower part of the cloud layer and a source when the sample fraction starts to increase. The sign of the term corresponds with the sign of the vertical velocity of the direct environment of the cumuli. Surrounded by a negative buoyant cloud shell in the lower part of the cloud layer (figure 3.9 and 4.12),

the updraft is slowed down by entrained parcels. Though reaching heights dominated by downdraft turbulence the mean vertical velocity has become quite small, whereas environmental vertical velocity fluctuations heavily increase. The largest velocities of all upward wPDF sampled updrafts are found in the middle of the stratocumulus cloud (figure 4.13). Furthermore the updrafts become part of the environmental turbulence structures, so the entrained parcels are able to contribute to the mean vertical velocity. The vertical velocity entrainment rate is calculated from the entrainment term:

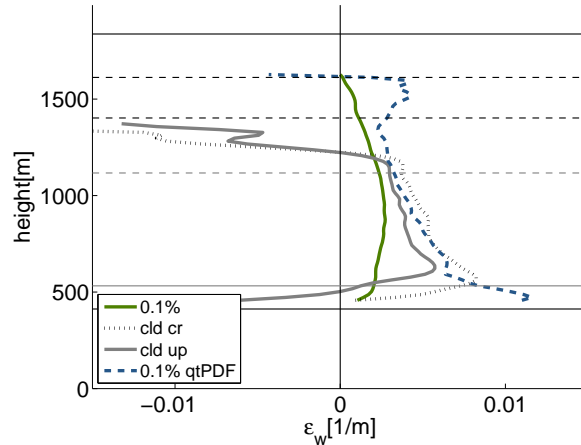


Figure 5.14: Cloudup, cloudcore, 1%wPDF and 1 % q_t PDF sampled vertical velocity entrainment rate. The entrainment rates are calculated from the residual vertical velocity budget term. All entrainment rates slowly decrease with height. In the upper part of the cloud layer, the cloud and cloudcore vertical velocity budget even start to benefit from the downdraft related turbulence. Horizontal lines in the left side figures indicate heights according to figure 3.3. (*LESlarge*)

All sample w entrainment rates are significant larger than the q_t and θ_l entrainment rates at the cloud base. The rates decrease with height and the cloudup and cloudcore entrainment rates change sign at heights with downdraft related turbulence. The rates even increase asymptotic.

The 0.1% q_t and wPDF sampled updrafts are continuously entraining slower parcels and therefore remain positive. In the upper part of the cloud layer the PDF sampled entrainment rates behave as extrapolation of the conditional sampled entrainment rates in the lower part of the cloud layer. The q_t PDF sampled entrainment rate even coincides with the cloudup and cloudcore rates for 500 meter below the deflection of the conditional sampled entrainment rates. The 0.1% wPDF sampled rate is close to the cloud base much smaller, since it had even a negative value in the sub-cloud layer (figure 5.8).

***a* and *b* factors**

The bimodal environment in the lower part and the strong cloud fraction increment in the upper part of the cloud-layer make it hard to relate the cloudcore and cloudup subplume and pressure to the buoyancy and entrainment terms. The subplume term is very small in the lower part of the boundary layer and increases strongly at a height 1100 m. The buoyancy term has opposed behaviour; in the lower part of the cloud layer it slowly increases, but it starts to decrease again at a height of 1100 m. The pressure has opposite sign to the entrainment term in almost all part of the cloud layer. Although the relation between these terms is not very strong, since the pressure term is decreasing

between updraft initiation and 1100 m, whereas the entrainment term on contrary is constantly increasing.

PDF based sample criteria

The pressure terms of the 0.1% wPDF and q_t PDF sampled updrafts remain a source up to slightly below the stratocumulus cloud, whereas the entrainment term continues to be the main sink term (5.15). The smallest PDF based criteria are kind of extrapolations of the conditional sampled updrafts in the lower part of the cloud layer. Similar to the earlier mentioned properties, the smallest PDF sampled updrafts show continuity from the lower into the upper part of the cloud layer for a 'core' updraft. The 0.1% q_t PDF based entrainment terms furthermore again show better continuity at the cumulus cloud base and the wPDF sampled updraft within the stratocumulus cloud.

The profiles of these terms give no clear relation for the subplume and pressure term either. The subplume term is very small and deviates in the stratocumulus cloud for the 0.1% q_t PDF updraft. The change of sign of the advection term in the top of the cloud layer is only related to the change of sign of the pressure term. Therefore also for these criteria an another model for the pressure is needed.

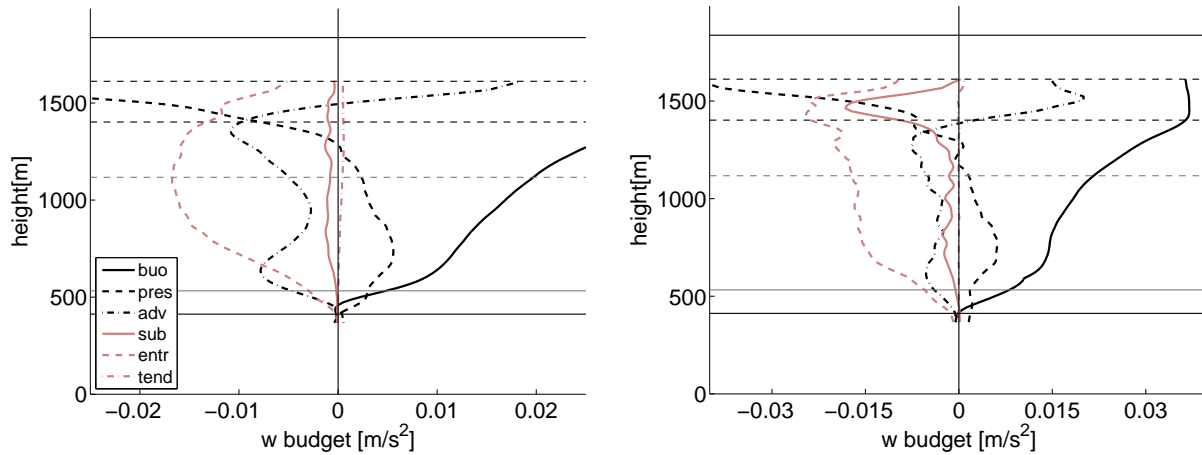


Figure 5.15: Terms of the 0.1 % w (left) and q_t PDF (right) sampled vertical velocity budget (eq 2.18) in the 30th hour of the ASTEX transition. Horizontal lines in the left side figures indicate heights according to figure 3.3. (*LESlarge*)

Chapter 6

Conclusion and discussion

6.1 Sub-cloud layer

Strong similarity is noticed between the massflux transport terms in the ASTEX sub-cloud layer and sub-cloud layers of earlier diagnosed cumulus cases (Neggers et al. (2009a)). The relative heat and water massflux transport contribution of the 10% wPDF sampled updraft increases up to 65% of the total transport budgets, slightly below the top of the layer and detrains afterwards. Only wPDF criteria with a larger percentile than 4% are appropriate to diagnose the non-local 'dry' updraft, because the smaller updrafts do not detrain in the top of the sub-cloud layer.

The relative massflux heat and water transport contributions of the 1% wPDF sampled updraft are smaller below the cumulus cloud base, although they increase up to 85% in the lowest 250 m of the cloud layer. In despite of the satisfying massflux contributions in the heat and water transport budget, *the 1% wPDF sampled updraft is not applicable to represent the moist updraft*. The fastest part of the wPDF spectrum does not evolve into the saturated updraft in the cloud layer. In the entire cloud layer, wPDF criteria select both the saturated updraft and turbulent parcels in the environment, which are found in opposite parts of the θ_t - and q_t - PDFs. The saturated updraft has more in common with the moistest part of the q_t PDF than with fastest part of the wPDF.

EDMF residual turbulent heat and water transport terms are well represented by eddy diffusivity *parameterization*. Only minor adjustments are needed to model the 10% wPDF sampled updraft. The parameterization of the mixed layer q_t entrainment rate (Siebesma et al. (2007)) collapses with the diagnosed entrainment rate using $c_\epsilon = 0.3$. The terms in the vertical velocity budget show strong similarity with these terms in the convective boundary layer (Siebesma et al. (2007)). Though the pressure term is found to be a significant larger sink term, whereas the advection term is smaller in the top of the sub-cloud layer. The vertical velocity entrainment rate scales with a factor 0.1 to $\epsilon_{q,t}$.

6.2 Cloud layer

After the decoupling from the sub-cloud layer dynamics, the **cloud layer environment** dynamics are characterized by a deep turbulent mixed layer in the top. The vertical velocity variance profiles have their maximum value in the top of the cloud

layer, with similar magnitude to nocturnal stratocumulus cases (Stevens et al. (2005)). Furthermore the concave-shaped vertical velocity skewness profiles indicate the presence of downdraft-related turbulence over 800 m below the stratocumulus top. At these heights a strong environmental subplume transport term is present, with a contribution of 40 to 80% of the total heat and water transport budget. Depending on the moment of the transition, a layer of 150 m to 800 m is found below, with undisturbed cumulus environment. At these heights over 80% of all heat and water transport is performed by the cloudup sampled updraft. The downdraft turbulence dominated environment and the undisturbed cumulus environment coexist at same heights but are spatially separated. In the 30th hour of the ASTEX transition a bimodal distribution is found in the joint w - q_t , w - θ_l and w - θ_v PDFs at heights between 675 and 1275 m.

Close to the cloudbase, the cloudup sampled **updraft q_t and θ_l budget** hardly changes due to a small entrainment rate. Though the detrainment rate is relative large. These rates are not constant in height, since the entrainment rate increases with height, whereas the detrainment becomes smaller and even negative. As a result the cloudup massflux and fraction increase heavily, far below the stratocumulus cloud. This phenomenon is accompanied with different uncommon effects. The offset of the updraft w_u , $p_{mod,u}$, $\theta_{v,u}$, $\theta_{l,u}$ and $q_{t,u}$ with respect to the horizontal mean sudden decreases and the updraft mean properties approaches the horizontal mean value. The cloud, cloudup and cloudcore criteria are not able to select the heat and water advecting updraft, whereas joint w - q_t and w - θ_l PDFs and q_t PDF and wPDF criteria show an updraft with more or less constant fraction, with distinct properties up into the stratocumulus cloud.

The sudden cloudup fraction increment in the middle of the cloud layer has also consequences for the **vertical velocity budget**. The pressure term turns into a sink in the middle of the cloud layer when the updraft fraction increases. The pressure term of the 0.1% q_t PDF and wPDF sampled updrafts in contrast, turns similar as found in the convective boundary layer into a sink in the top of the layer. A similar abnormality applies to the subplume term at the height of the cloudup fraction increment. This term is very small below the stratocumulus cloud for all criteria, except for the cloud-condition based updrafts. For these criteria the term becomes even the largest sink at the heights with large sample fraction increment.

The cloudcore buoyancy term is quite small in the lower part of the cloud layer and even almost negligible for the cloudup sampled updraft. An explanation is found in the large θ_v variance in the bimodal environment. The entrainment term (calculated as a residual term, similar to de Roode et al. (2012)) is negative in the lower part of the cloud layer. A sink is needed since the buoyancy and pressure terms have to be balanced. In contrast with the lower part of the cloud layer, the entrainment term is a major source term in upper part. de Roode et al. (2012) found in contrast to these results a positive entrainment in the entire cloud-layer of the BOMEX, ARM and RICO cases.

Though the resulting w entrainment rate is quite reasonable. Since the updraft has a strong negative buoyant cloud shell in the lower part of the cloud layer the entrained parcels are quite likely to entrain downward moving parcels. In the upper part of the cloud layer, w_u is small due to the increased cloudup fraction, whereas the environment is accelerating due to increasing turbulent cloud dynamics. Entrainment of faster rising parcels causes a positive entrainment rate.

The vertical velocity budget of the 0.1% q_t and wPDF sampled updrafts have different properties of both cumulus updrafts and wPDF sampled updraft in the CBL. Close to the cloudbase the entrainment rates are large, but they slowly decrease with height. The subplume term of these small updrafts is very small. Furthermore the pressure term turns similar as found in CBL's into a sink term in the top of the layer. The decrement of the advection term and w_u in the stratocumulus cloud is mainly caused by the pressure term. In similarity with the sub-cloud layer, the pressure term in this situation needs an another parameterization than a factorization of the buoyancy or advection term.

The three most significant subjects for **further diagnosis** of the dual massflux model during the ASTEX case are:

- q_t PDF sampled updrafts in the cloud-layer, with percentiles in the order of the cloud fractions. Large subplume terms for the cloud-condition criteria gives the opportunity to improve updraft selection. The 0.1% q_t PDF sampled updraft and joint w - q_t PDF's show good perspectives for the moistest part of the q_t PDF to achieve this. This furthermore connects to the approach of parameterization of the $\sigma_{q,t}$ budget by Neggers et al. (2009b).
- Transport by downdraft turbulence is not yet modelled for a decoupled boundary layer. A dual environment model is recommended, in which the downdraft turbulent decomposition could be diagnosed by a criterion based on the stratocumulus cloud mean properties.
- The pressure term appears of great importance in the vertical velocity budget of the wPDF, cloudup and q_t PDF criteria in the entire boundary layer and uncorrelated to any other term. Another model than a relation with buoyancy or entrainment term is recommended.

Chapter 7

Appendix - Vertical plane plots

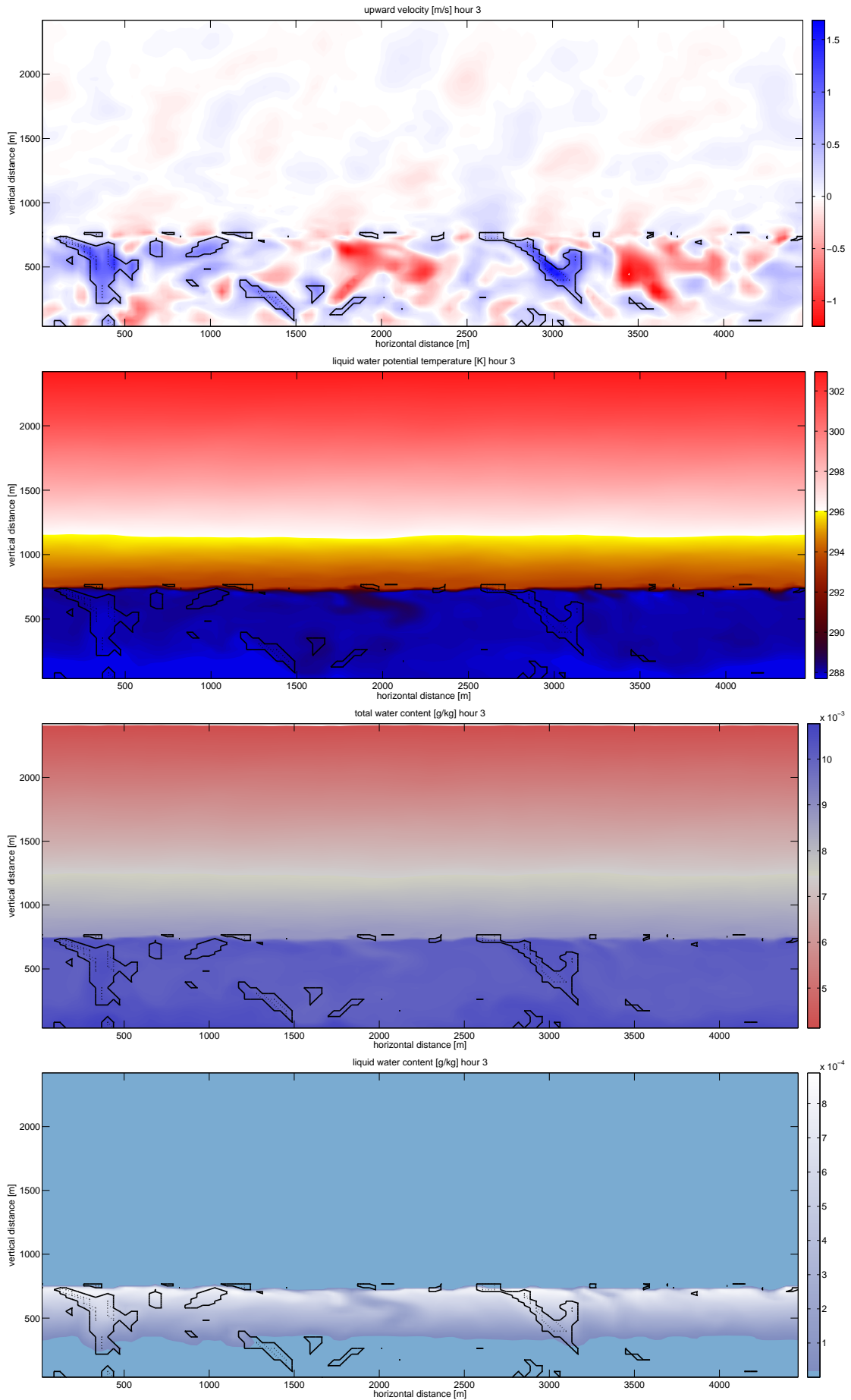


Figure 7.1: hour 3, horizontal plane fastest 2 (dotted) and 10(solid) percent(*LESsmall*)

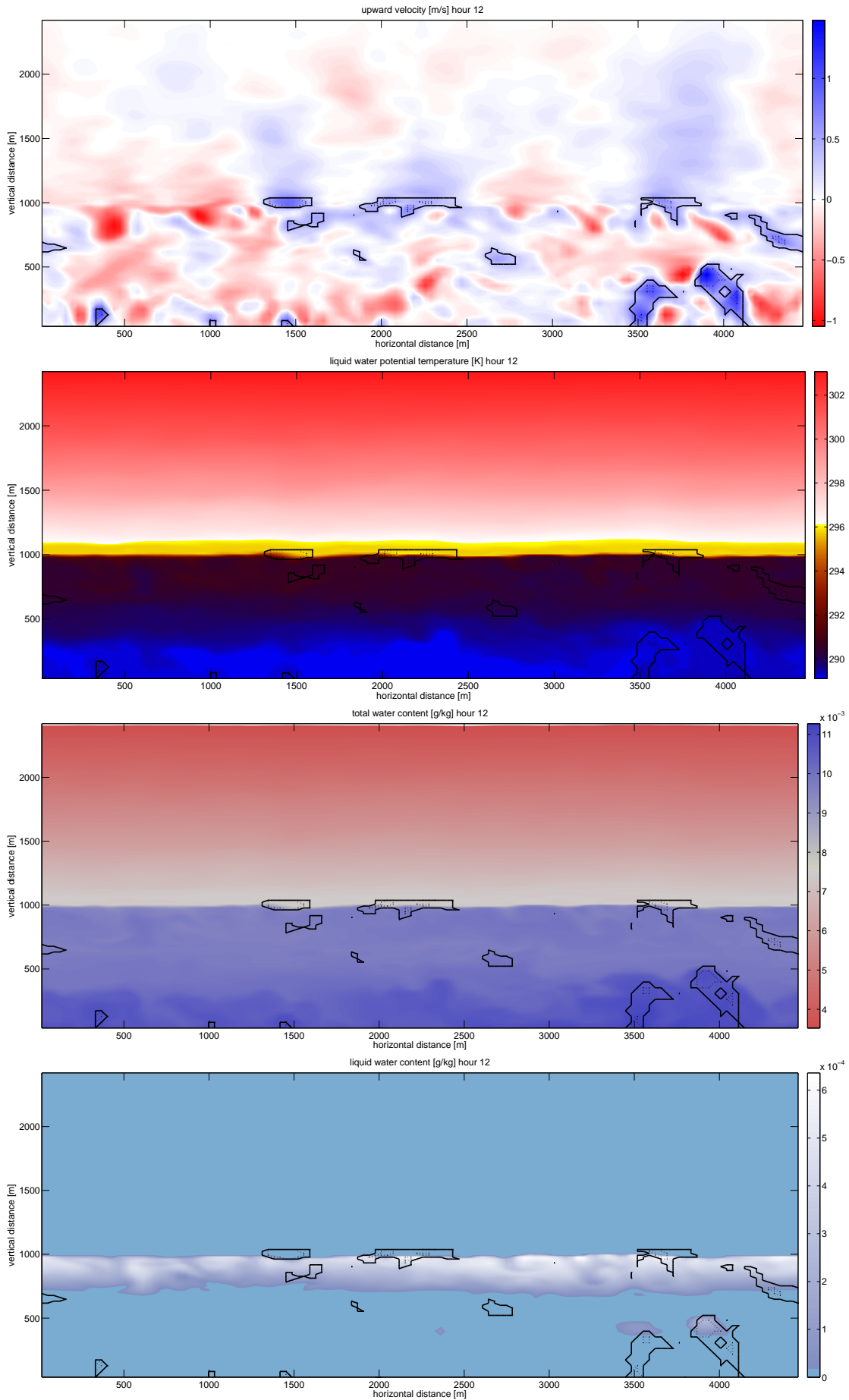


Figure 7.2: hour 12, horizontal plane fastest 2 (dotted) and 10(solid) percent(*LESsmall*)

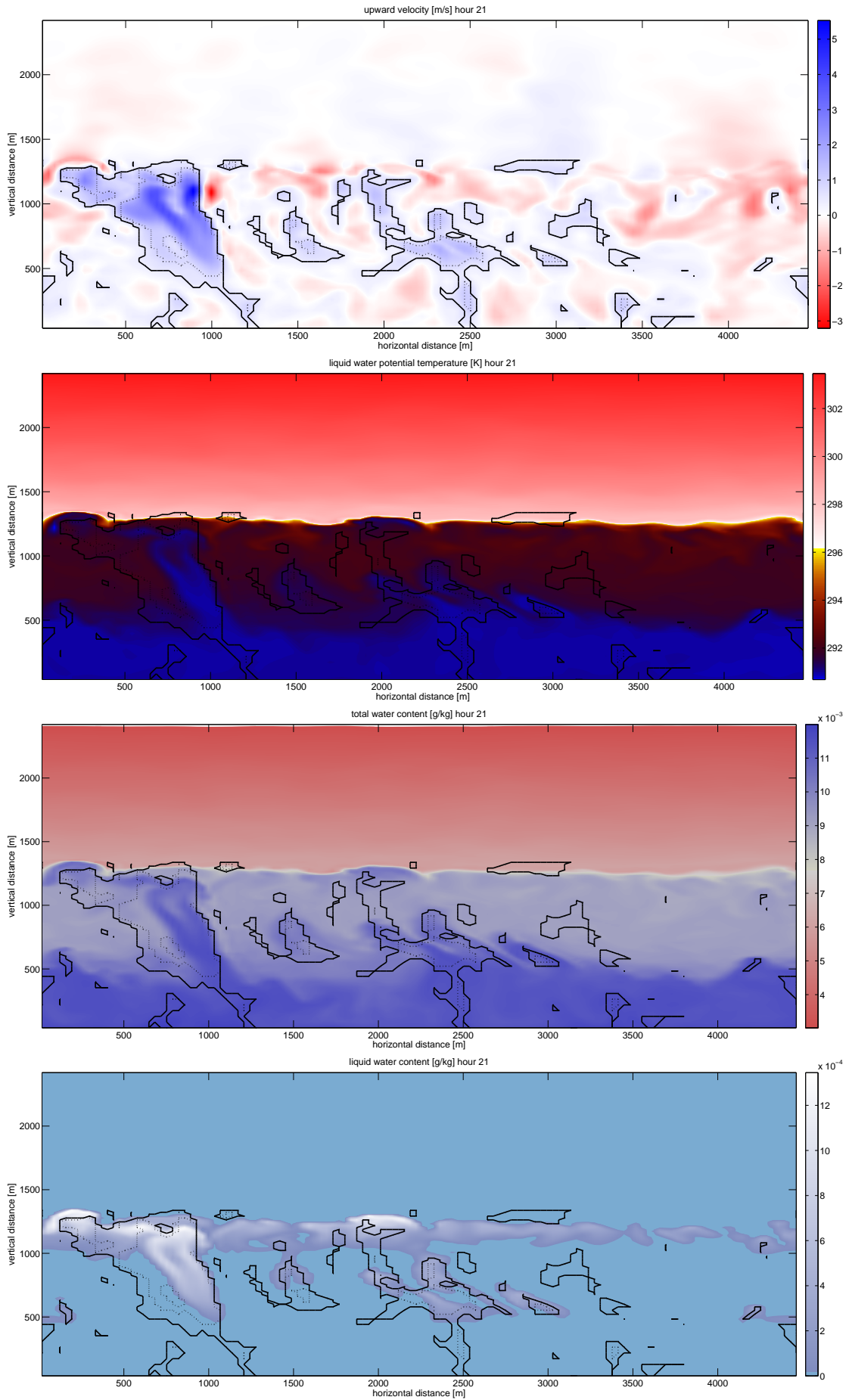


Figure 7.3: hour 21, horizontal plane fastest 2 (dotted) and 10(solid) percent(*LES_{small}*)

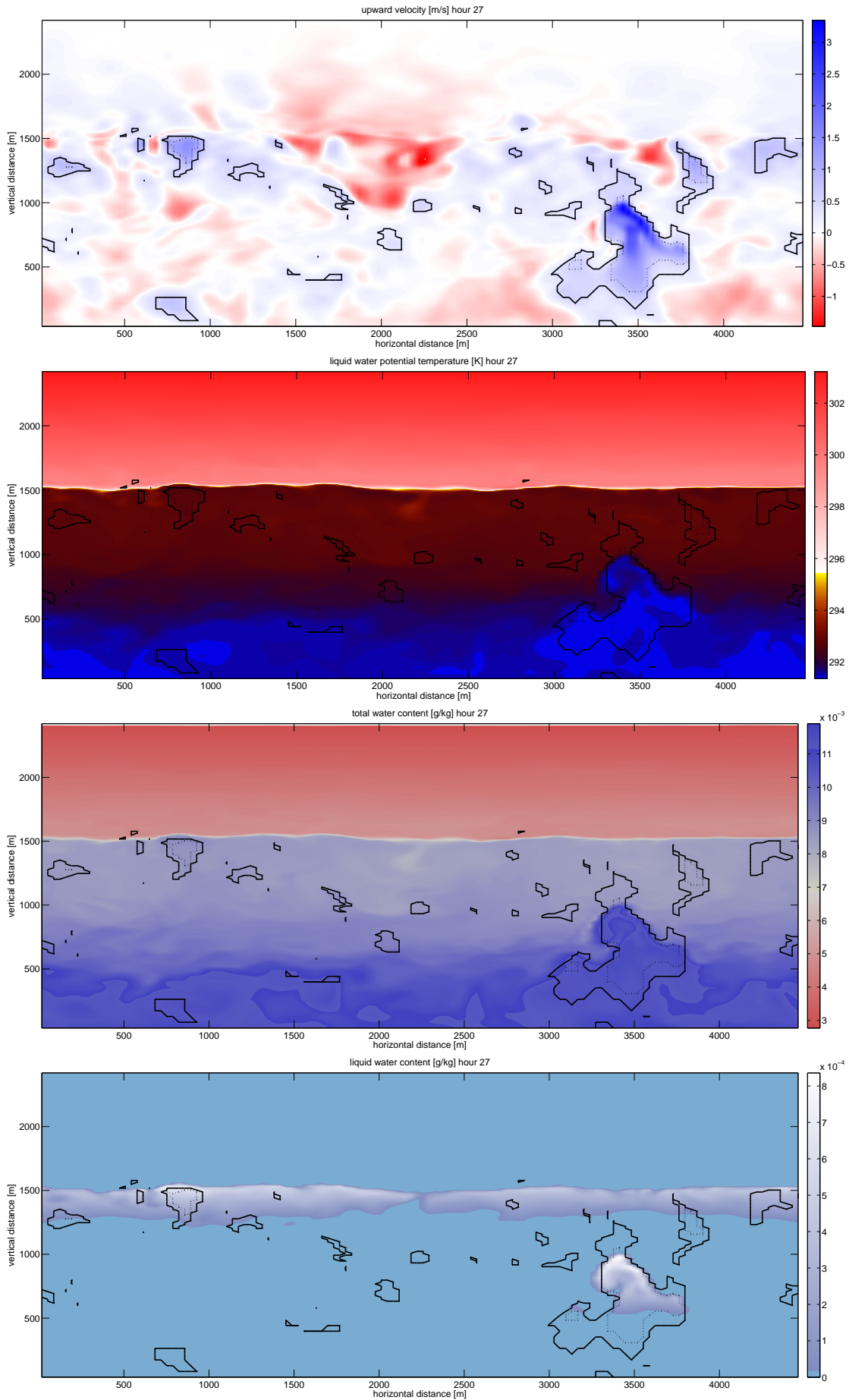


Figure 7.4: hour 27, horizontal plane fastest 2 (dotted) and 10(solid) percent(*LES_{small}*)

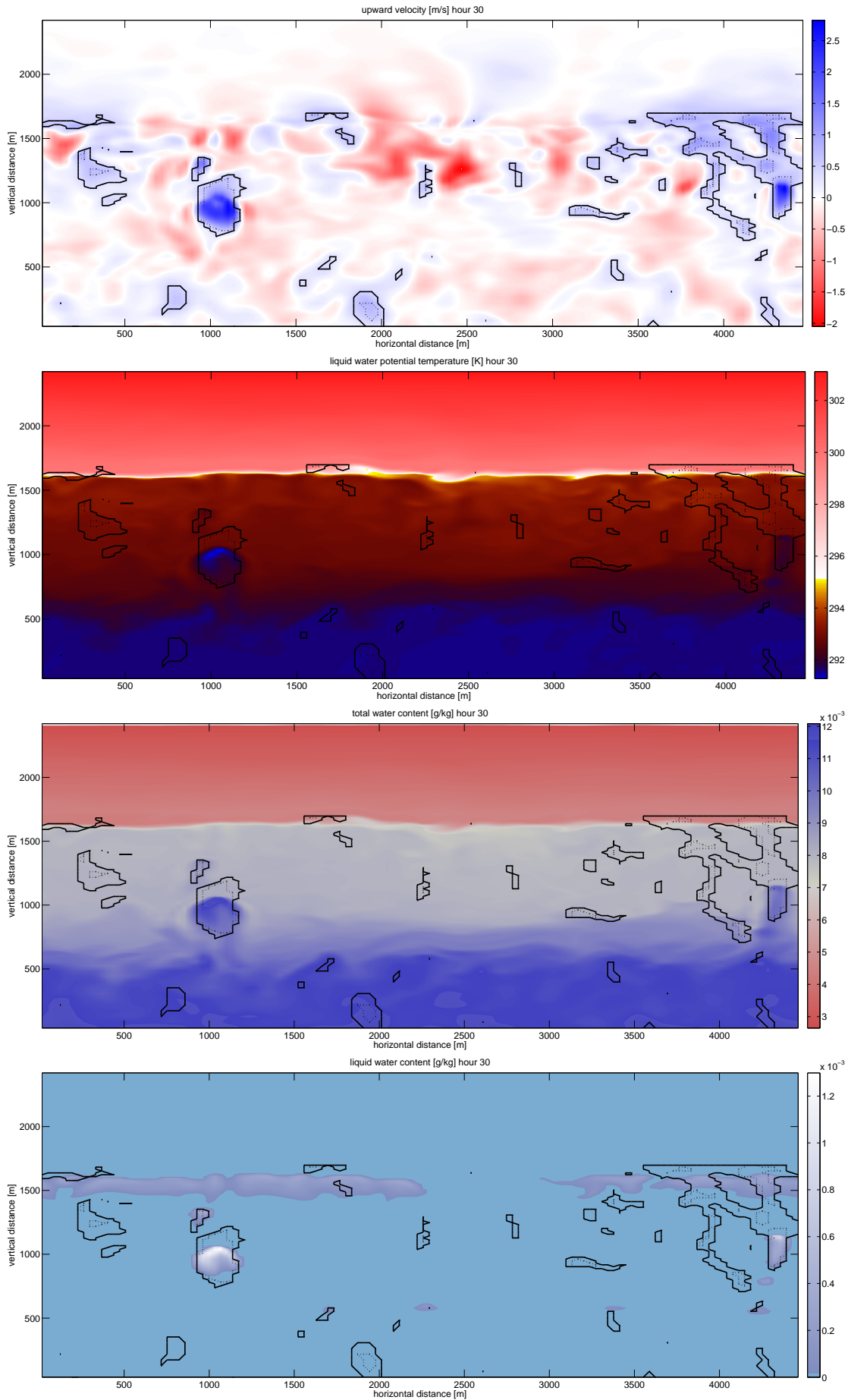


Figure 7.5: hour 30, horizontal plane fastest 2 (dotted) and 10(solid) percent(*LESsmall*)

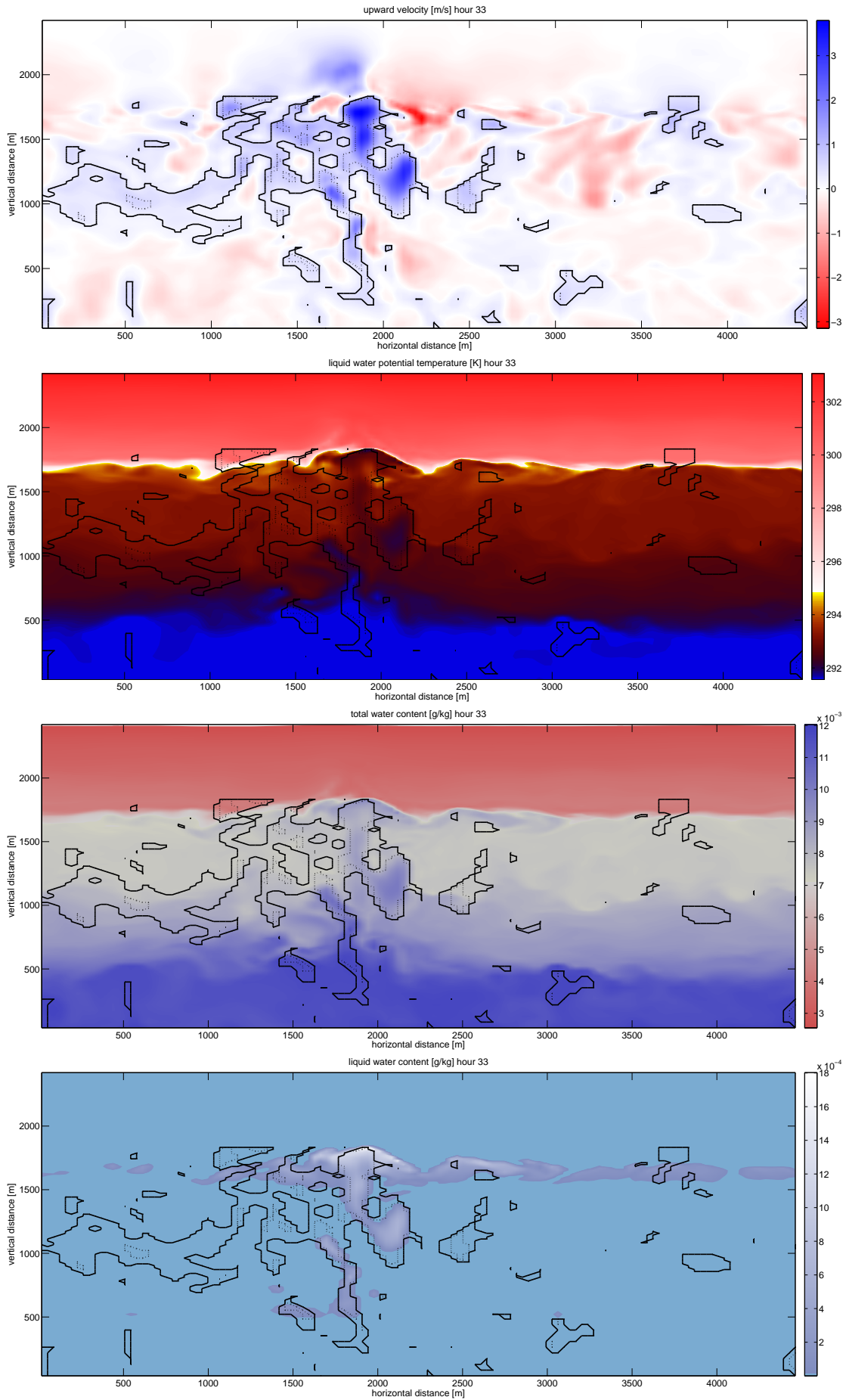


Figure 7.6: hour 33, horizontal plane fastest 2 (dotted) and 10(solid) percent(*LES_{small}*)

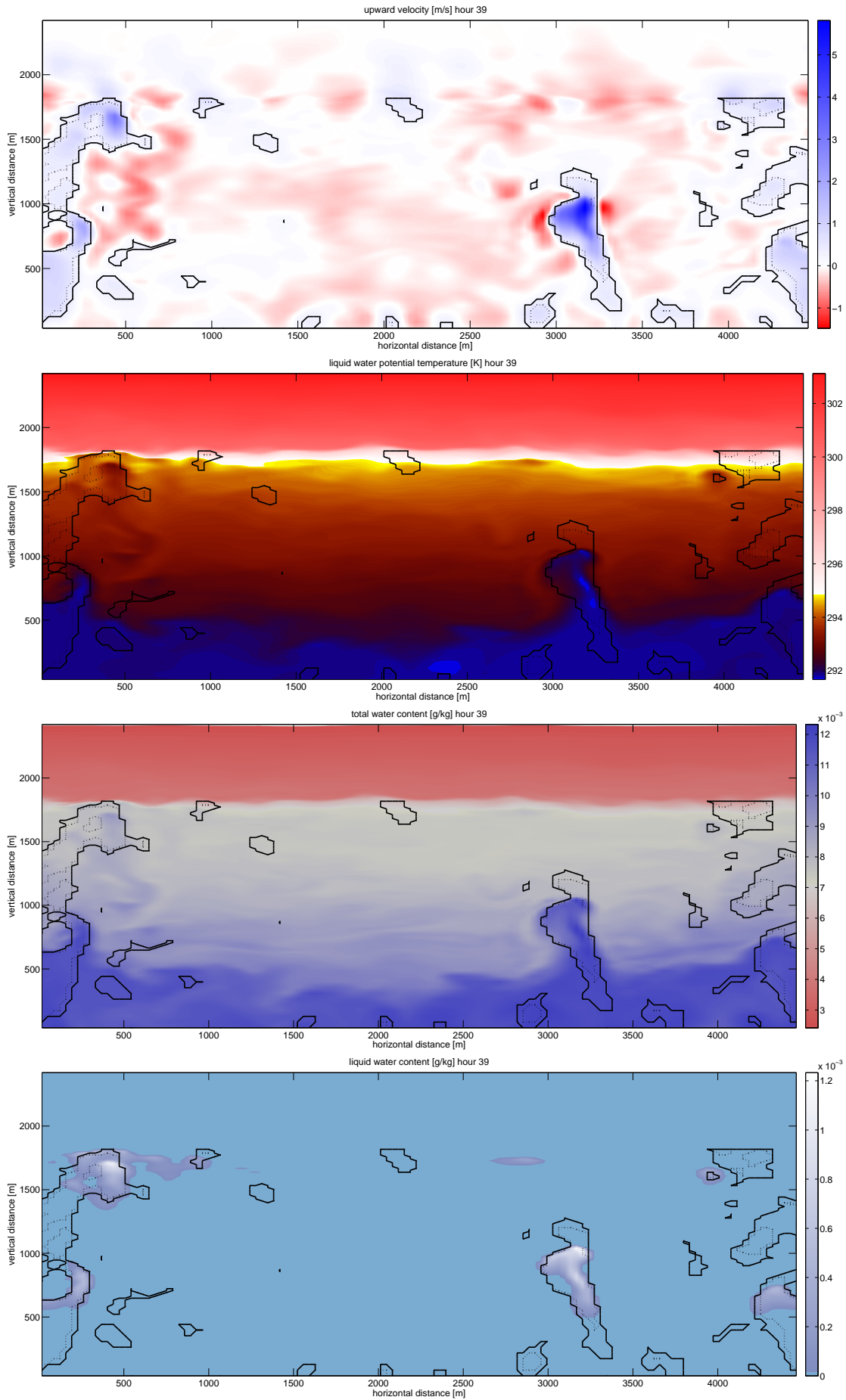


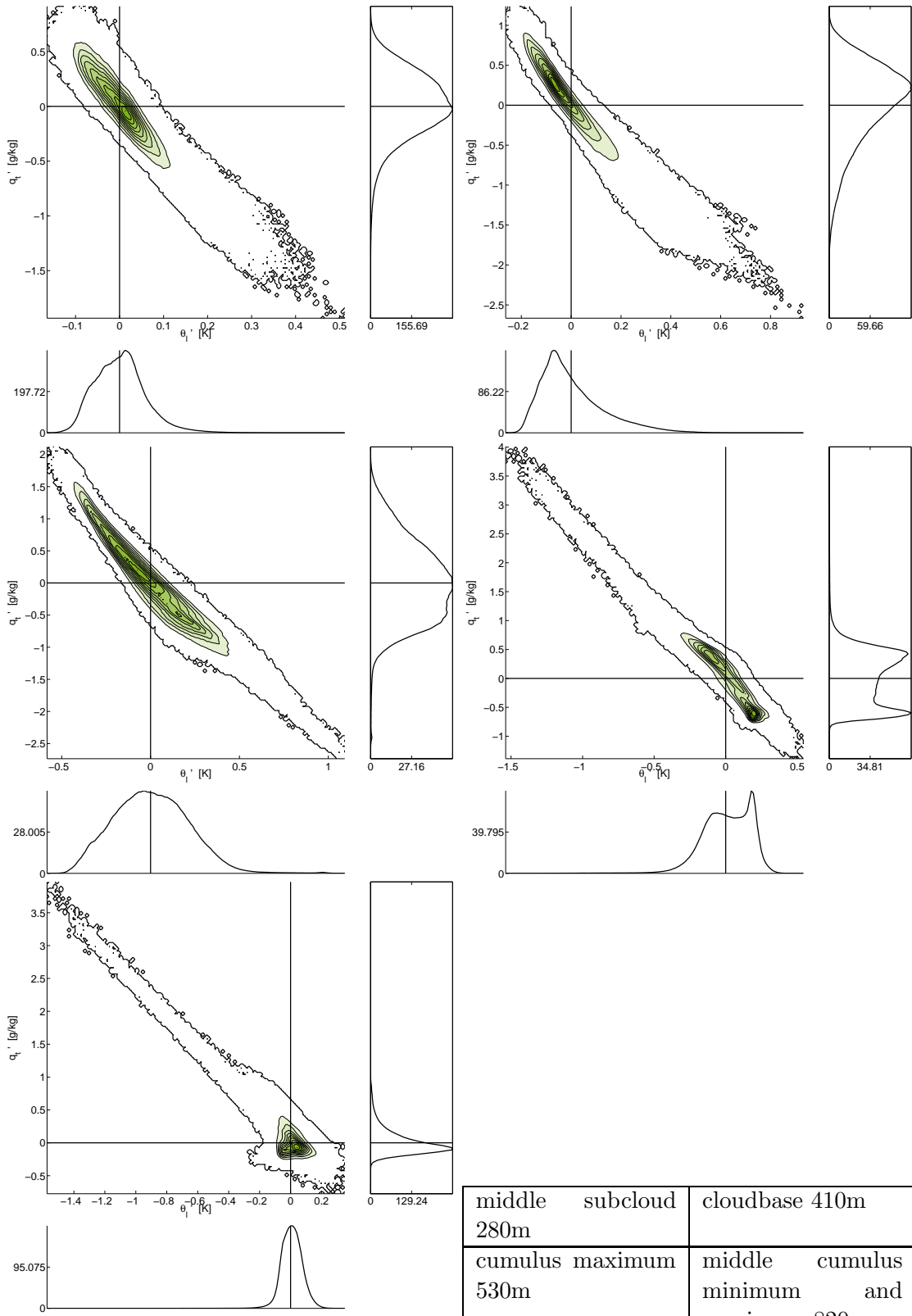
Figure 7.7: hour 39, horizontal plane fastest 2 (dotted) and 10(solid) percent(*LES_{small}*)

Chapter 8

Appendix - Joint PDF plots large domain LES

Joint density plots in this appendix have different line-style to joint density plots in chapter 4. In this chapter the part of the PDF with:

- PDF 0 are surrounded by the outer black lines.
- PDF 10% PDF_{peak} are surrounded by the first green filled black line
- PDF 20% PDF_{peak} are surrounded by the second green filled black line
-
- PDF 90% PDF_{peak} are surrounded by the ninth green filled black line



middle subcloud 280m	cloudbase 410m
cumulus maximum 530m	middle cumulus minimum and maximum 820 m
cumulus minimum 1180m	

hour 30 ASTEX

Figure 8.1: Joint probability density plots at heights according to table (*LESlarge*)

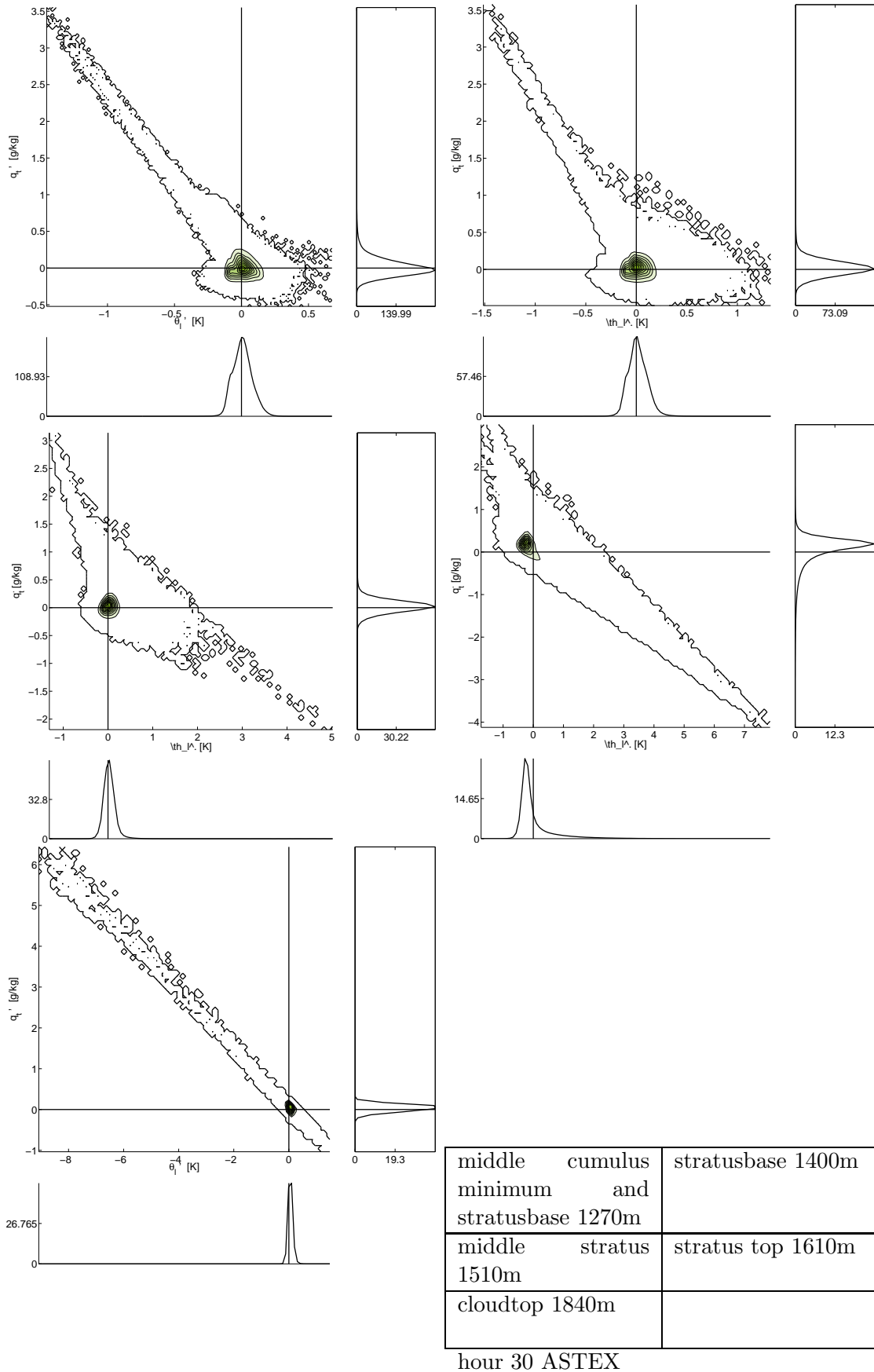
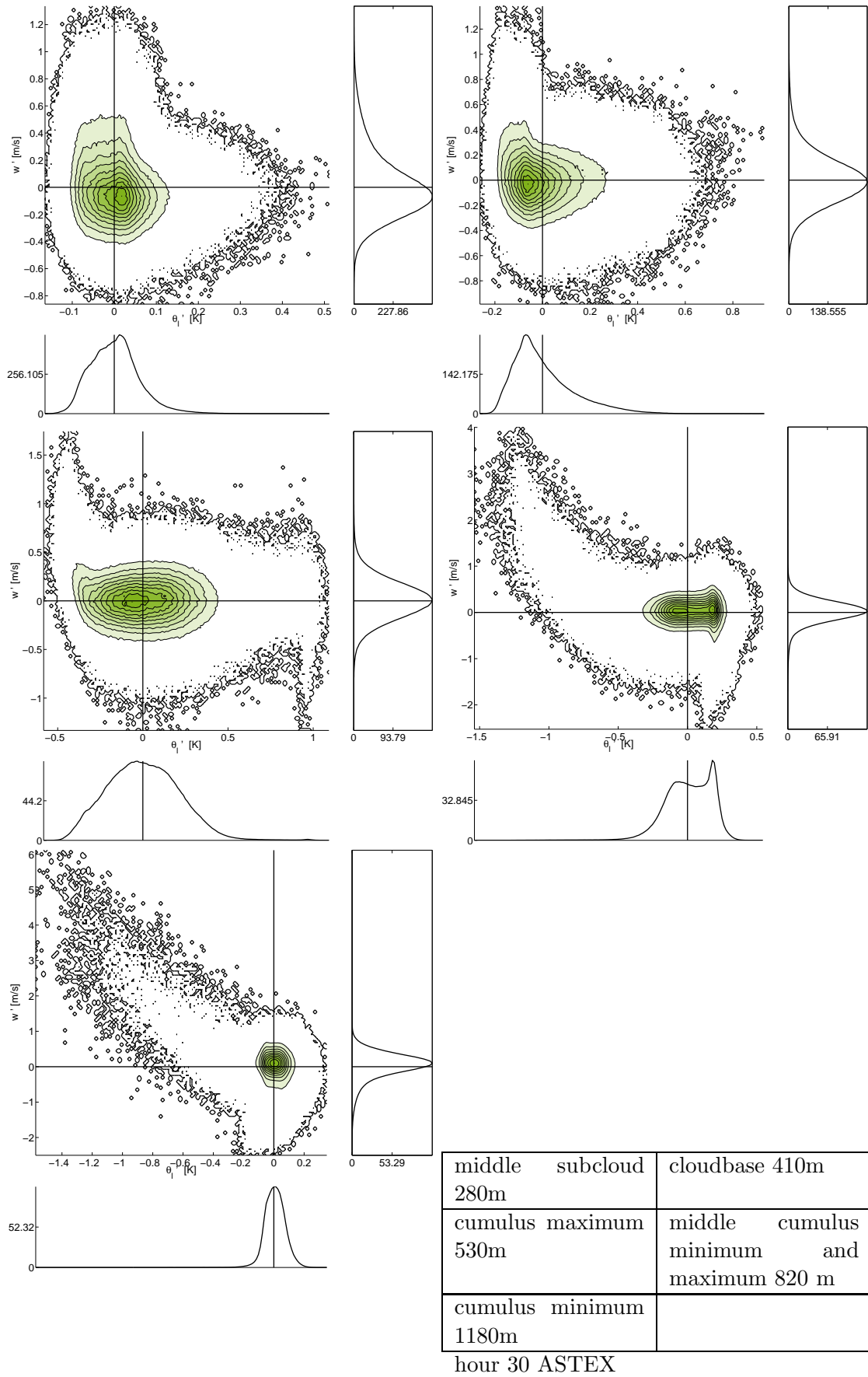


Figure 8.2: Joint probability density plots at heights according to table (*LESlarge*)



76 Figure 8.3: Joint probability density plots at heights according to table (*LESlarge*)

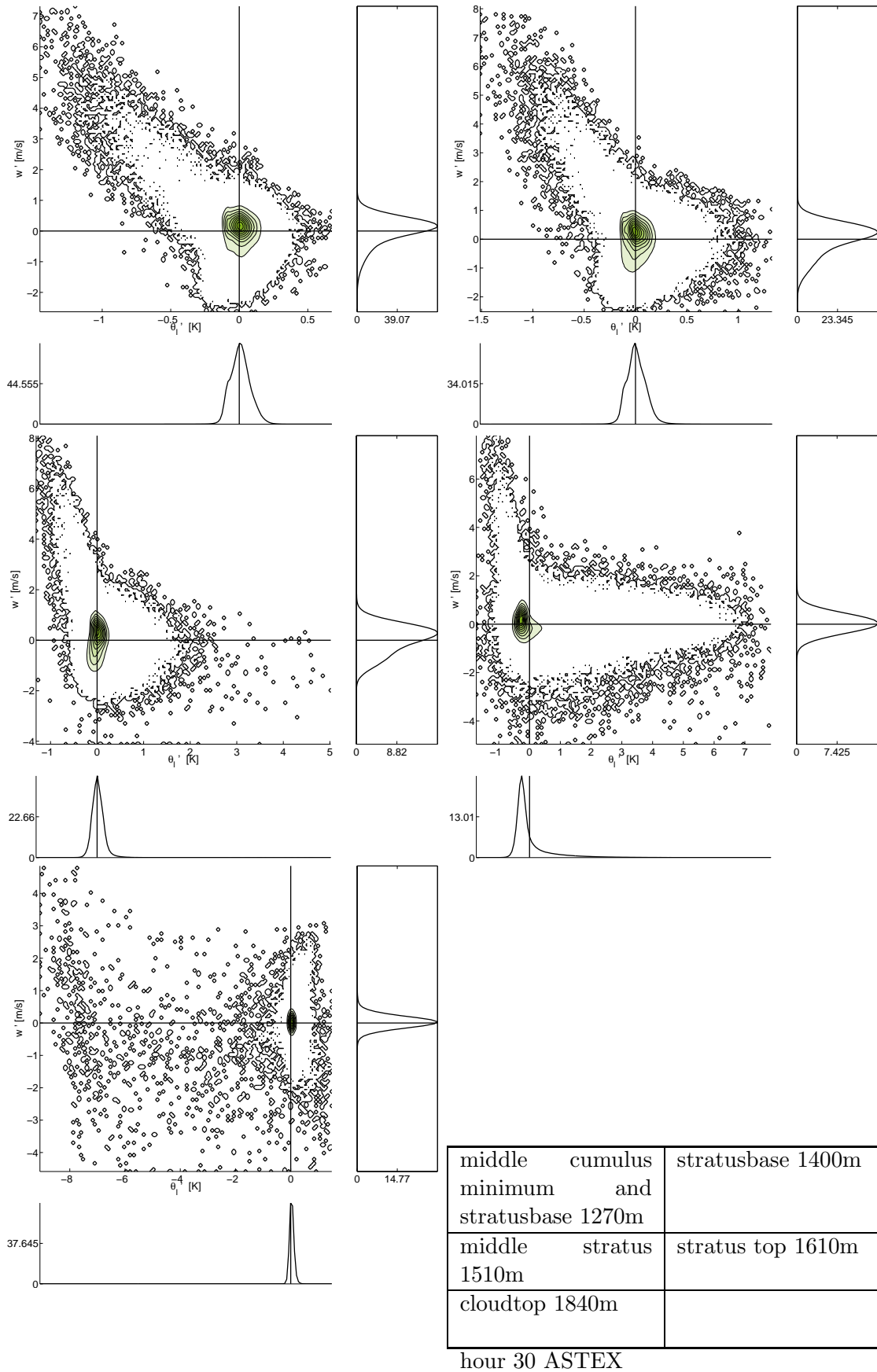
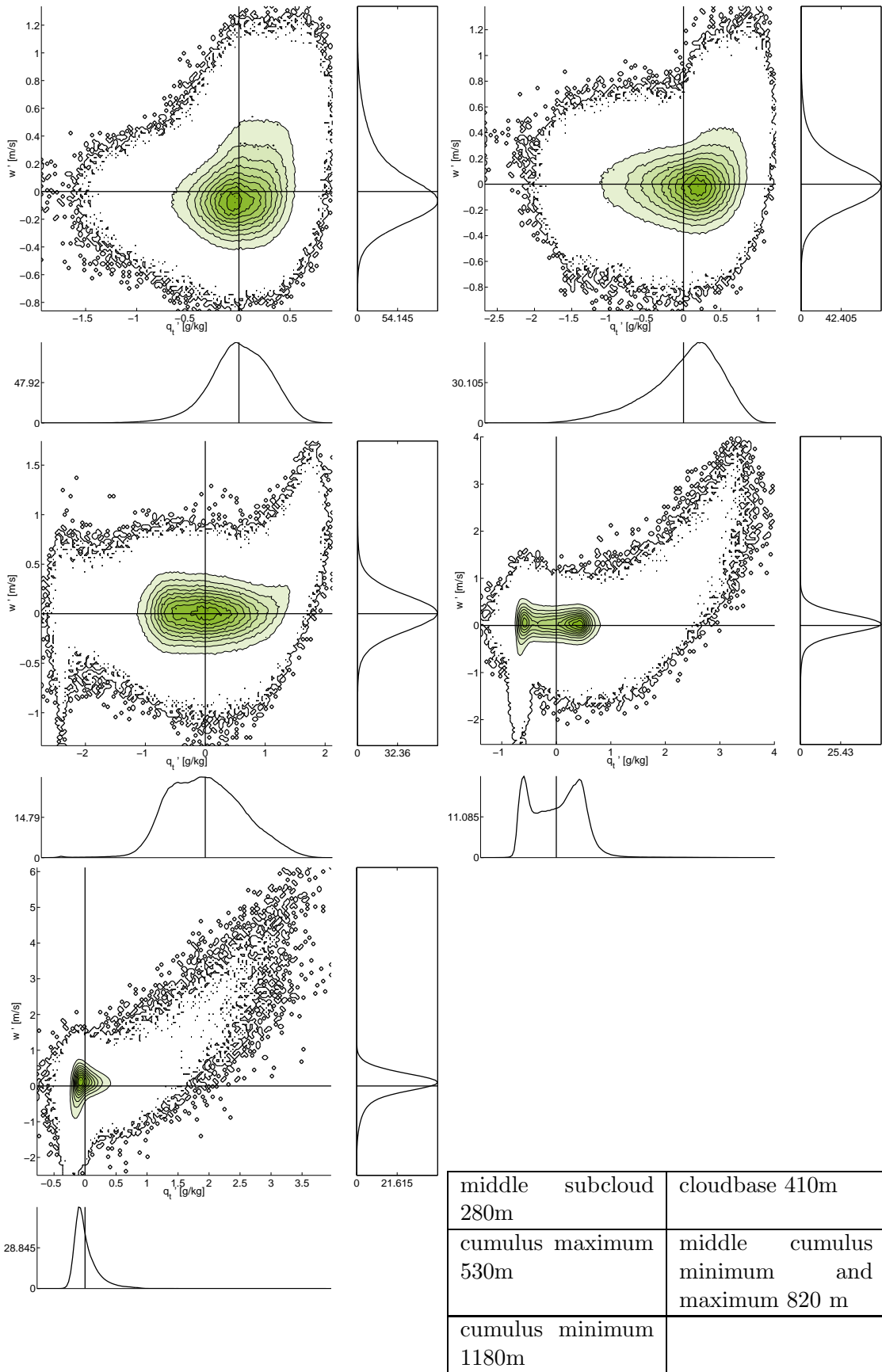


Figure 8.4: Joint probability density plots at heights according to table. (*LESlarge*)



middle subcloud 280m	cloudbase 410m
cumulus maximum 530m	middle cumulus minimum and maximum 820 m
cumulus minimum 1180m	

hour 30 ASTEX

78 Figure 8.5: Joint probability density plots at heights according to table (*LESlarge*)

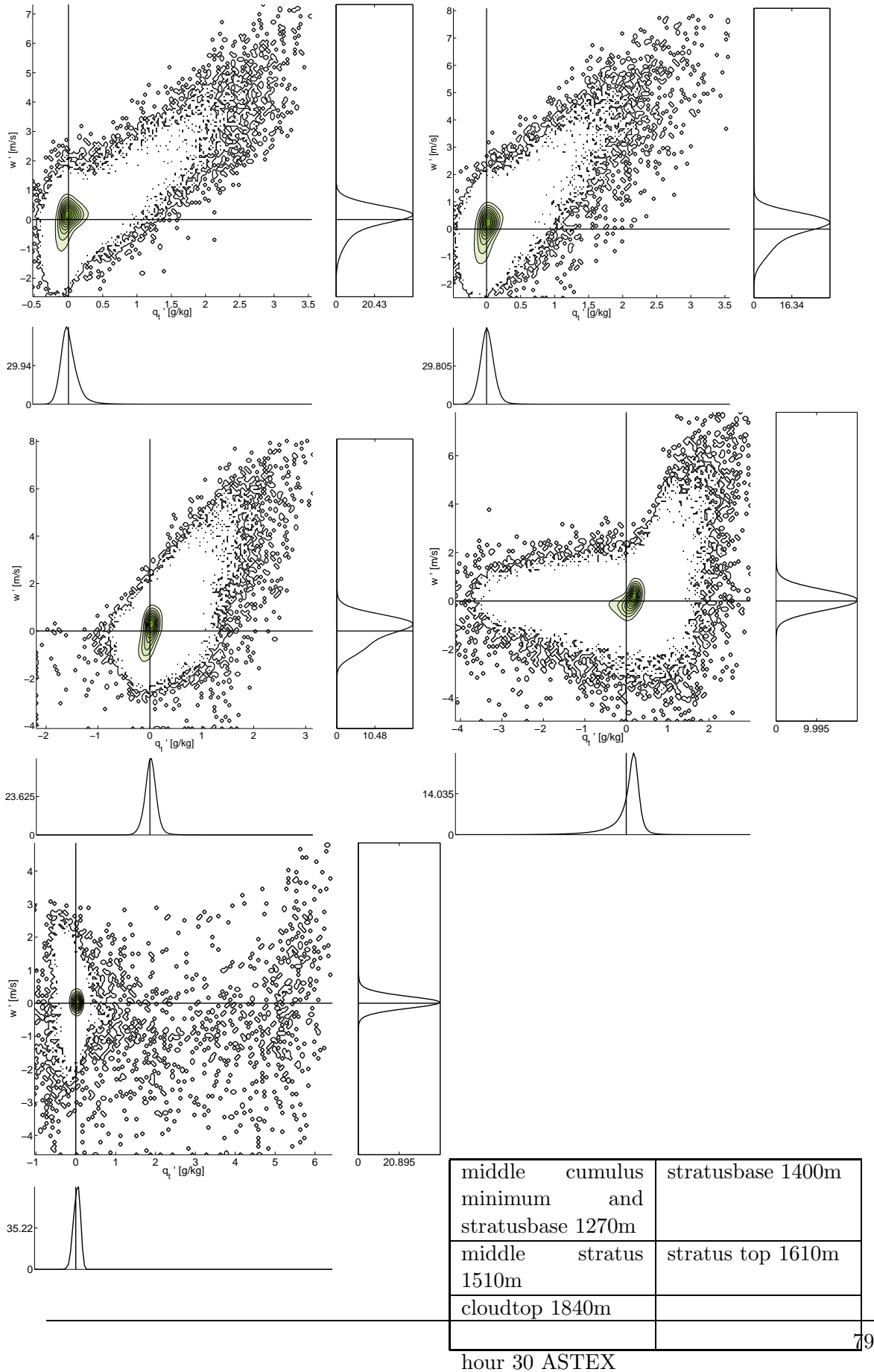
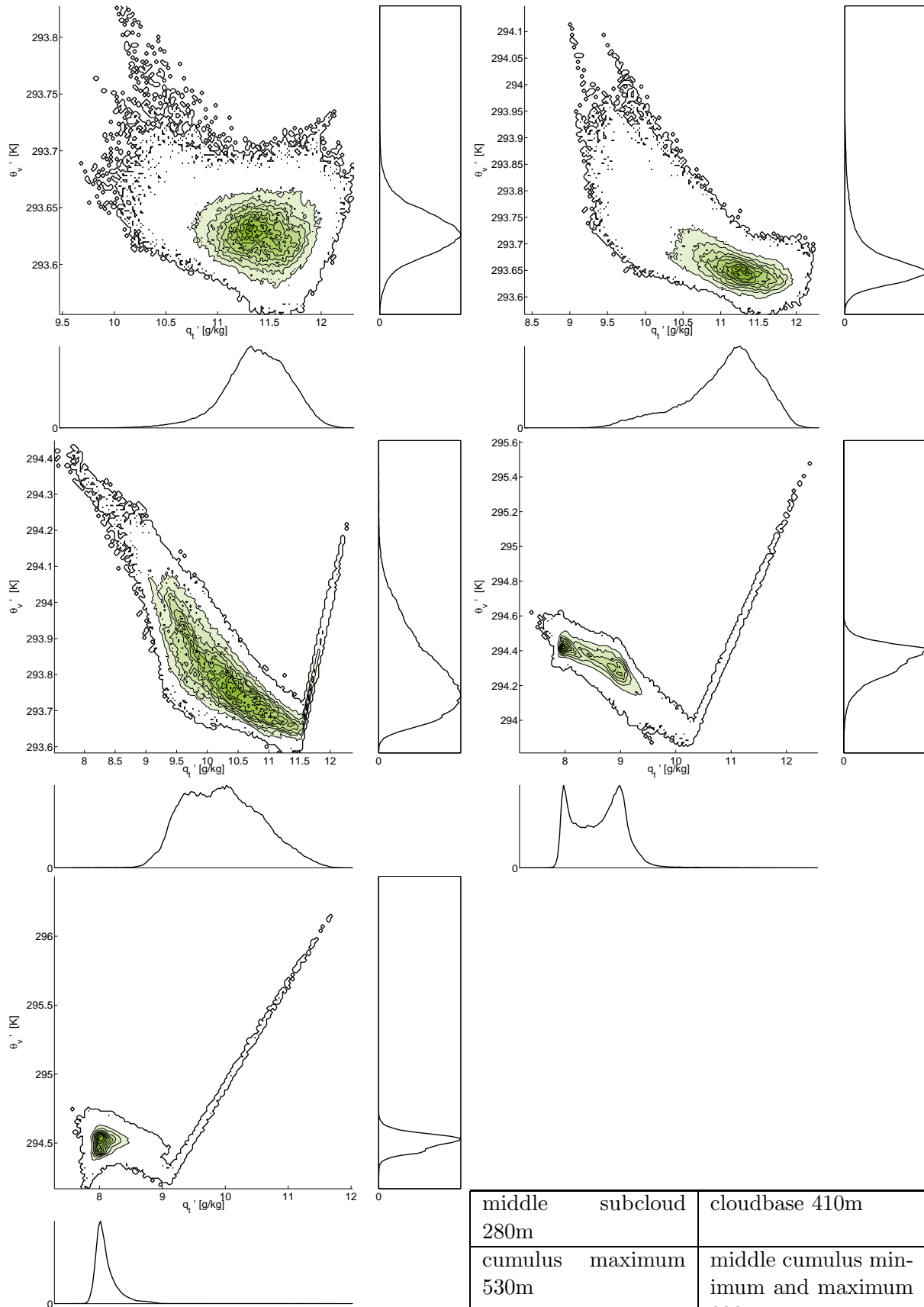
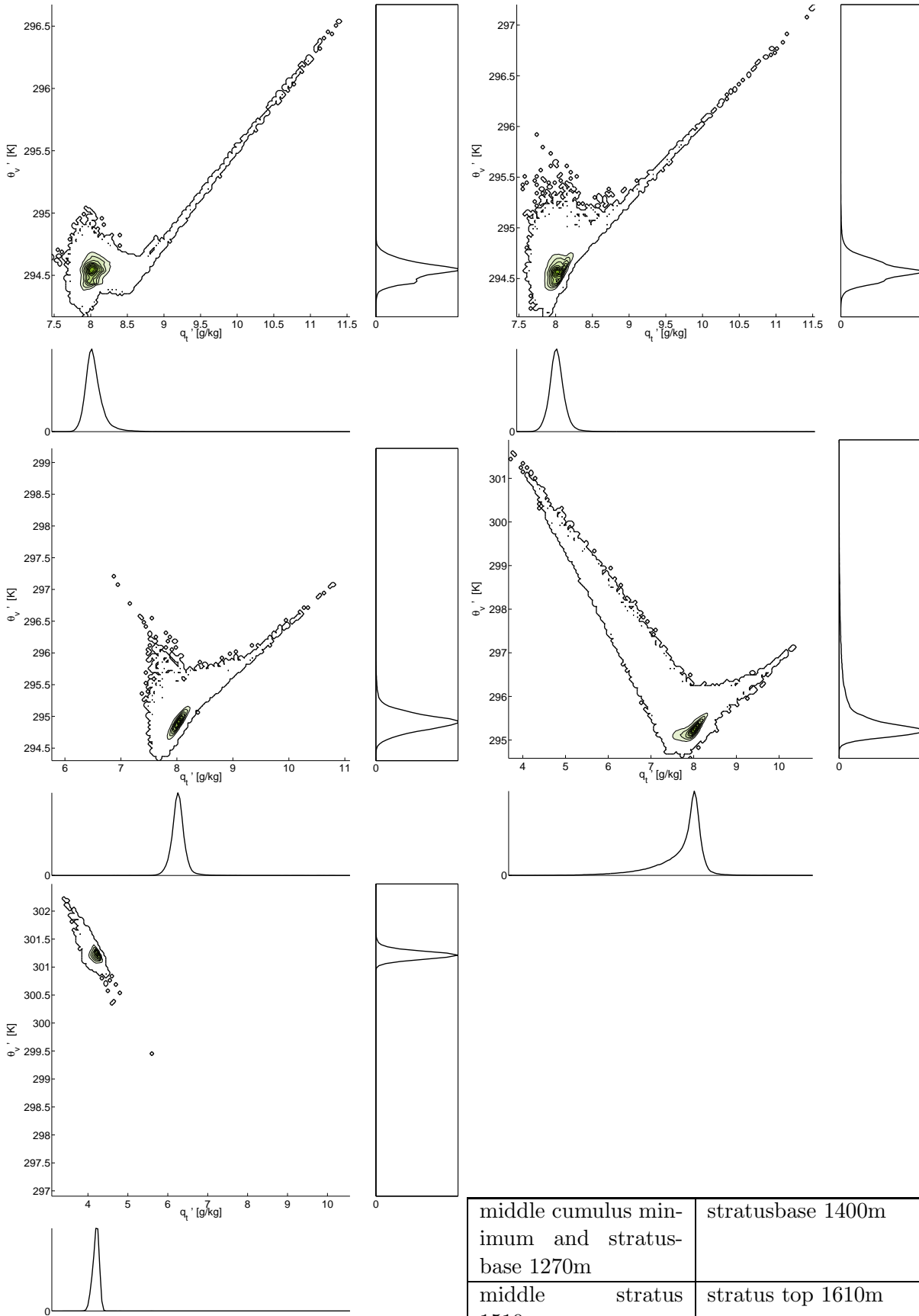


Figure 8.6: Joint probability density plots at heights according to table (*LESlarge*)

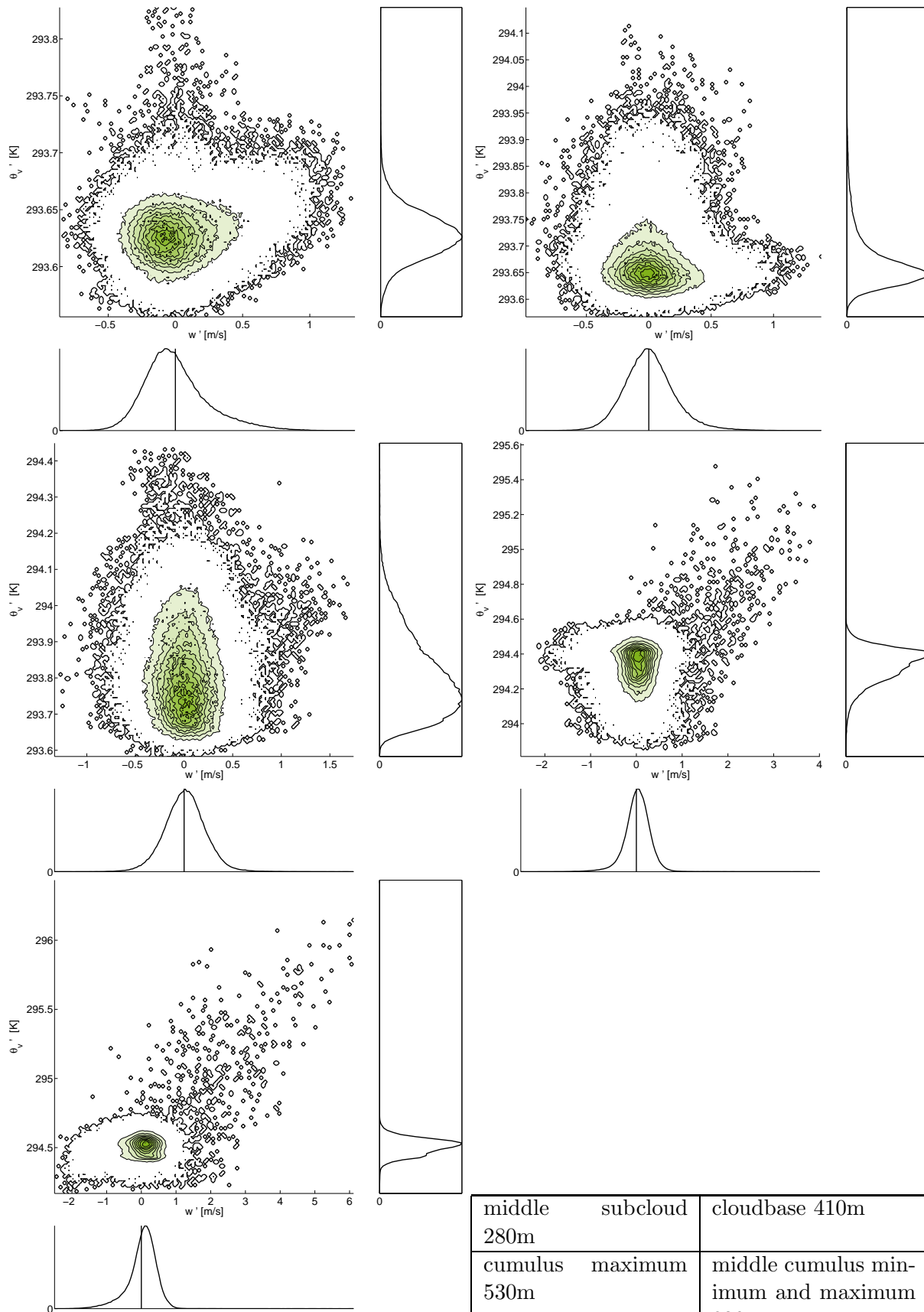


middle 280m	subcloud	cloudbase 410m
cumulus 530m	maximum	middle cumulus min- imum and maximum 820 m
cumulus 1180m	minimum	

8. Appendix - Joint PDF plots large domain LES

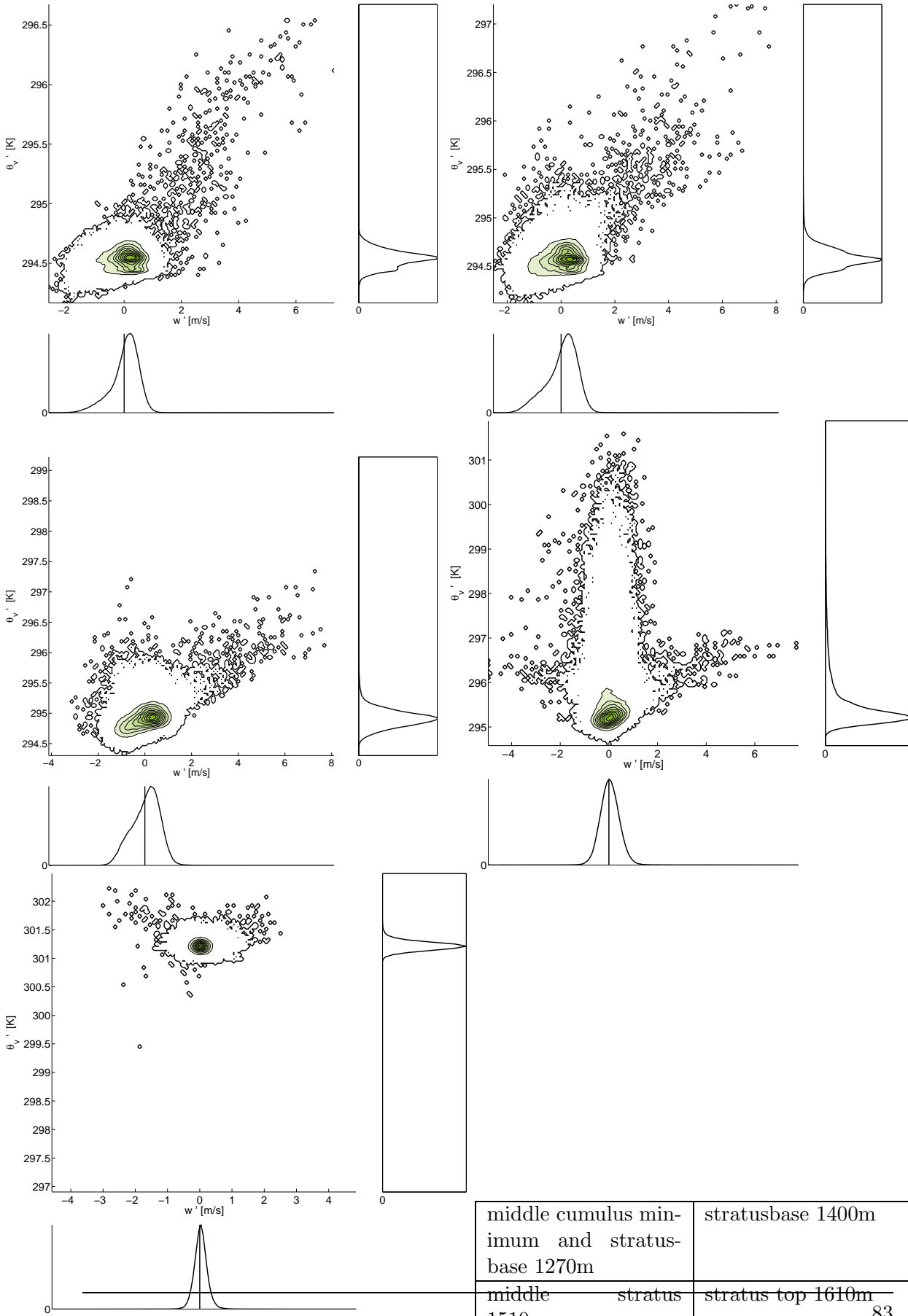


middle cumulus minimum and stratus base 1270m	stratus base 1400m
middle stratus 1510m	stratus top 1610m
cloud top 1840m	



middle 280m	subcloud	cloudbase 410m
cumulus 530m	maximum	middle cumulus min- imum and maximum 820 m
cumulus 1180m	minimum	

8. Appendix - Joint PDF plots large domain LES



middle cumulus minimum and stratus-base 1270m	stratusbase 1400m
middle stratus 1510m	stratus top 1610m
cloudtop 1840m	83

Bibliography

- Bruce A Albrecht, Christopher S Bretherton, Doug Johnson, Wayne H Scubert, and A Shelby Frisch. The atlantic stratocumulus transition experiment-astex. *Bulletin of the American Meteorological Society*, 76(6):889–904, 1995.
- R. Pincus C. S. Bretherton. Cloudiness and marine boundary layer dynamics in the astex lagrangian experiments. part i: Synoptic setting and vertical structure. *Journal of the atmospheric sciences*, 15 aug 1995.
- J.T. Dawe and P.H. Austin. Influence of the cloud shell on tracer budget measurements of les cloud entrainment. 2011.
- S.R. de Roode and P.G. Duynkerke. Observed lagrangian transition of stratocumulus into cumulus during astex: Mean state and turbulence structure. *Journal of the atmospheric sciences*, 54(17):2157–2173, 1997.
- S.R. de Roode, H.J.J. Jonker, P.G. Duynkerke, and B. Stevens. Countergradient fluxes of conserved variables in the clear convective and stratocumulus-topped boundary layer: The role of the entrainment flux. *Boundary-Layer Meteorology*, 112(1):179–196, 2004.
- Stephan R de Roode, A Pier Siebesma, Harm JJ Jonker, and Yoerik de Voogd. Parameterization of the vertical velocity equation for shallow cumulus clouds. *Monthly Weather Review*, 140(8), 2012.
- JW Deardorff. The counter-gradient heat flux in the lower atmosphere and in the laboratory. *Journal of the Atmospheric Sciences*, 23(5):503–506, 1966.
- JW Deardorff. Theoretical expression for the countergradient vertical heat flux. *Journal of Geophysical Research*, 77(30):5900–5904, 1972.
- ECMWF. Horizontal resolution increase, January 2010. URL http://www.ecmwf.int/products/changes//horizontal_resolution..._2009/#gaussian.
- T. Heus and H.J.J. Jonker. Subsiding shells around shallow cumulus clouds. *Journal of the Atmospheric Sciences*, 65(3):1003–1018, 2008.
- T. Heus, CC Van Heerwaarden, HJJ Jonker, A.P. Siebesma, S. Axelsen, K. van den Dries, O. Geoffroy, AF Moene, D. Pino, SR de Roode, et al. Formulation of and numerical studies with the dutch atmospheric large-eddy simulation (dales). *Geosci. Model Dev. Dis*, 3:99–180, 2010.

-
- HIRLAM. General description of the harmonie model, 2009. URL <http://hirlam.org/index.php/hirlam-programme-53/general-model-...description/mesoscale-harmonie>.
- AAM Holtslag and C.H. Moeng. Eddy diffusivity and countergradient transport in the convective atmospheric boundary layer. *Journal of Atmospheric Sciences*, 48:1690–1700, 1991.
- IPCC. Climate change 2007: the physical science basis. *Agenda*, 6:07, 2007.
- Karim Muhammad Mahdi. Clouds over africa. personal picture, 2012.
- NASA. Earth global circulation. public domain, 6 2005. <http://sealevel.jpl.nasa.gov/overview/climate-climatic.html>.
- R.A.J. Neggers, M. k/ohler, and A.C.M. Beljaars. A dual mass flux framework for boundary layer convection. part i: Transport. *Journal of the atmospheric sciences*, 66(6):1465–1487, 2009a.
- R.A.J. Neggers, M. Köhler, and A.C.M. Beljaars. A dual mass flux framework for boundary layer convection. part ii: Clouds. *Journal of the atmospheric sciences*, 66(6):1489–1506, 2009b.
- AP Siebesma and JWM Cuijpers. Evaluation of parametric assumptions for shallow cumulus convection. *Journal of the atmospheric sciences*, 52(6):650–666, 1995.
- A.P. Siebesma, C.S. Bretherton, A. Brown, A. Chlond, J. Cuxart, P.G. Duynkerke, H. Jiang, M. Khairoutdinov, D. Lewellen, C.H. Moeng, et al. A large eddy simulation intercomparison study of shallow cumulus convection. *Journal of the Atmospheric Sciences*, 60(10):1201–1219, 2003.
- A.P. Siebesma, P.M.M. Soares, and J. Teixeira. A combined eddy-diffusivity mass-flux approach for the convective boundary layer. *Journal of the atmospheric sciences*, 64(4):1230–1248, 2007.
- PMM Soares, PMA Miranda, AP Siebesma, and J. Teixeira. An eddy-diffusivity/mass-flux parametrization for dry and shallow cumulus convection. *Quarterly Journal of the Royal Meteorological Society*, 130(604):3365–3383, 2004.
- P.M.M. Soares, P. Miranda, J. Teixeira, and AP Siebesma. An eddy-diffusivity/mass-flux boundary layer parameterization based on the tke equation: a dry convection case study. *Física de la Tierra*, 19:147–161, 2008.
- B. Stevens. Quasi-steady analysis of a pbl model with an eddy-diffusivity profile and nonlocal fluxes. *Monthly weather review*, 128(3):824–836, 2000.
- B. Stevens, A.S. Ackerman, B.A. Albrecht, A.R. Brown, A. Chlond, J. Cuxart, P.G. Duynkerke, D.C. Lewellen, M.K. Macvean, R.A.J. Neggers, et al. Simulations of trade wind cumuli under a strong inversion. *Journal of the atmospheric sciences*, 58(14):1870–1891, 2001.

- B. Stevens, C.H. Moeng, A.S. Ackerman, C.S. Bretherton, A. Chlond, S. de Roode, J. Edwards, J.C. Golaz, H. Jiang, M. Khairoutdinov, et al. Evaluation of large-eddy simulations via observations of nocturnal marine stratocumulus. *Monthly weather review*, 133(6):1443–1462, 2005.
- JJ Van der Dussen, SR de Roode, AS Ackerman, PN Blossey, CS Bretherton, MJ Kurowski, AP Lock, RAJ Neggers, I Sandu, and AP Siebesma. The gass/euclipse model intercomparison of the stratocumulus transition as observed during astex: Les results. *Journal of Advances in Modeling Earth Systems*, 2013.